Development of substituted 2-(4-(sulfonyl)piperazin-1-yl)quinazoline molecular hybrids as a new class of antimalarials

Hari Madhav[1,2,‡], Ashutosh Panda[2,‡], Dipanwita Datta[2], Kashfa Shaheen[1], Abdur Rahman[3], Azhar Tariq Khan[1], Souvik Bhattacharjee[3], Dhiraj Kumar[2], Pawan Malhotra[2,*], and Nasimul Hoda[1,*]

[1]Drug Design and Synthesis Laboratory, Department of Chemistry, Jamia Millia Islamia, New Delhi-110025, India.

[2]International Centre for Genetic Engineering and Biotechnology (ICGEB), New Delhi-110067, India.

[3]Special Centre for Molecular Medicine, Jawaharlal Nehru University, New Delhi-110067, India.

[‡]These authors contributed equally to the article (Joint First Authors).

[*]Corresponding Authors

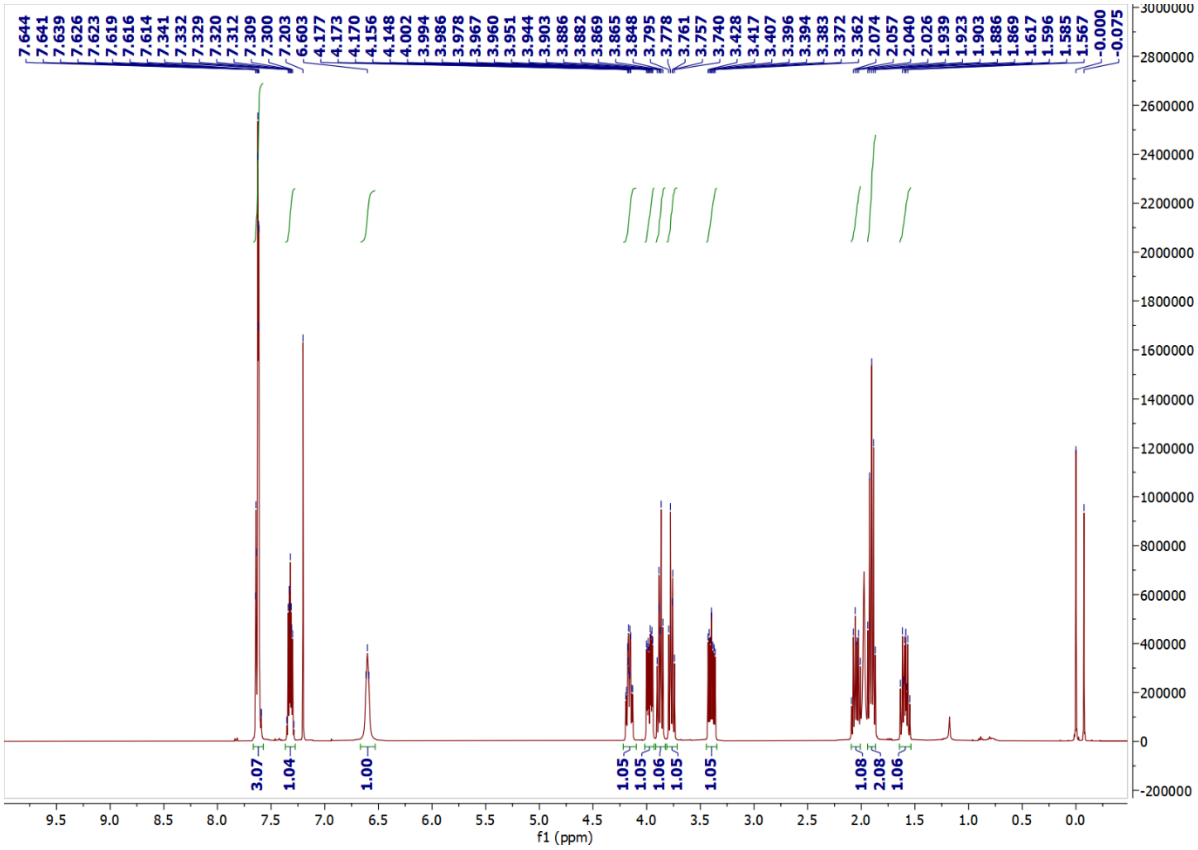

Figure S1: ^{1}H NMR Spectra of **12**.

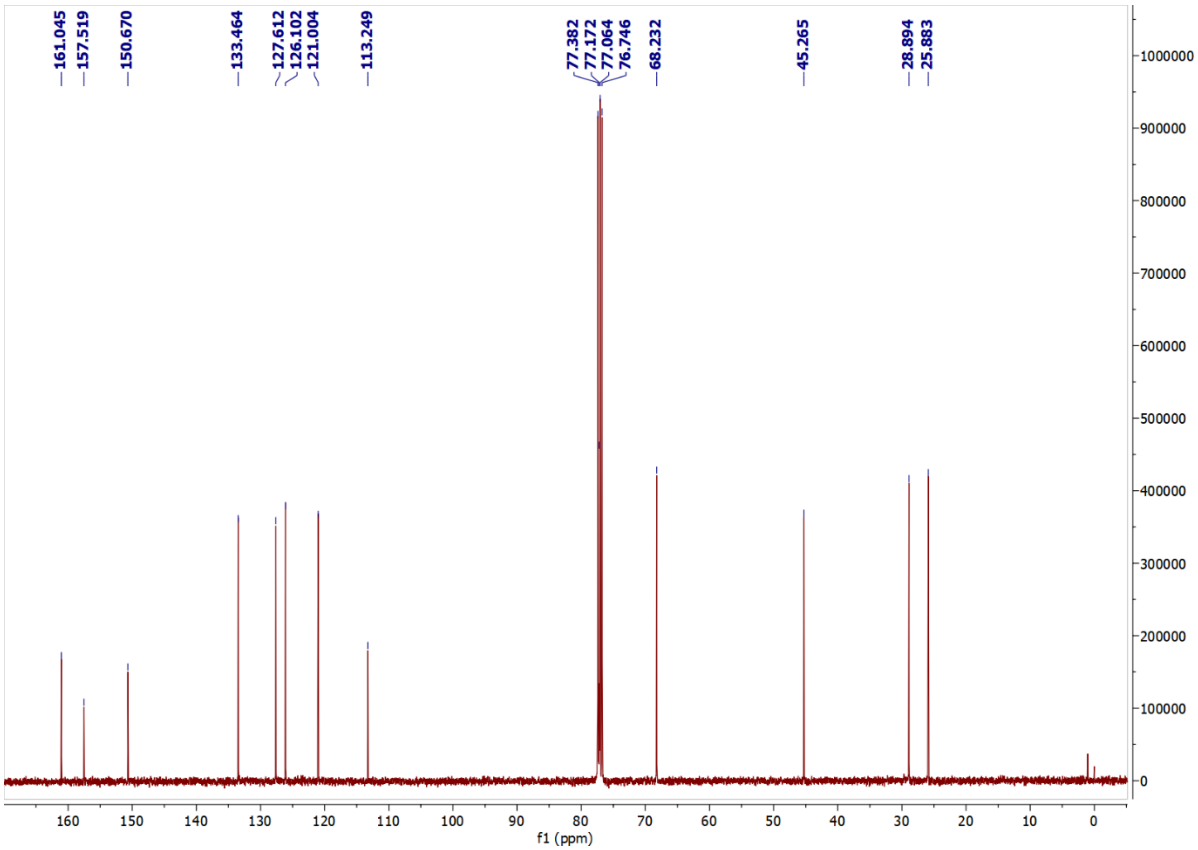

Figure S2: ^{13}C NMR Spectra of **12**.

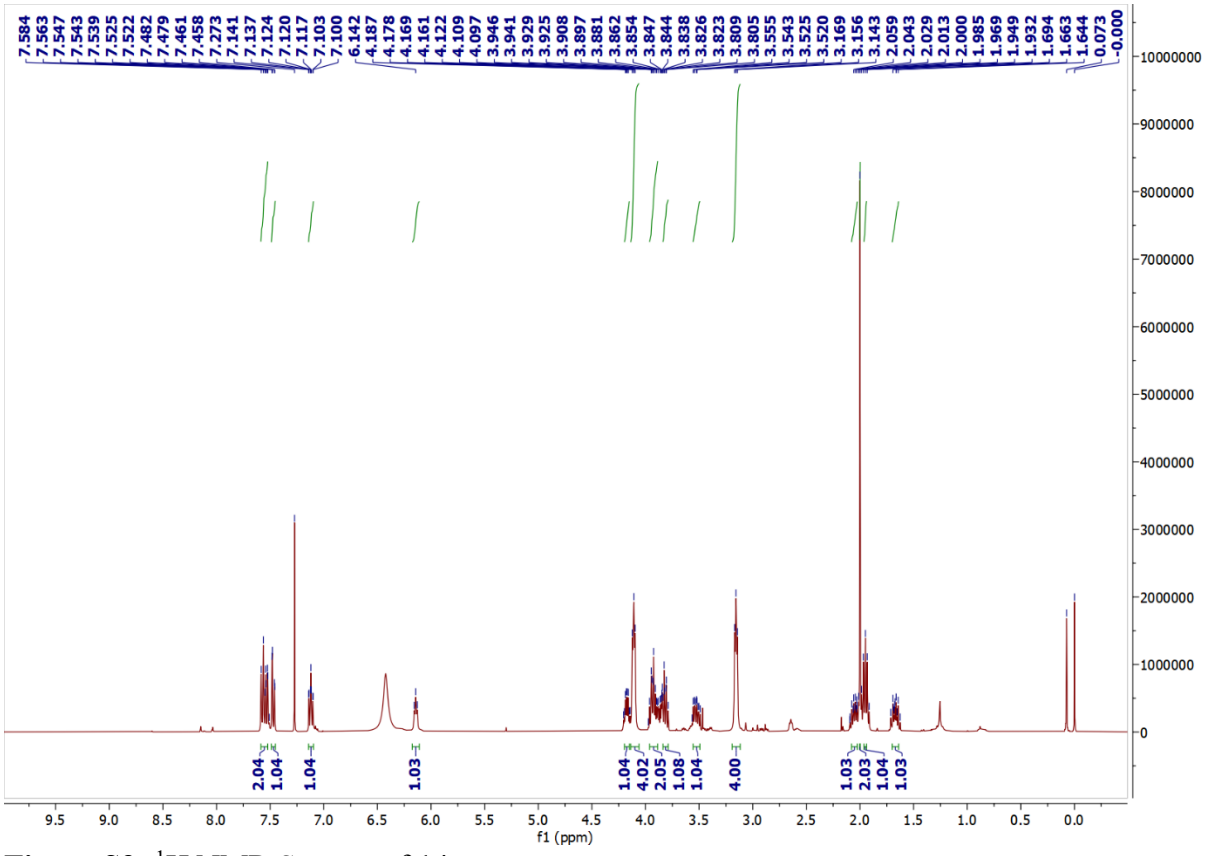

Figure S3: ^{1}H NMR Spectra of **14a**.

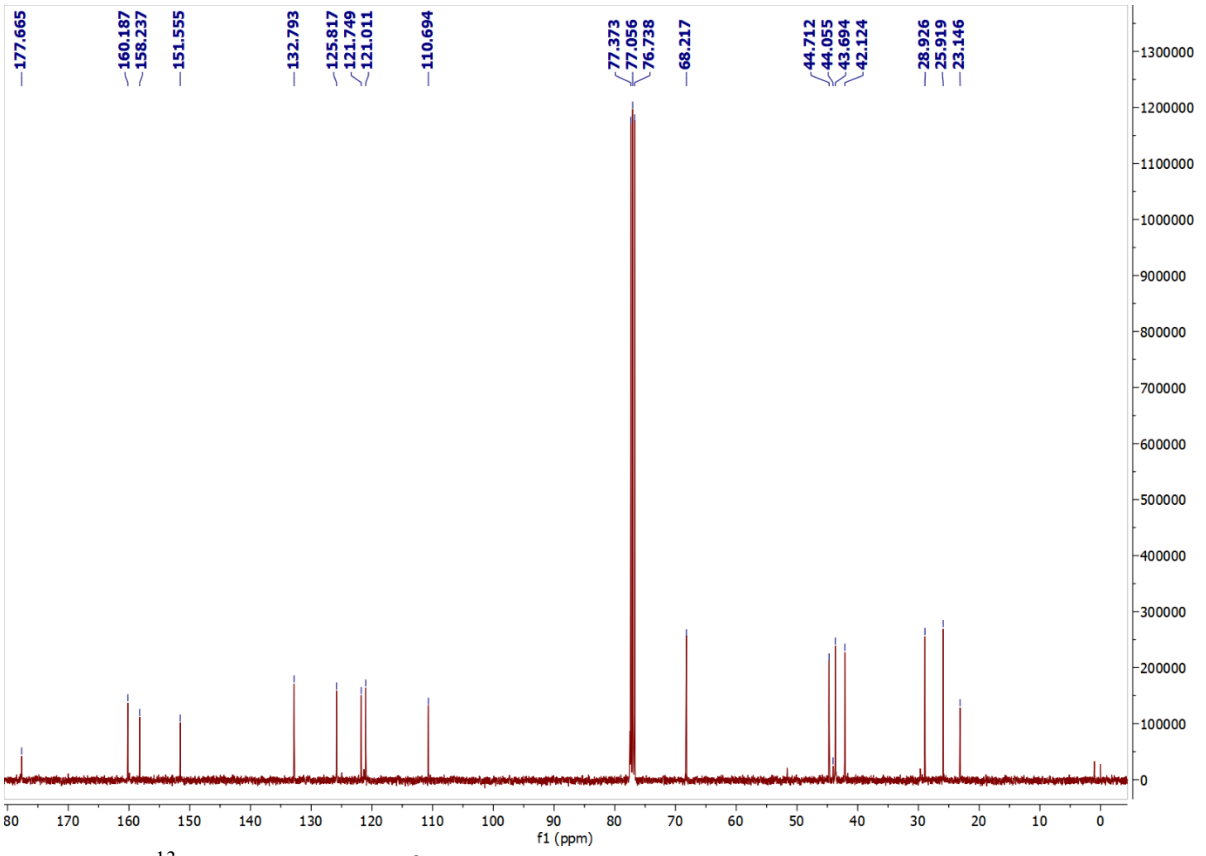

Figure S4: ^{13}C NMR Spectra of **14a**.

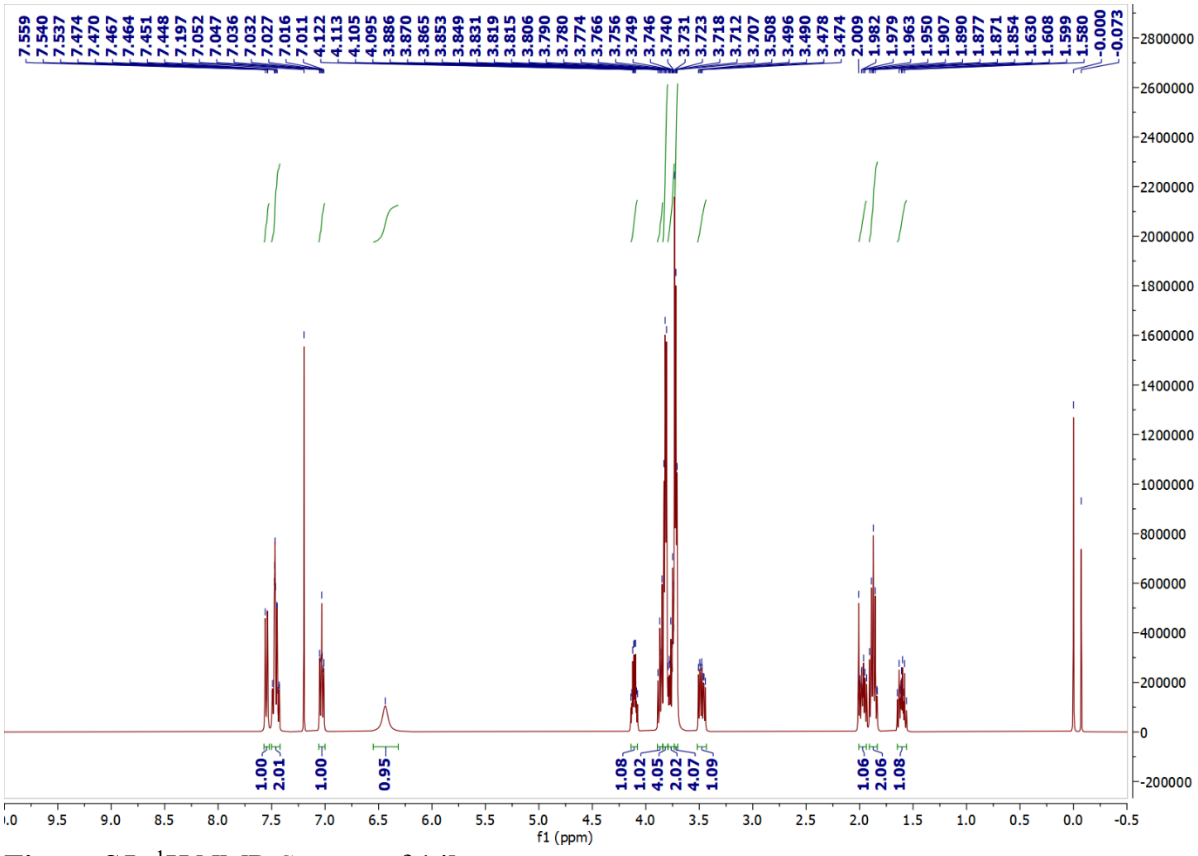

Figure S5: ^{1}H NMR Spectra of **14b**.

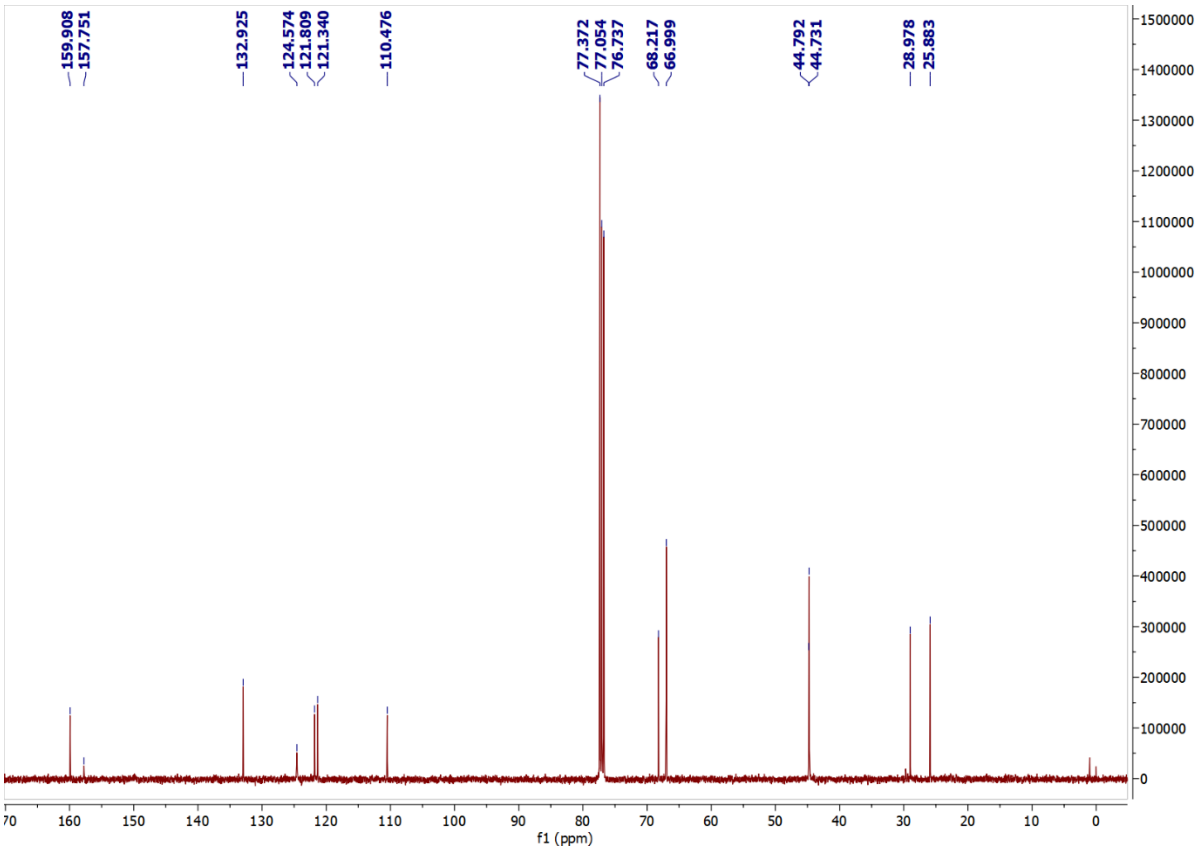

Figure S6: ^{13}C NMR Spectra of **14b**.

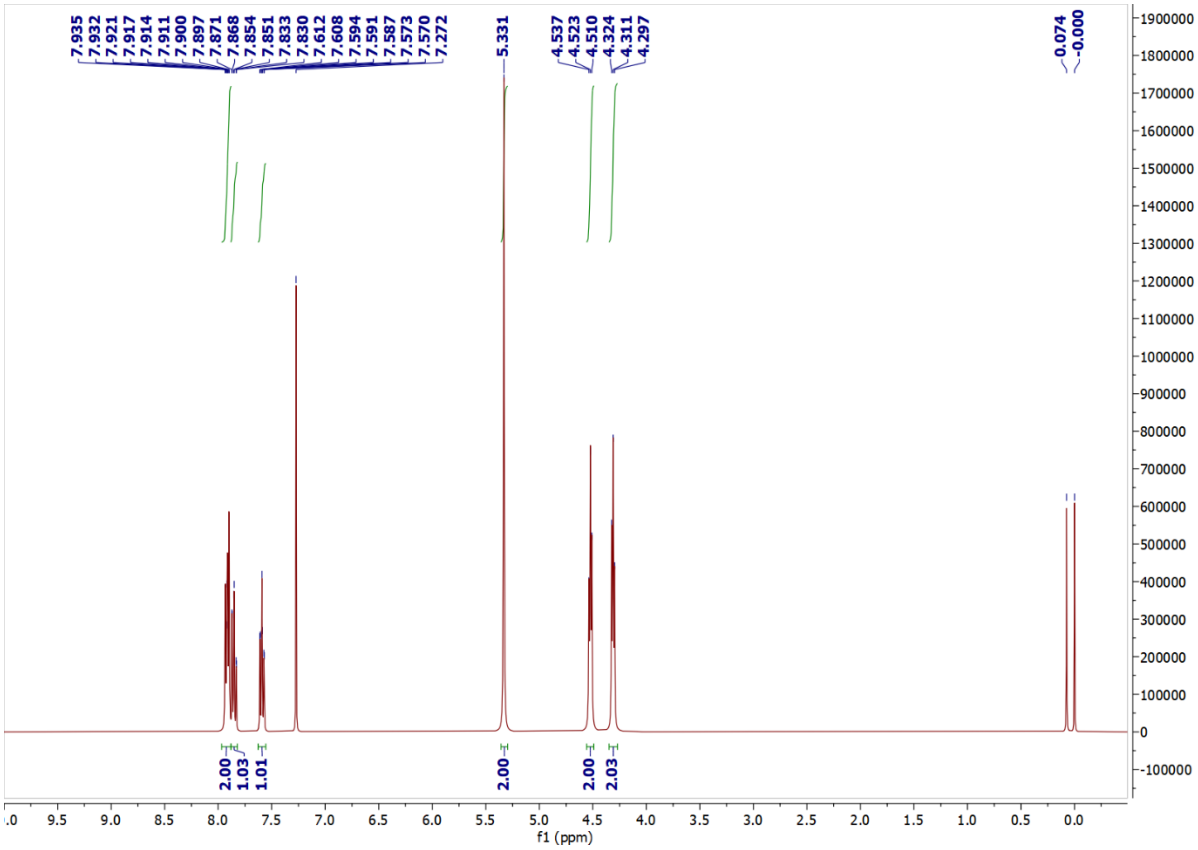

Figure S7: ^{1}H NMR Spectra of **16**.

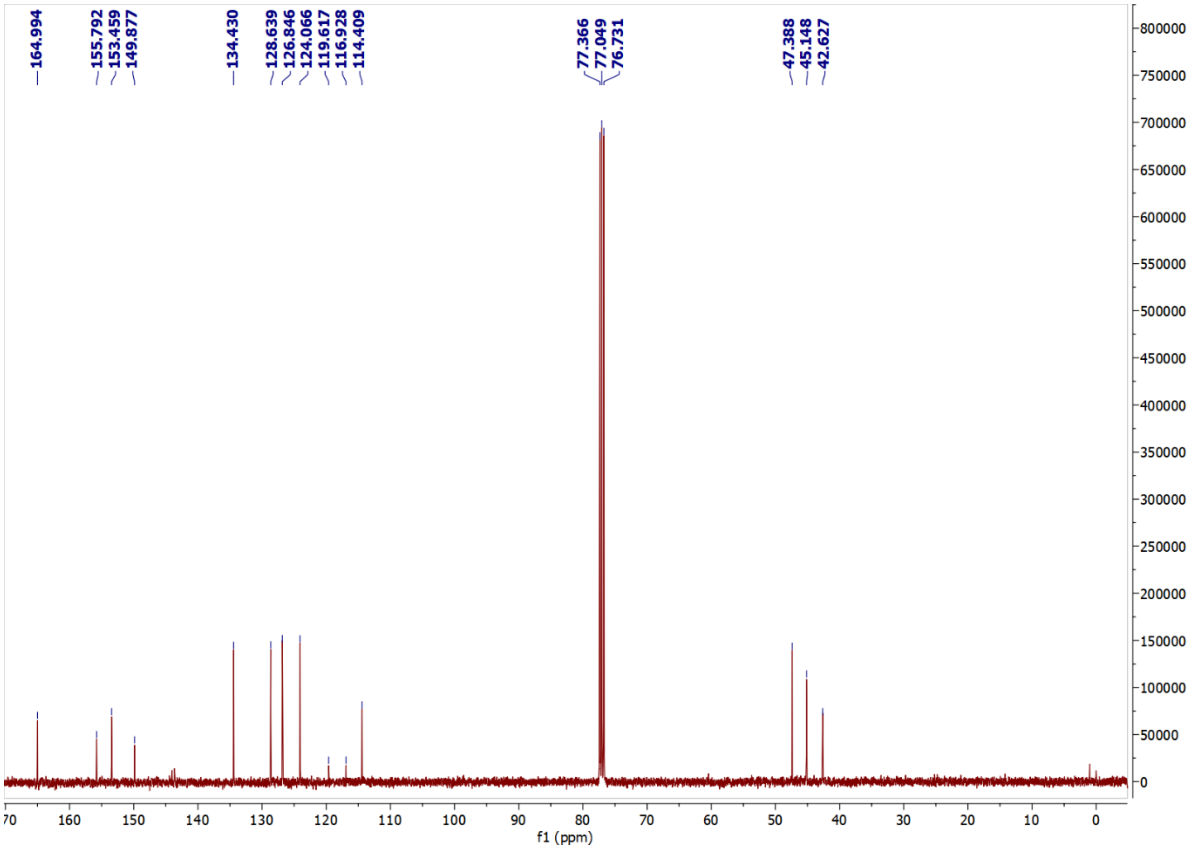

Figure S8: ^{13}C NMR Spectra of **16**.

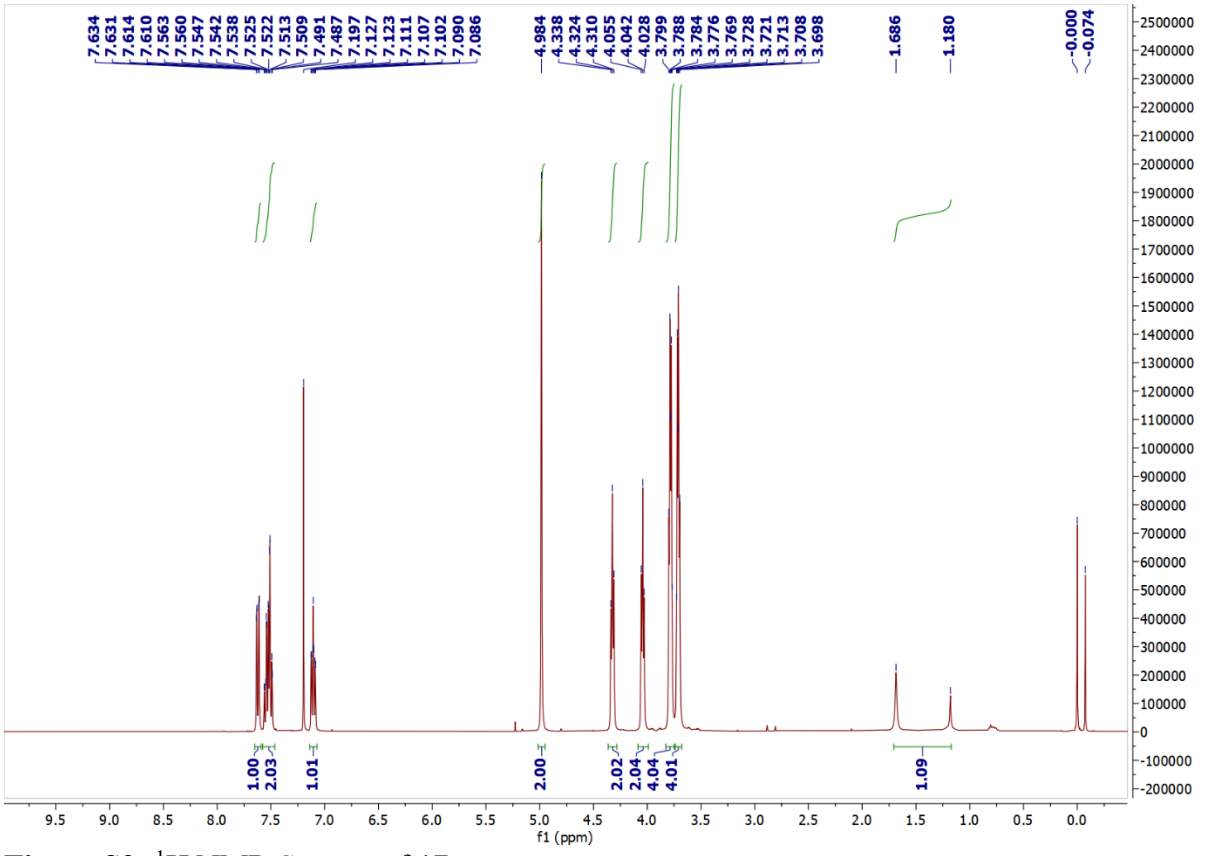

Figure S9: ^{1}H NMR Spectra of **17a**.

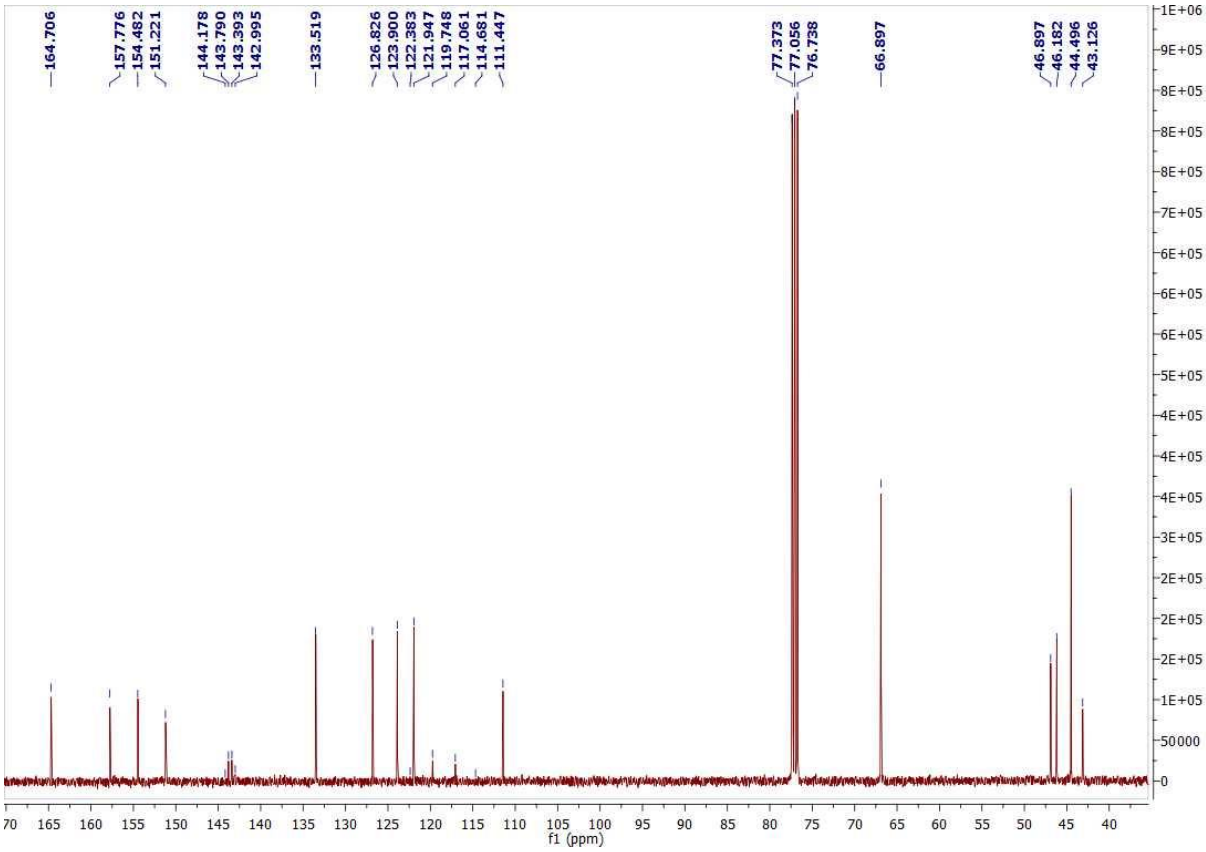

Figure S10: ^{13}C NMR Spectra of **17a**.

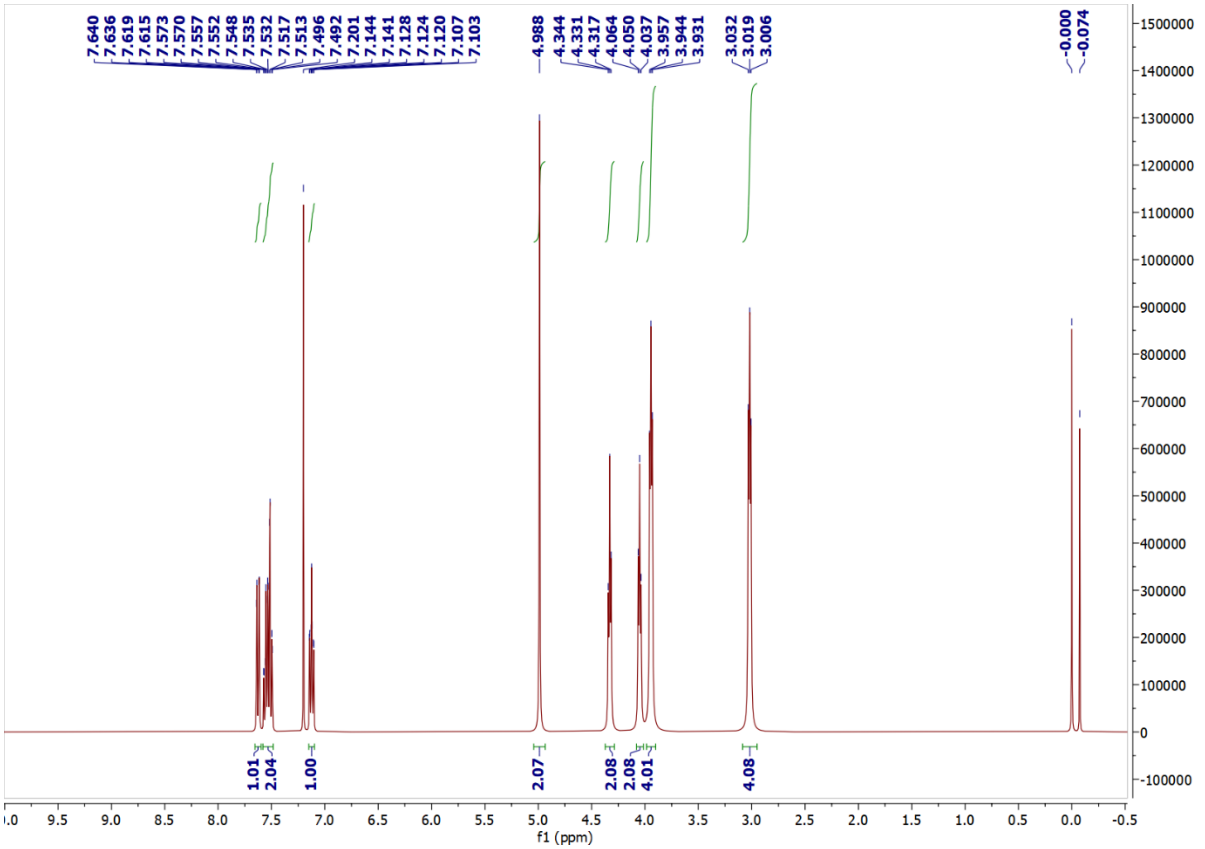

Figure S11: ^{1}H NMR Spectra of **17b**.

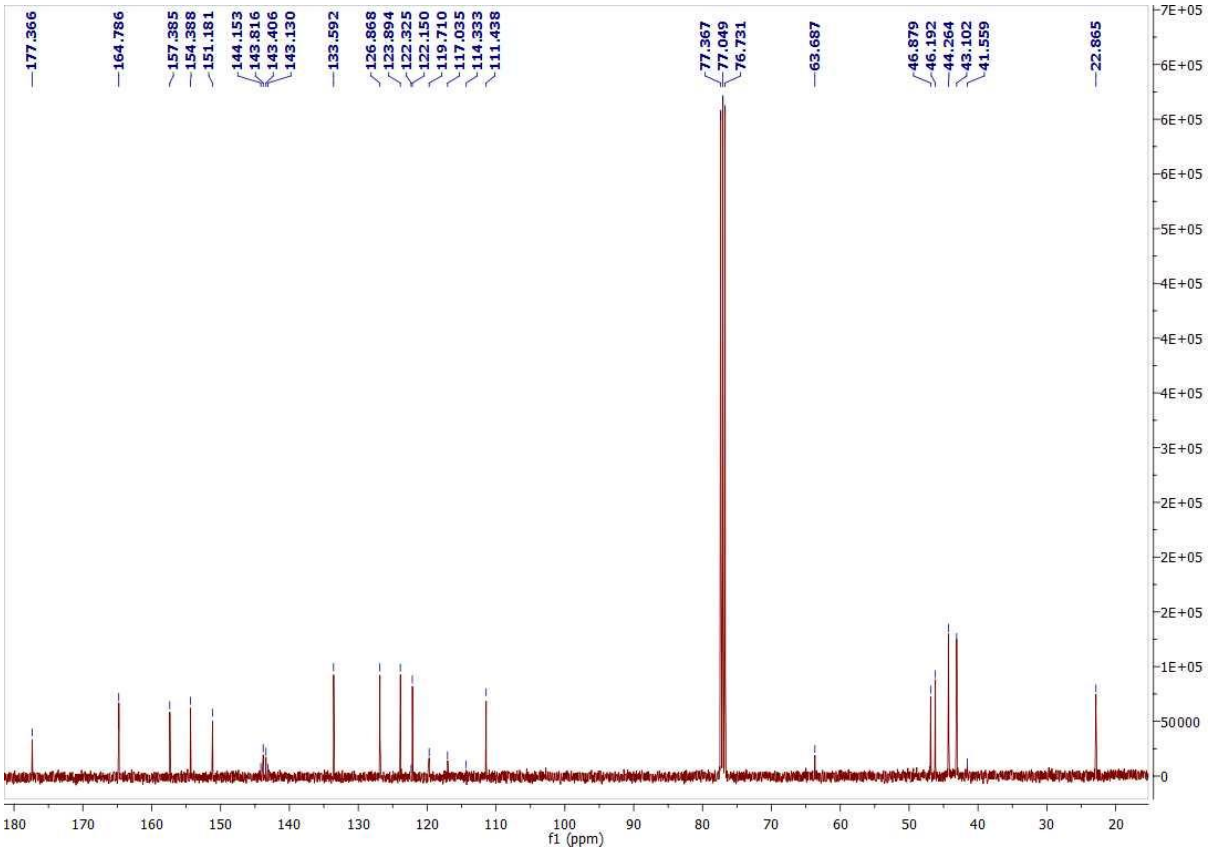

Figure S12: ^{13}C NMR Spectra of **17b**.

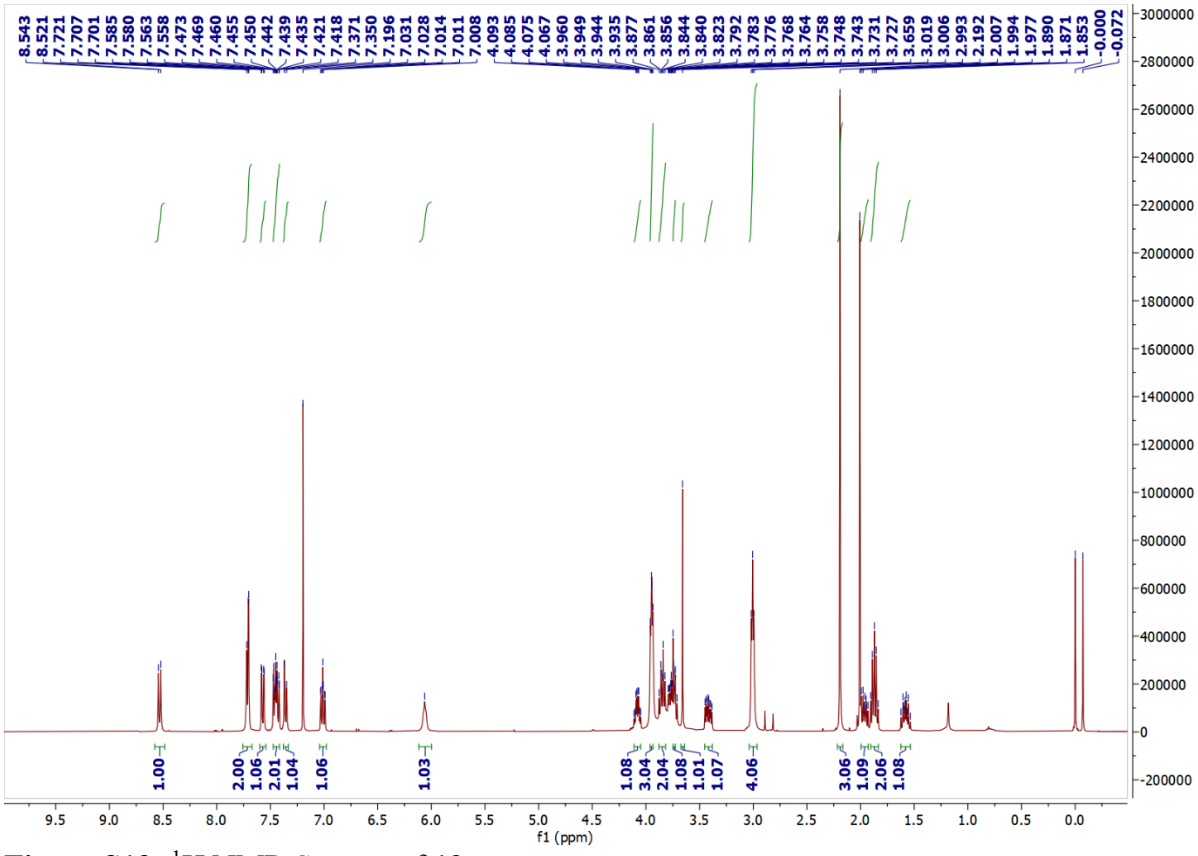

Figure S13: ^{1}H NMR Spectra of **19**.

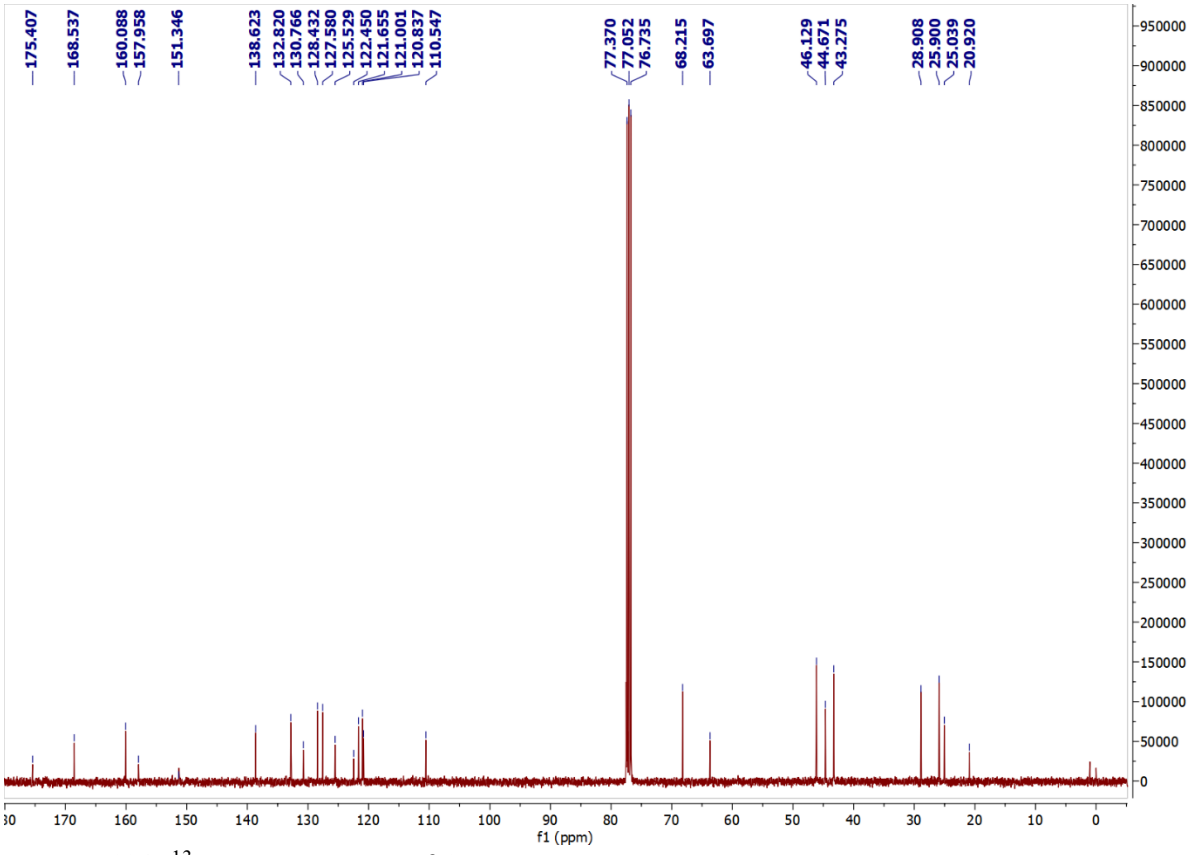

Figure S14: ^{13}C NMR Spectra of **19**.

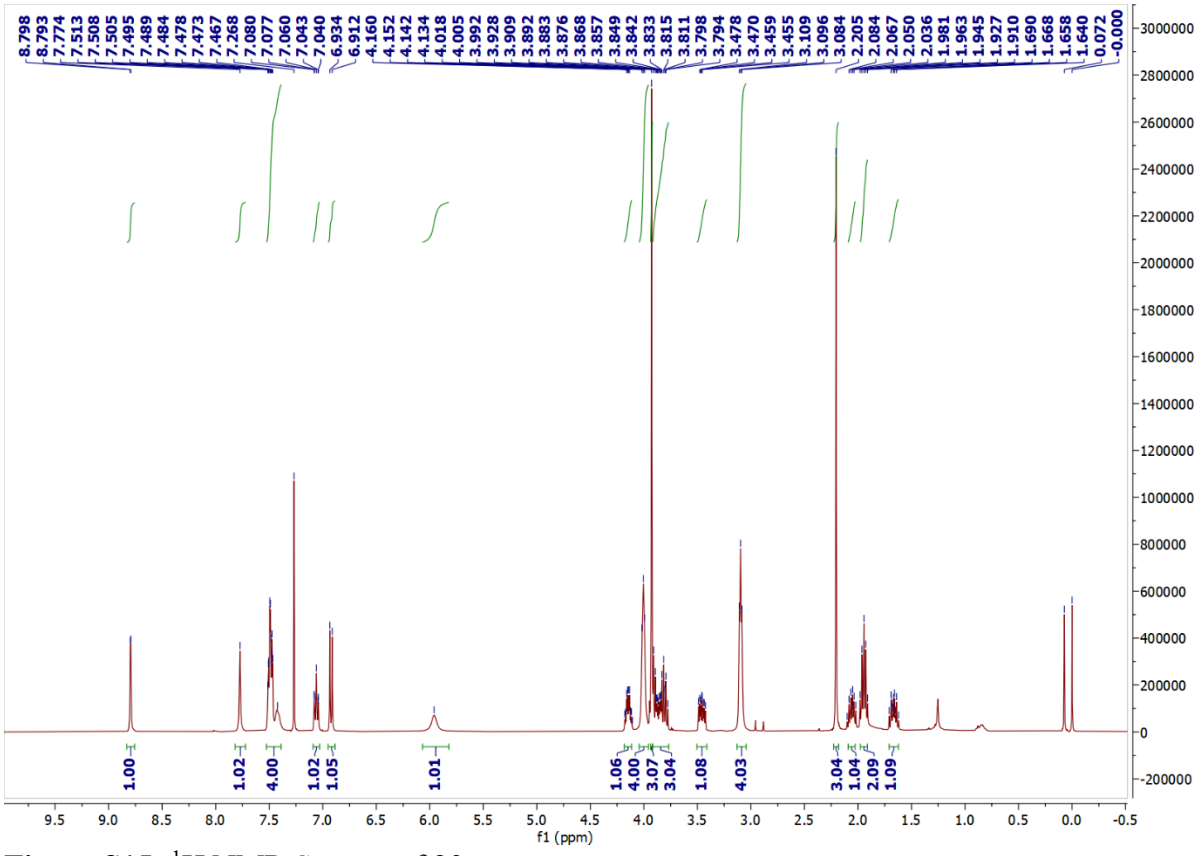

Figure S15: ^{1}H NMR Spectra of **20**.

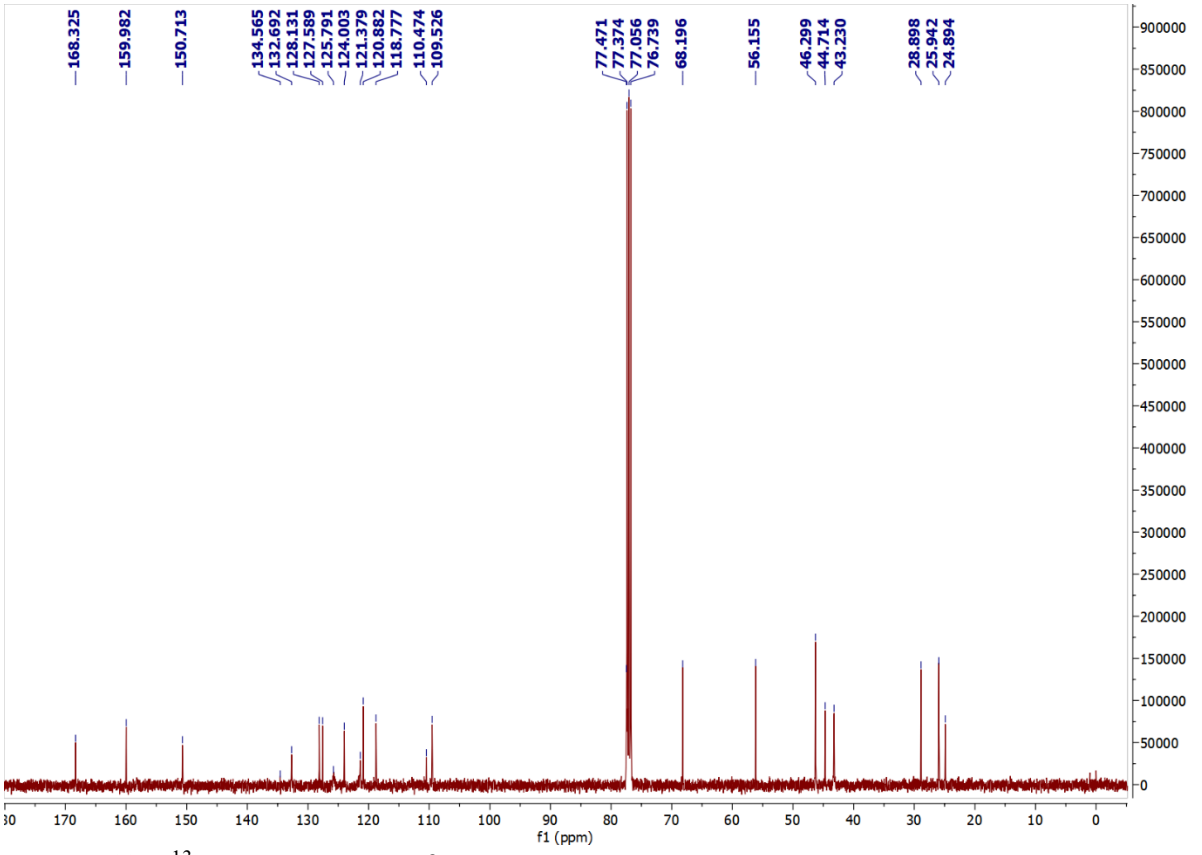

Figure S16: ^{13}C NMR Spectra of **20**.

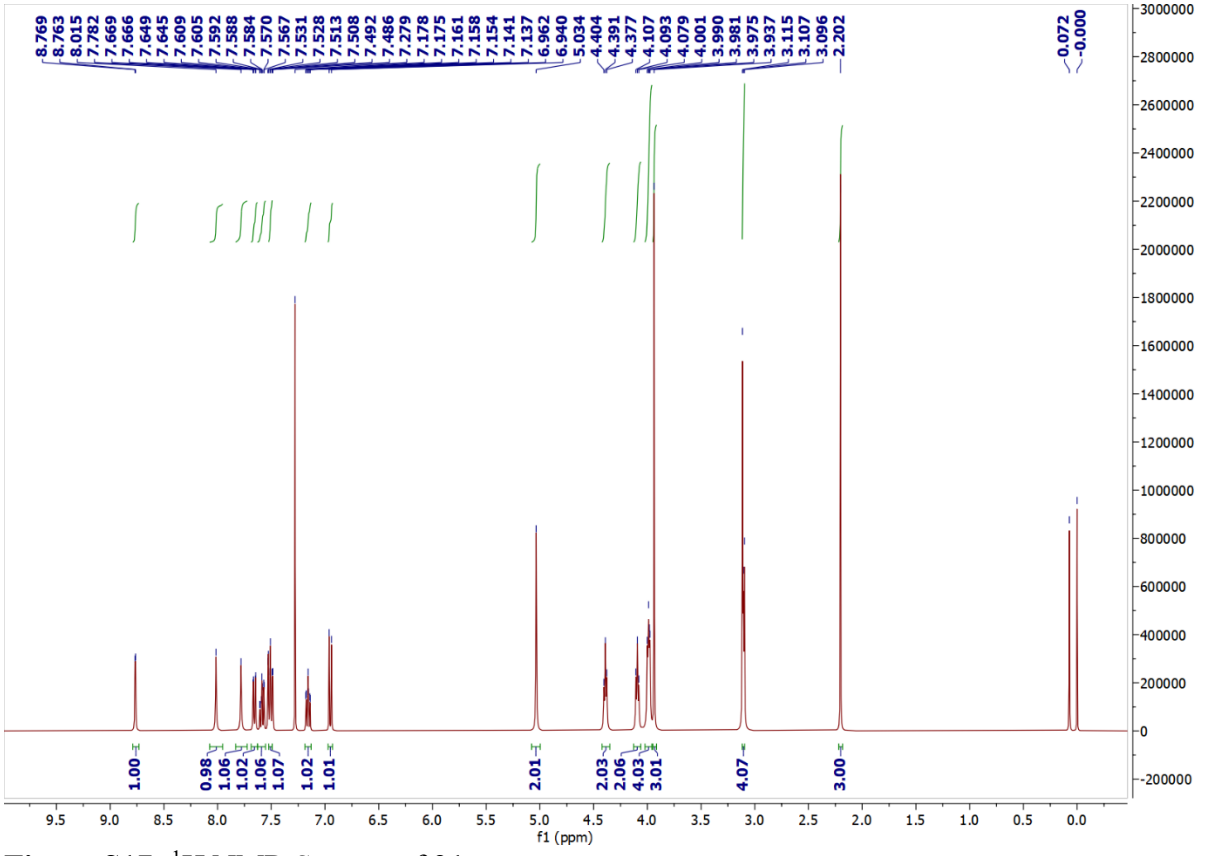

Figure S17: ^{1}H NMR Spectra of **21**.

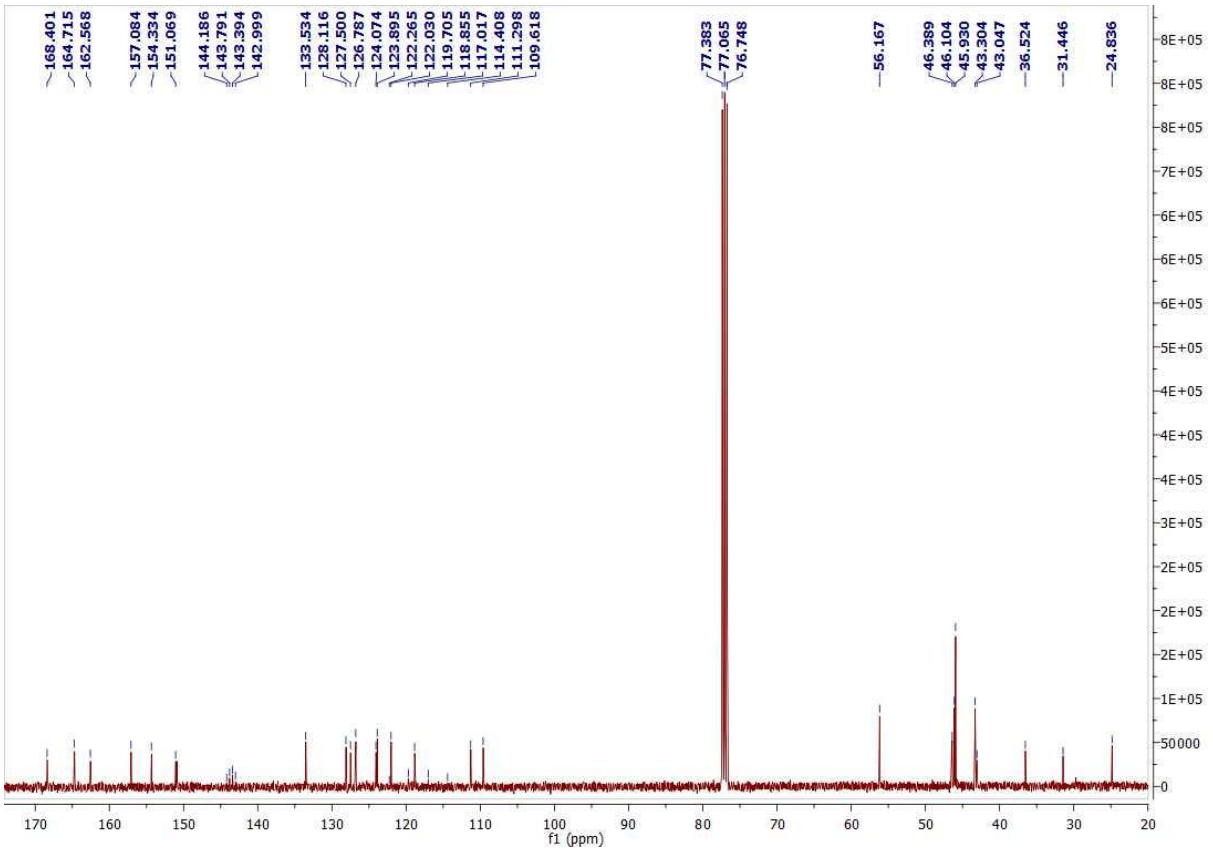

Figure S18: ^{13}C NMR Spectra of **21**.

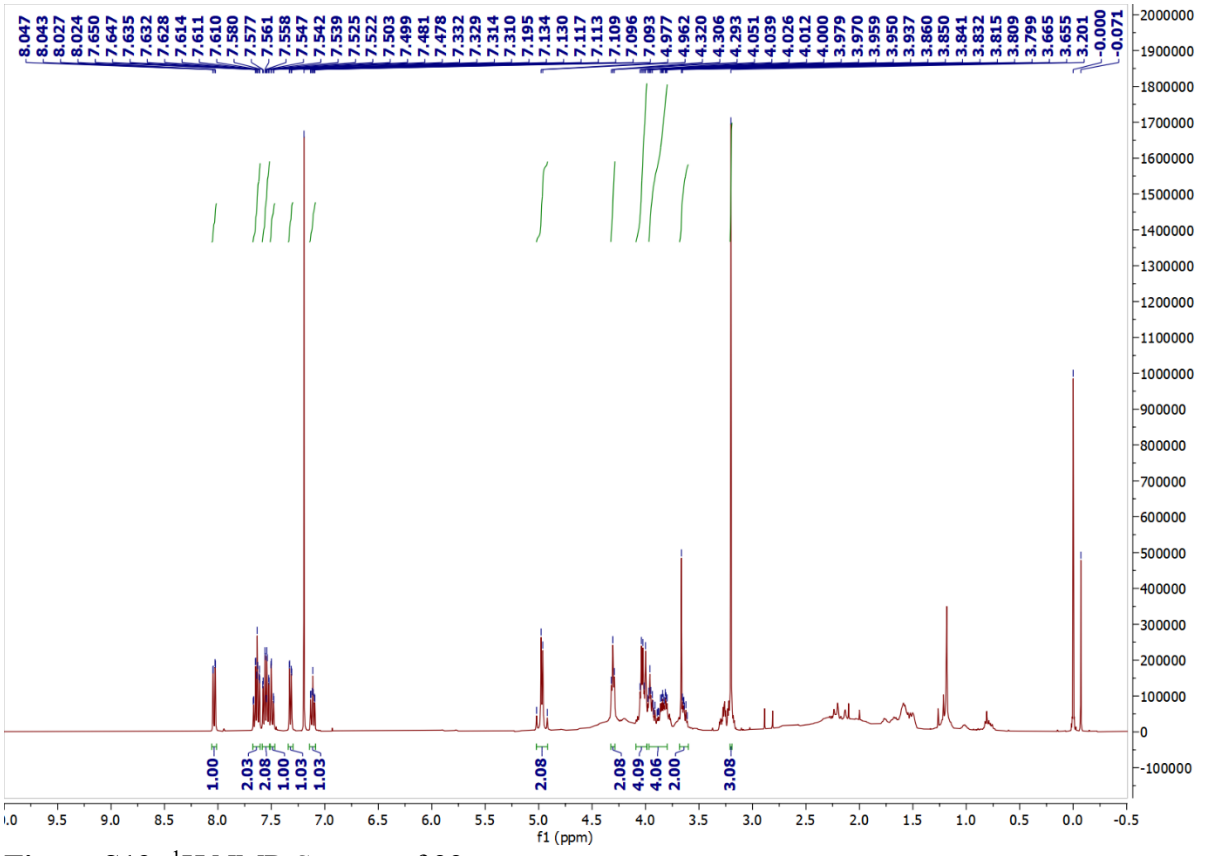

Figure S19: ^{1}H NMR Spectra of **22**.

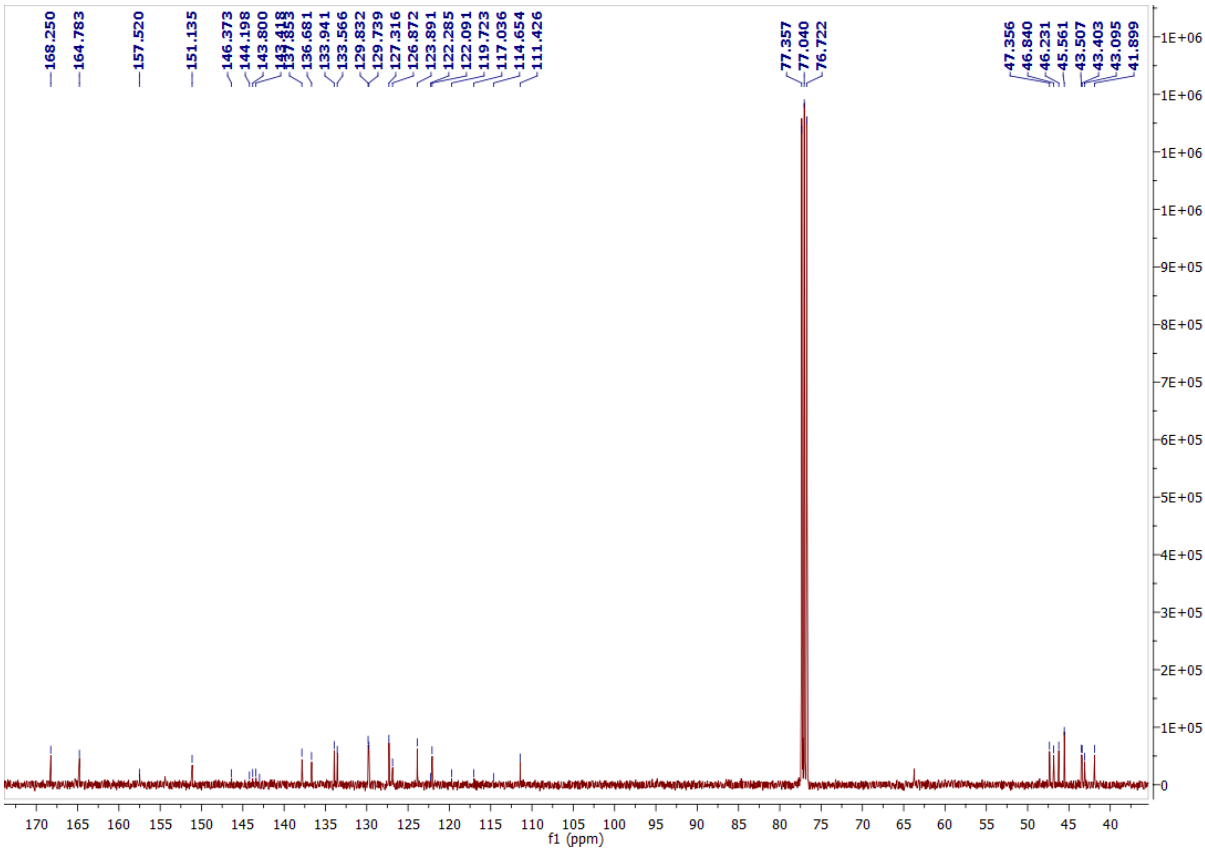

Figure S20: ^{13}C NMR Spectra of **22**.

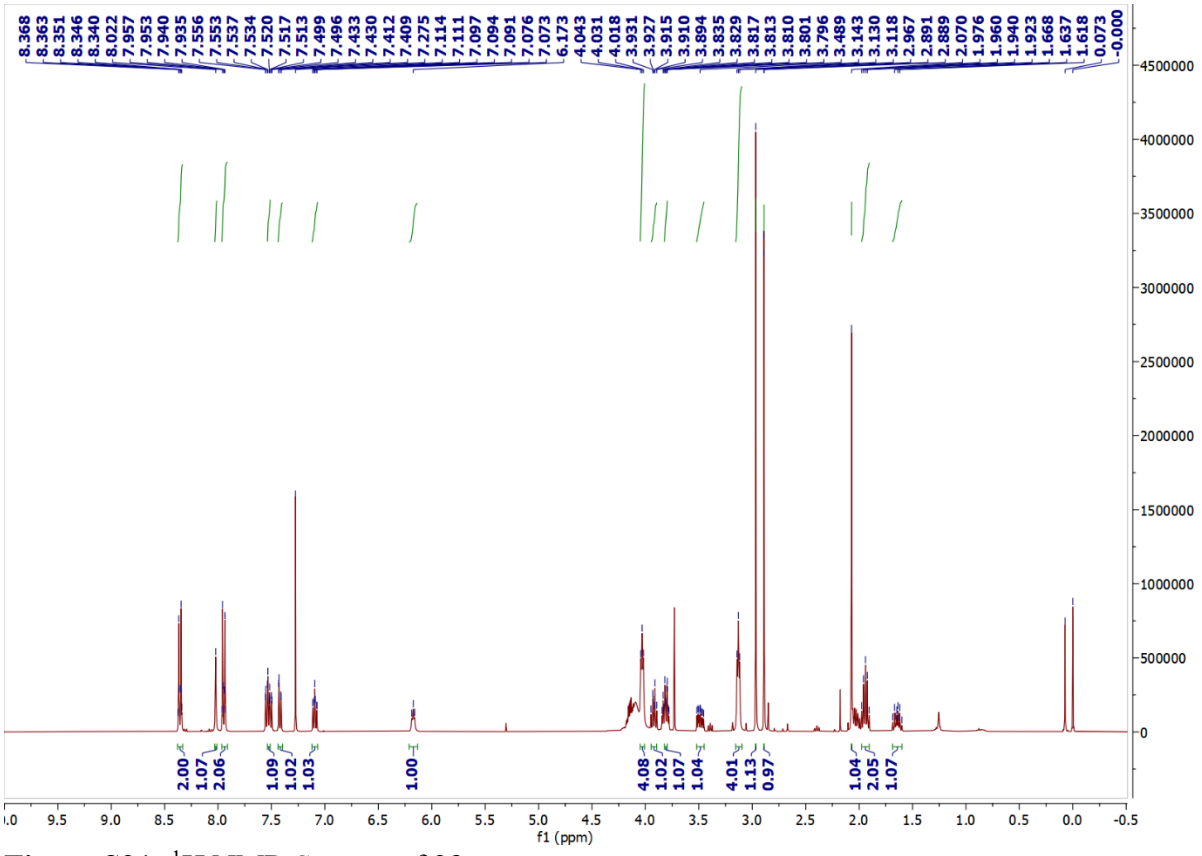

Figure S21: ^{1}H NMR Spectra of **23**.

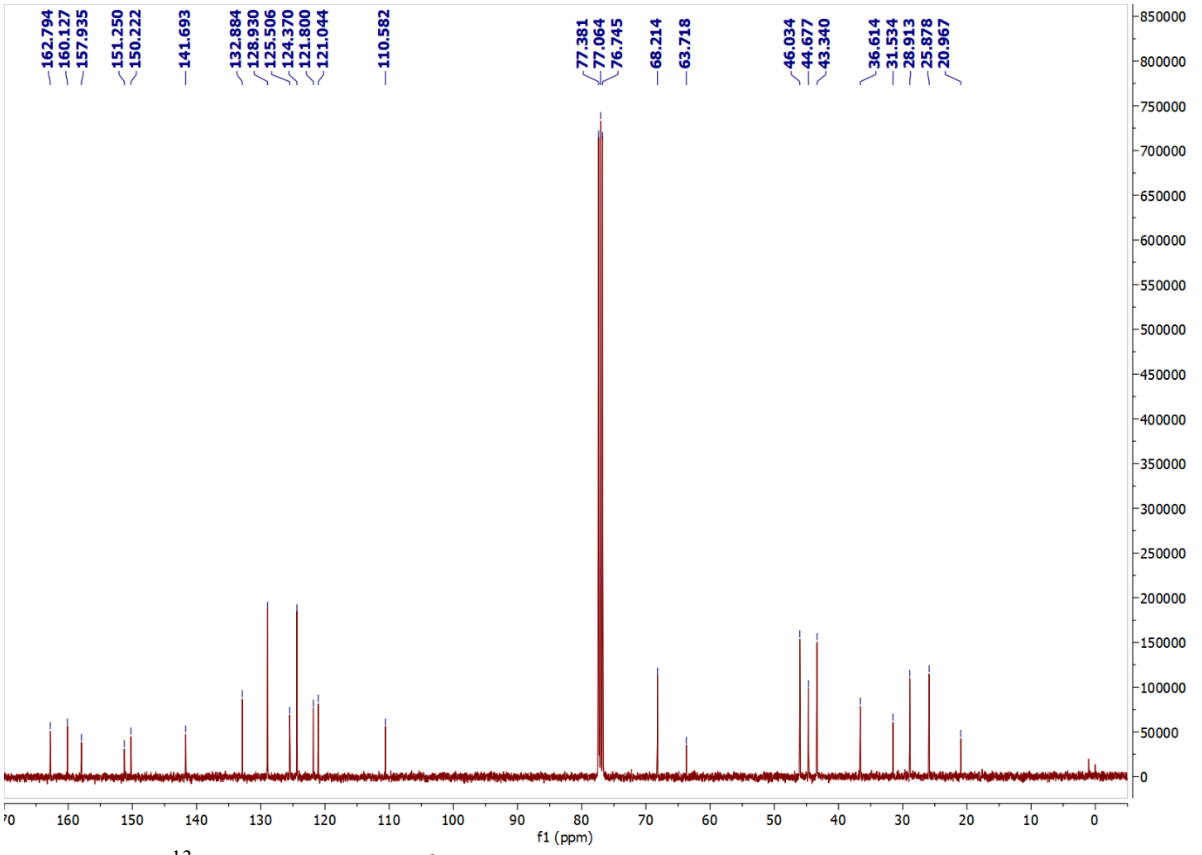

Figure S22: ^{13}C NMR Spectra of **23**.

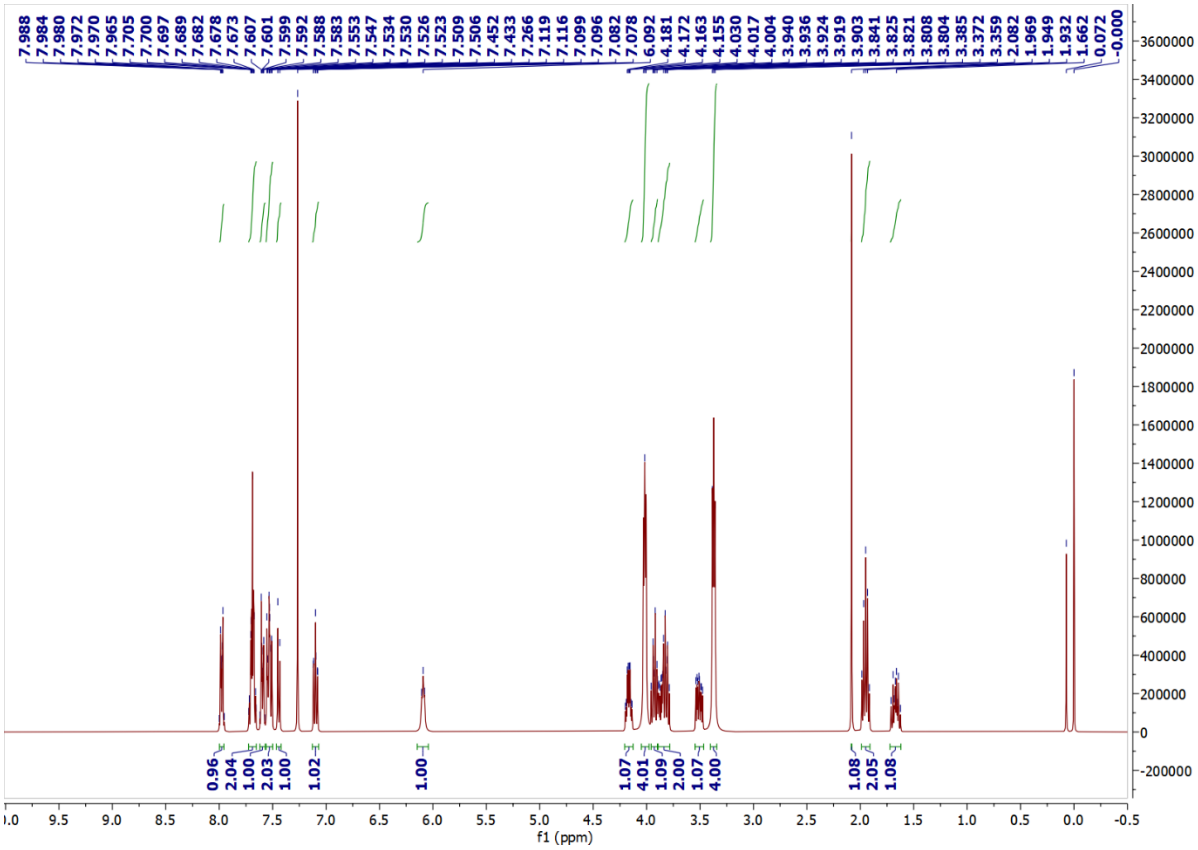

Figure S23: ^{1}H NMR Spectra of **24**.

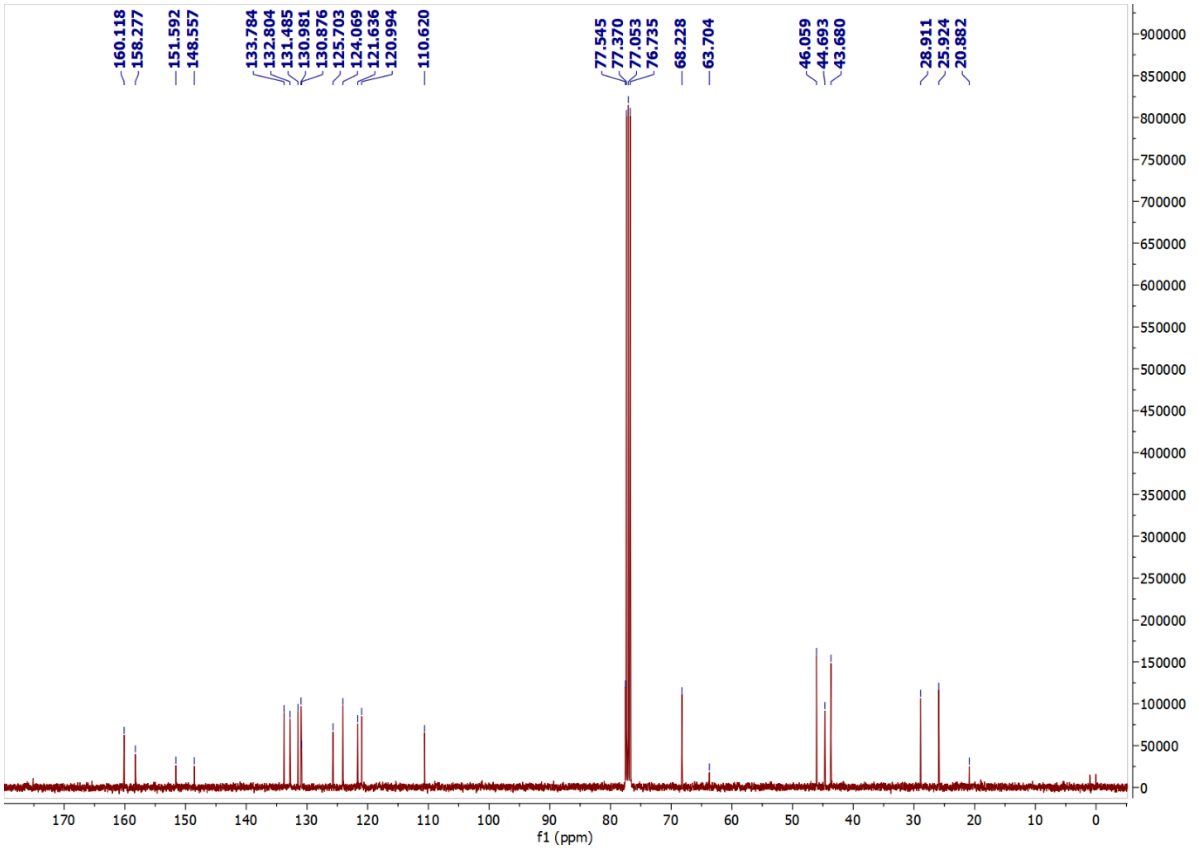

Figure S24: ^{13}C NMR Spectra of **24**.

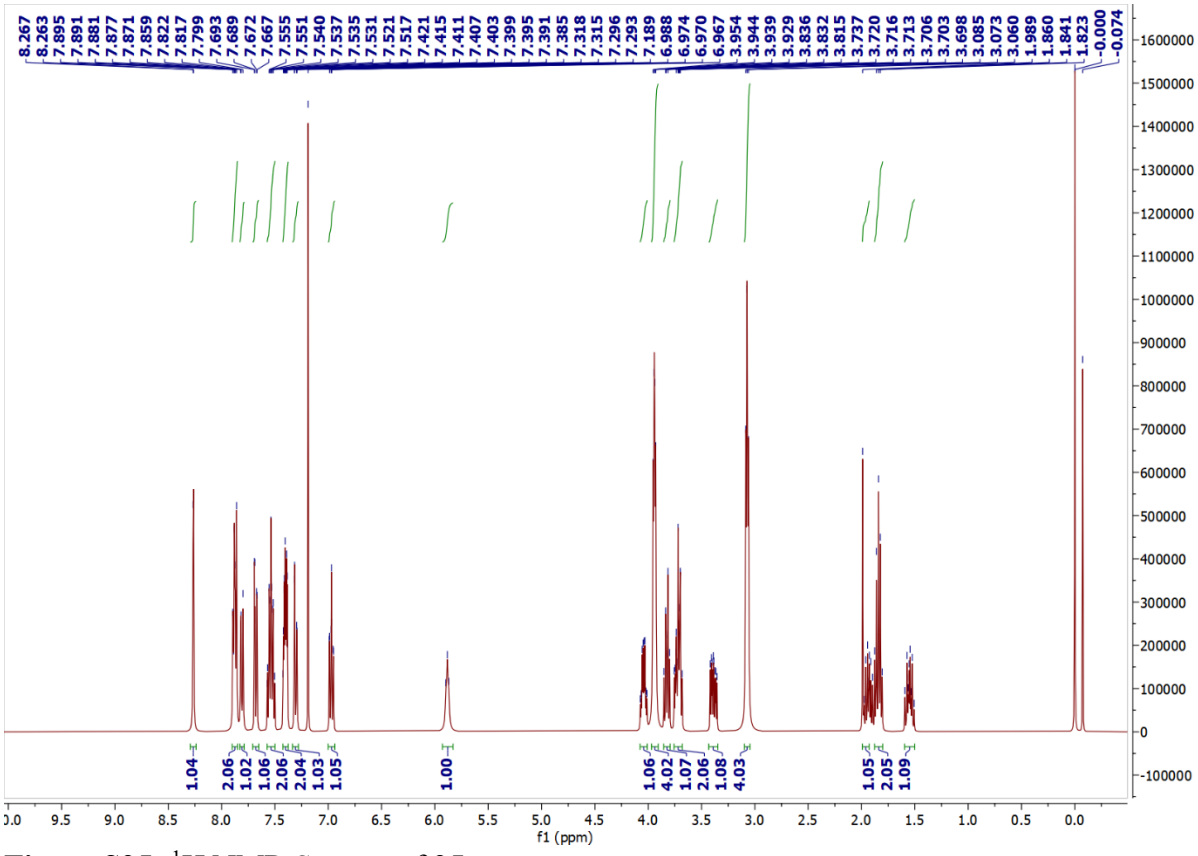

Figure S25: ^{1}H NMR Spectra of **25**.

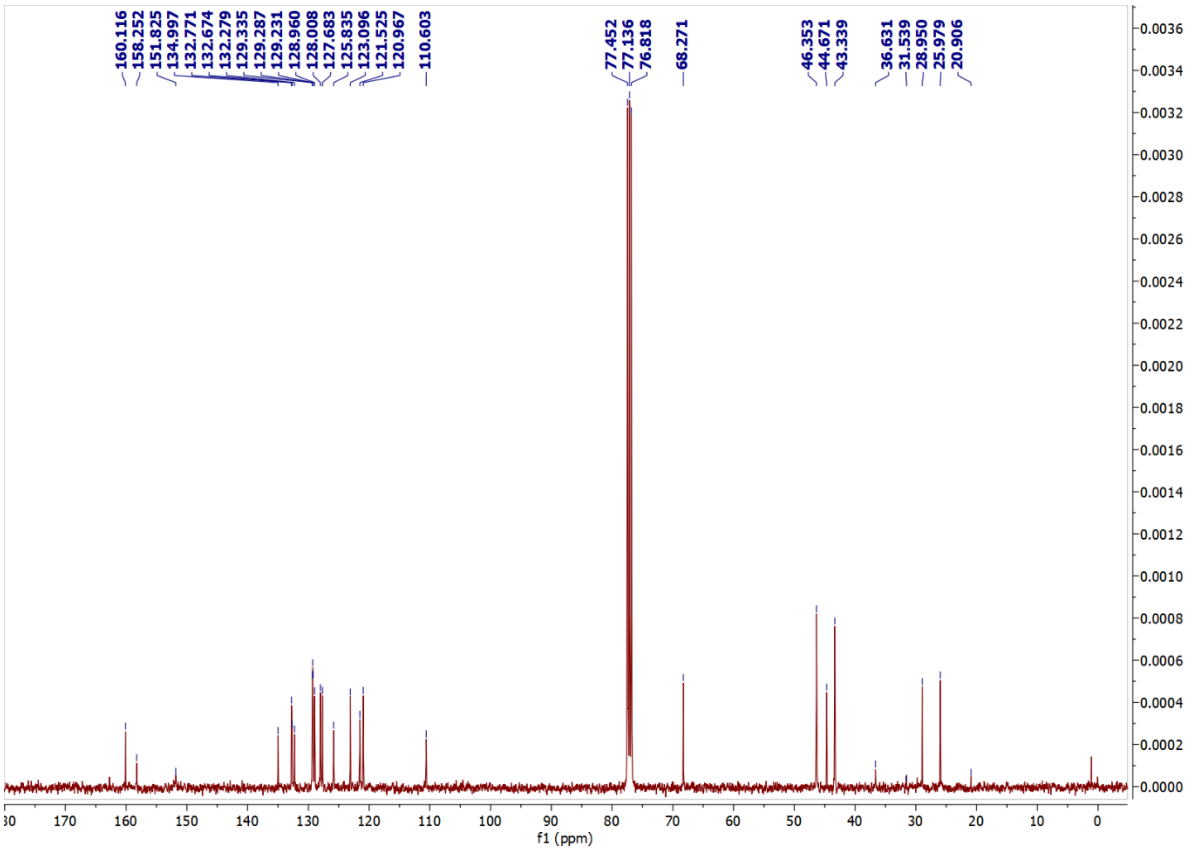

Figure S26: ^{13}C NMR Spectra of **25**.

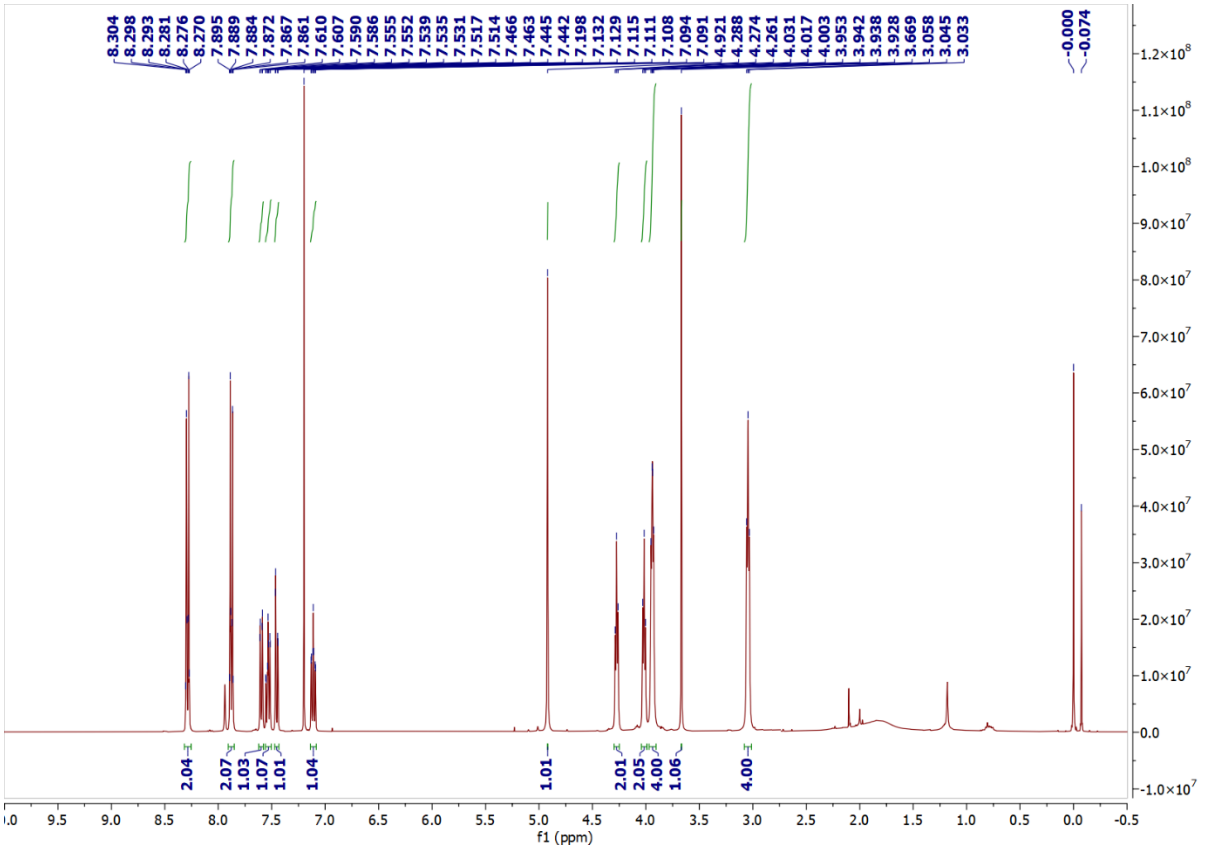

Figure S27: ^{1}H NMR Spectra of **26**.

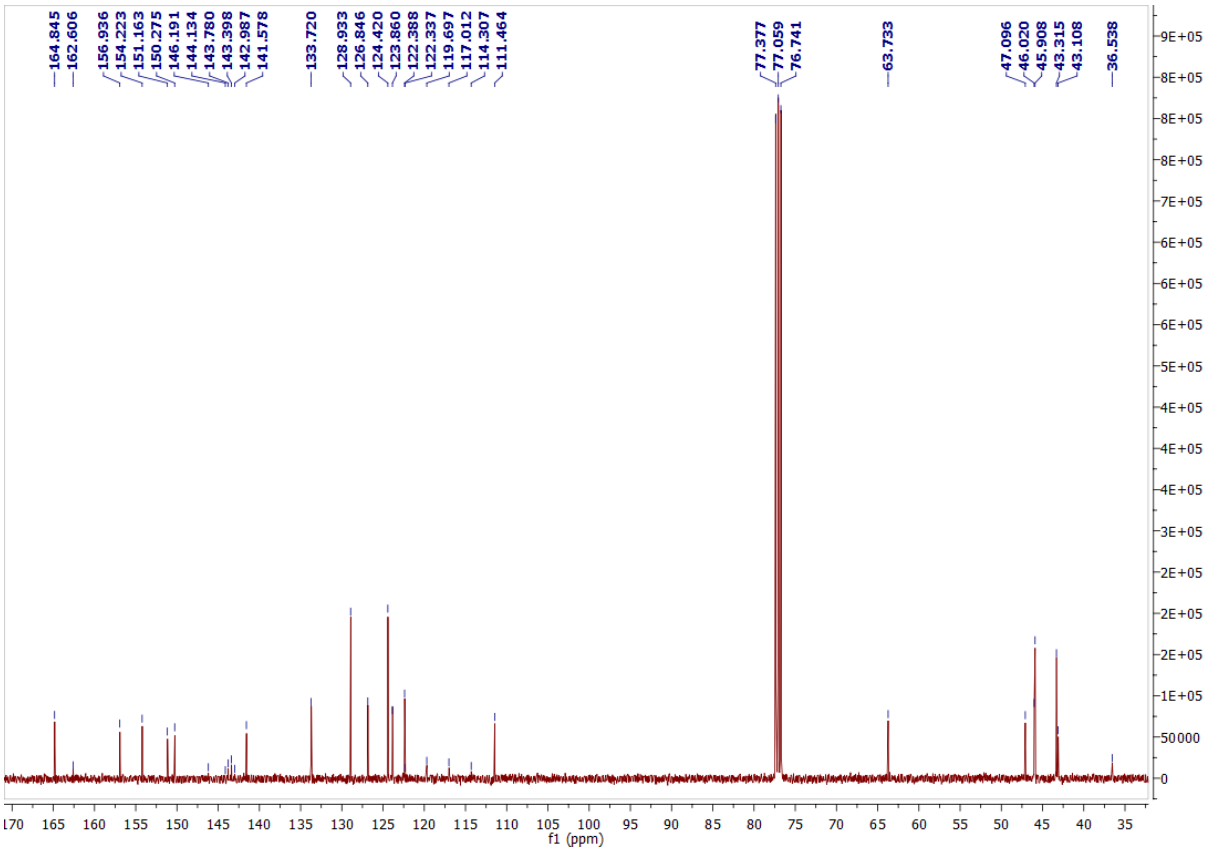

Figure S28: ^{13}C NMR Spectra of **26**.

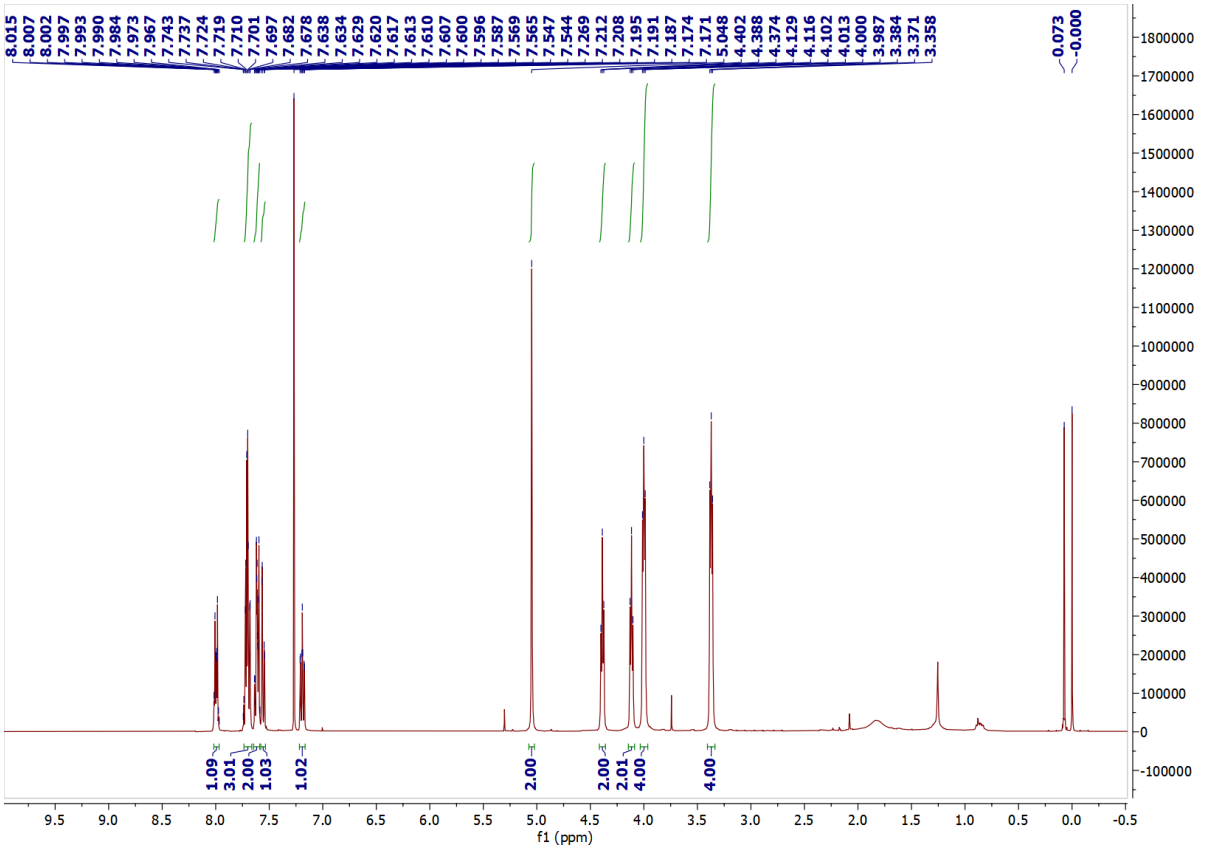

Figure S29: ^{1}H NMR Spectra of **27**.

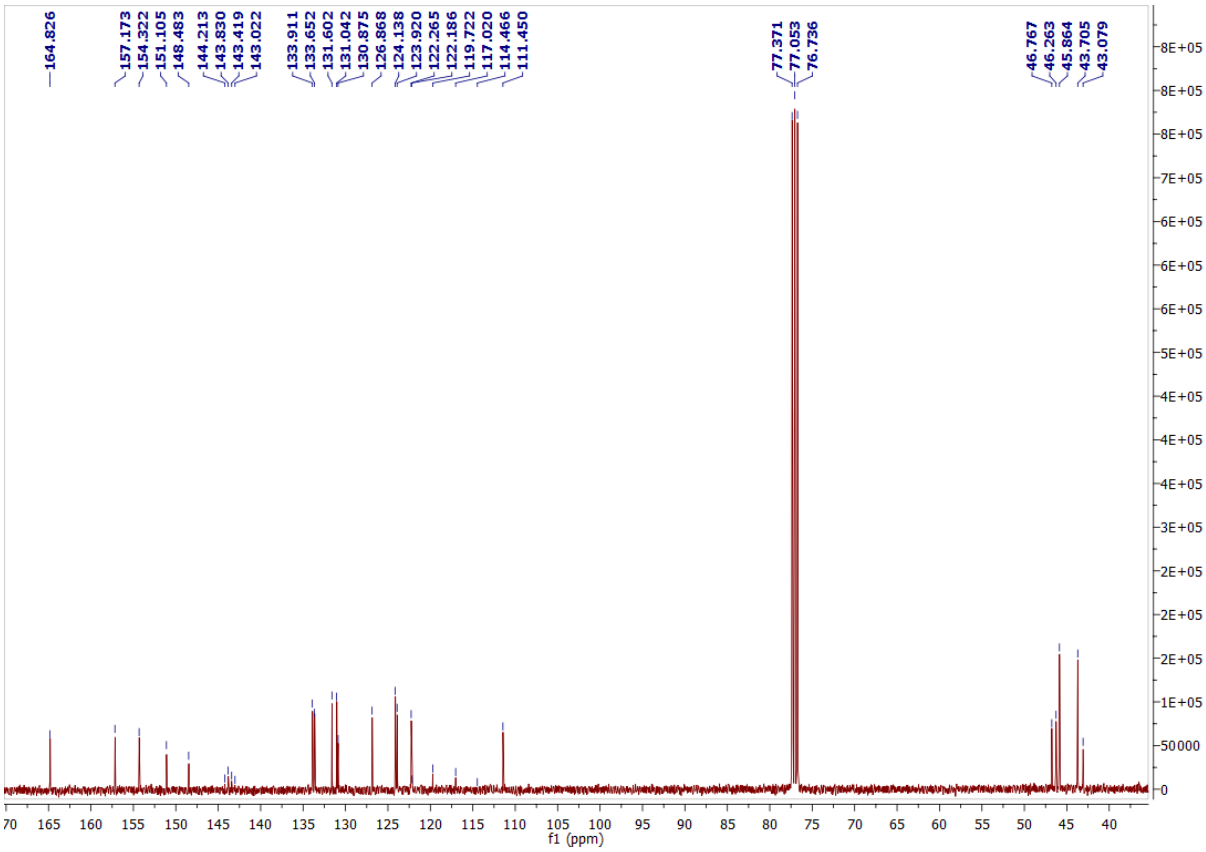

Figure S30: ^{13}C NMR Spectra of **27**.

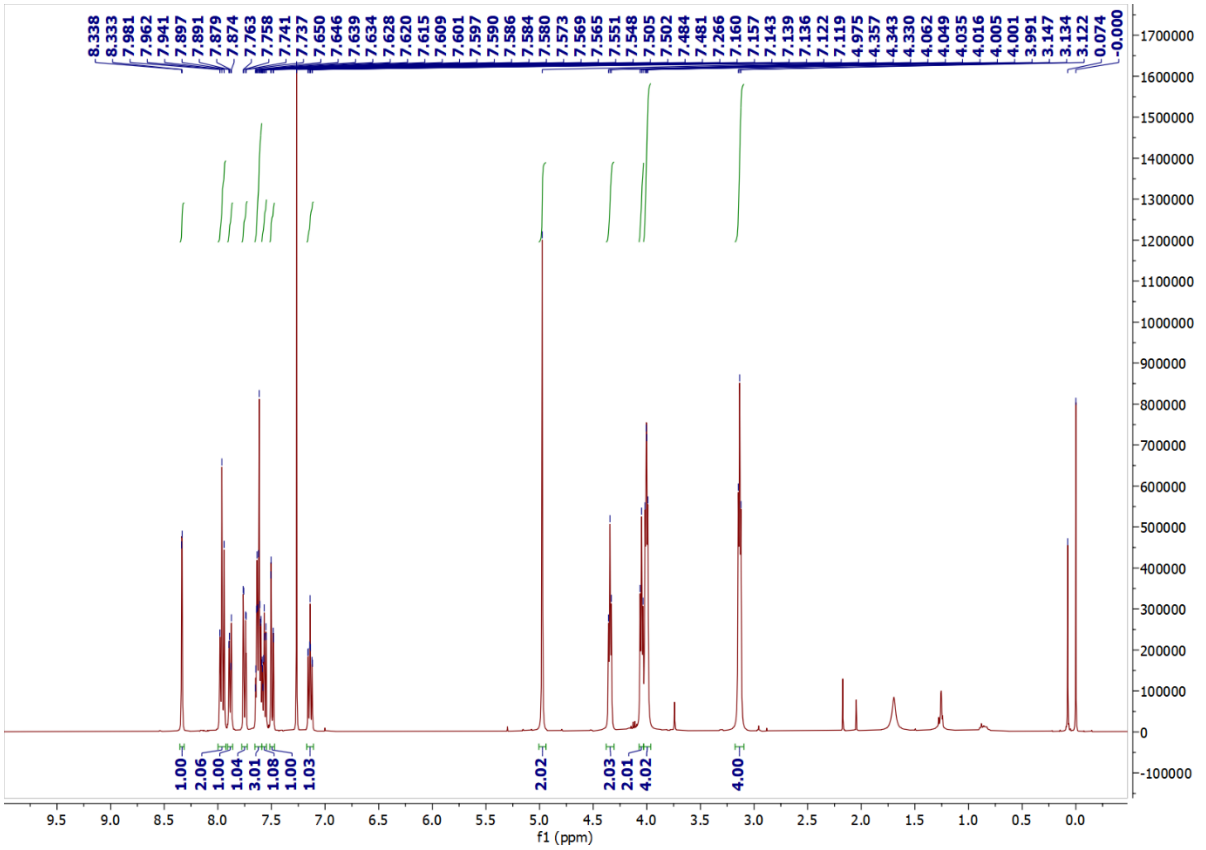

Figure S31: ^{1}H NMR Spectra of **28**.

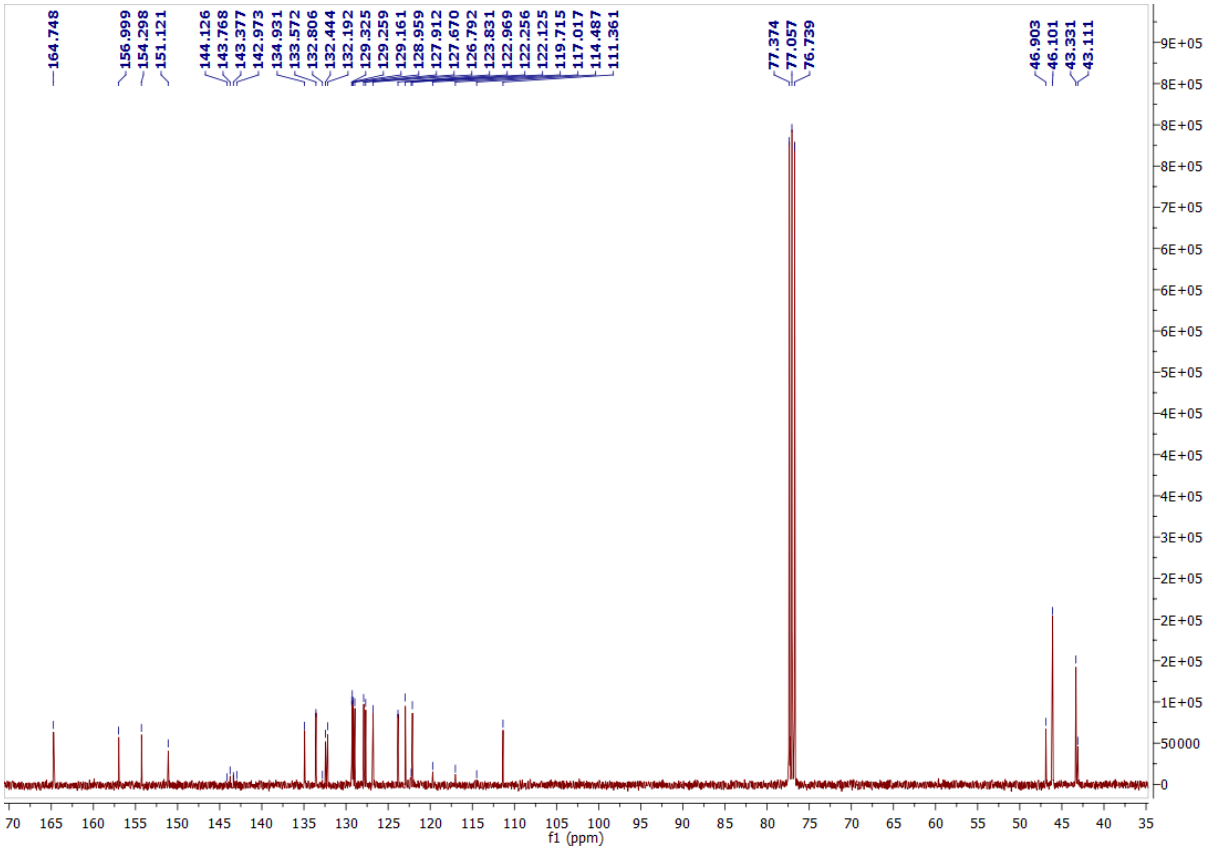

Figure S32: ^{13}C NMR Spectra of **28**.

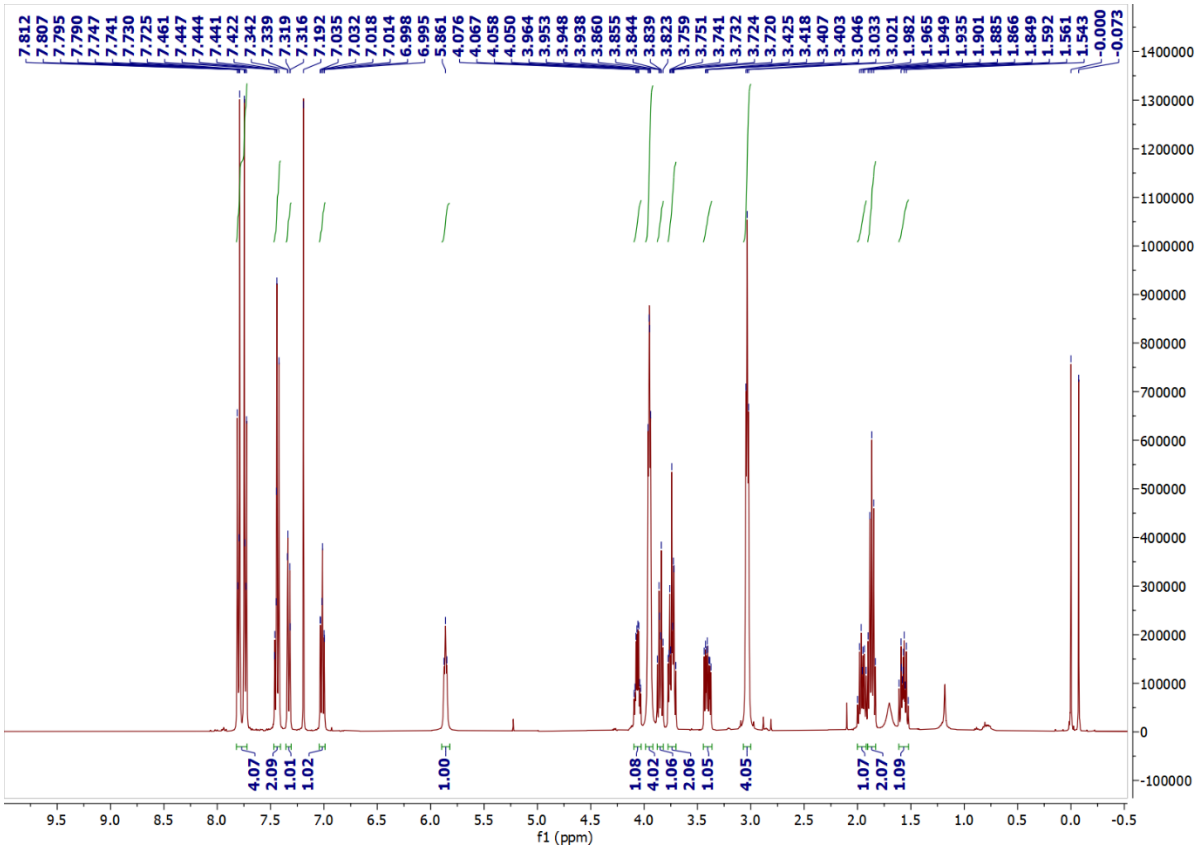

Figure S33: ^{1}H NMR Spectra of **29**.

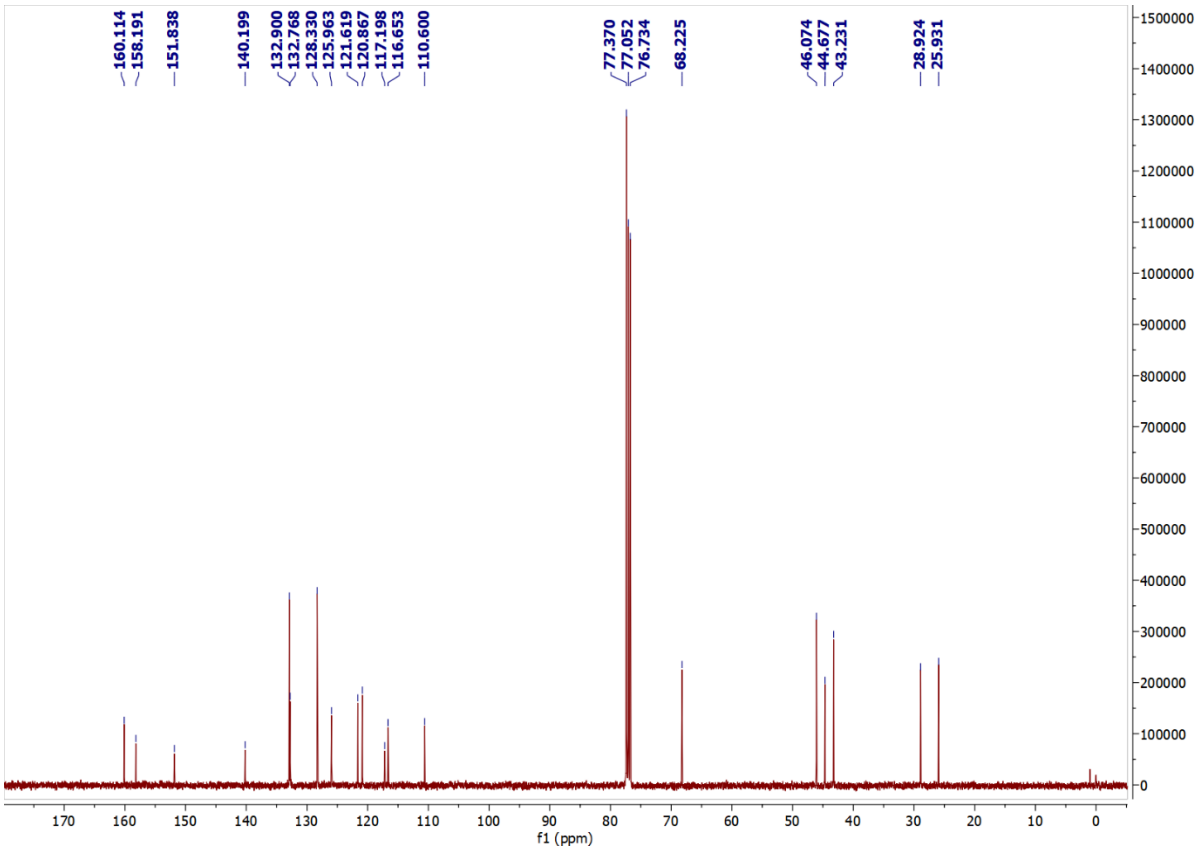

Figure S34: ^{13}C NMR Spectra of **29**.

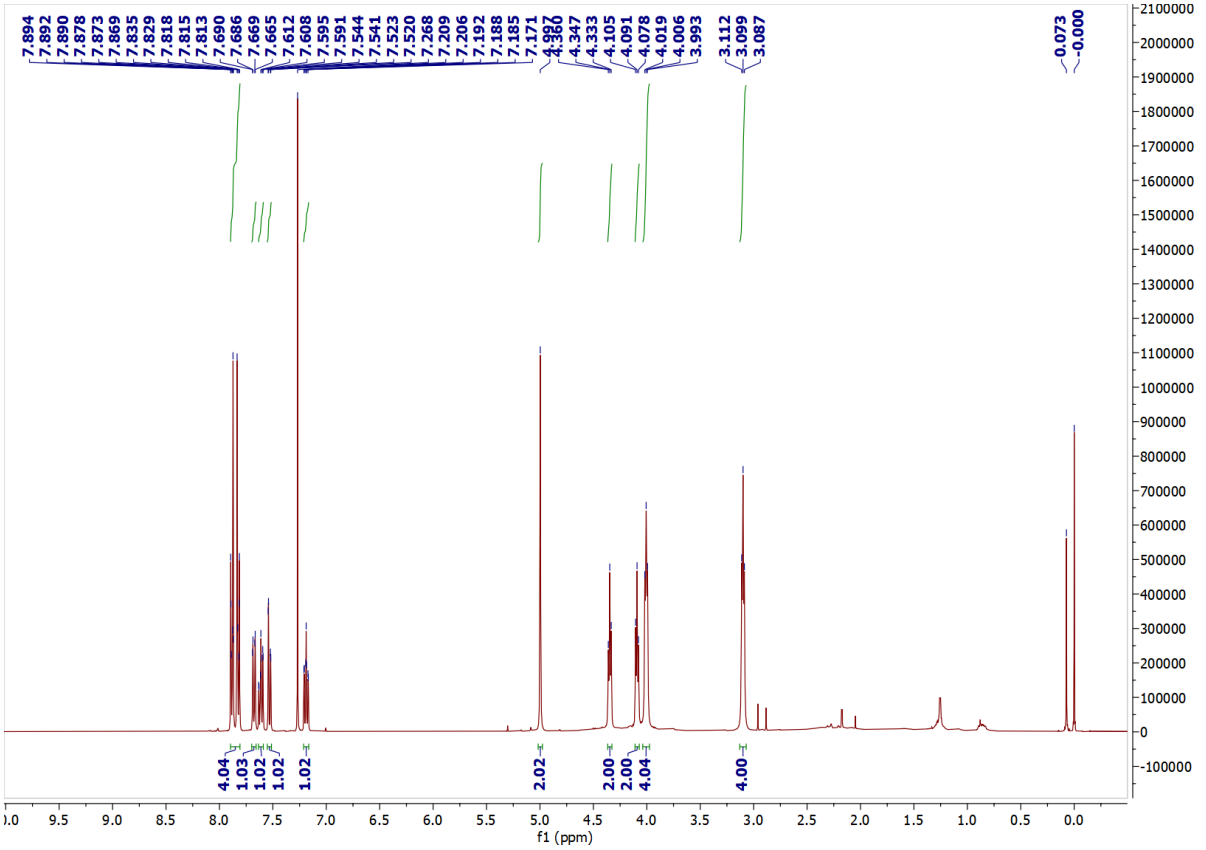

Figure S35: ^{1}H NMR Spectra of **30**.

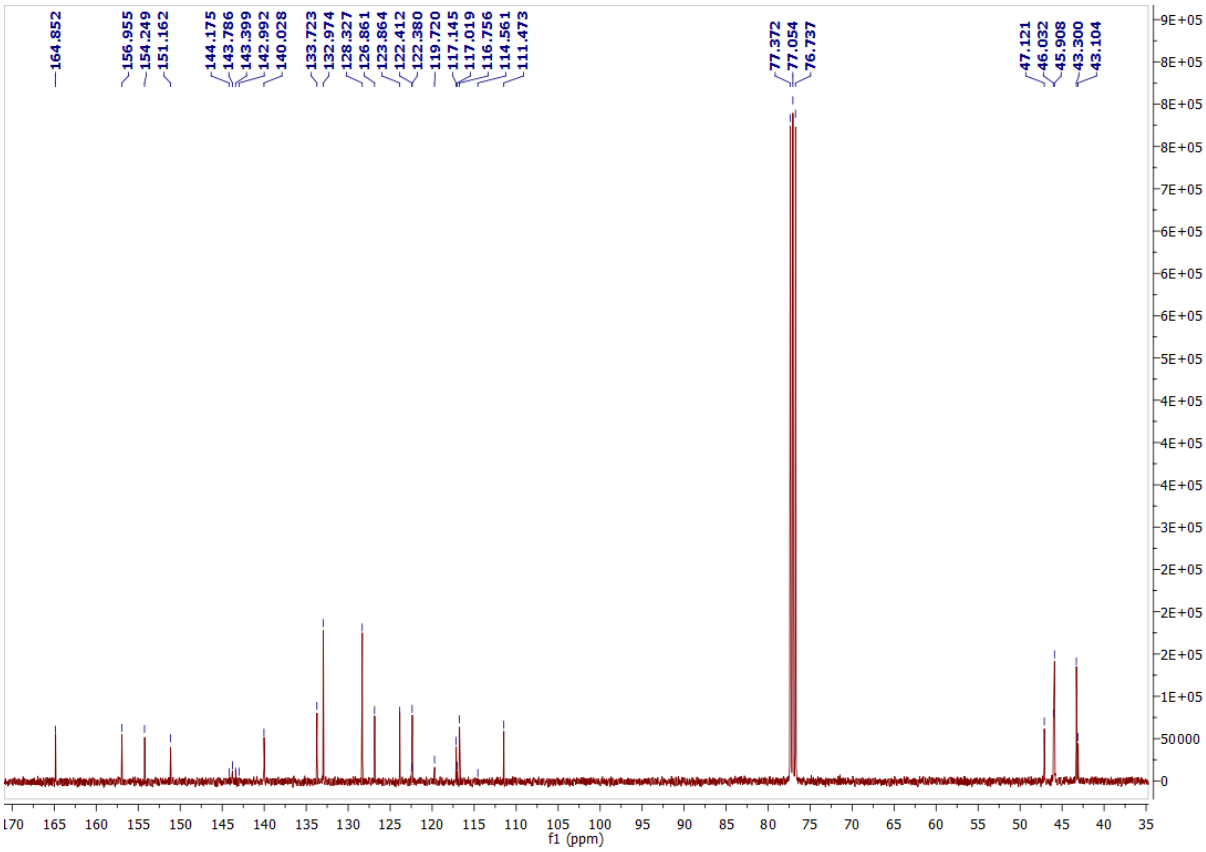

Figure S36: ^{13}C NMR Spectra of **30**.

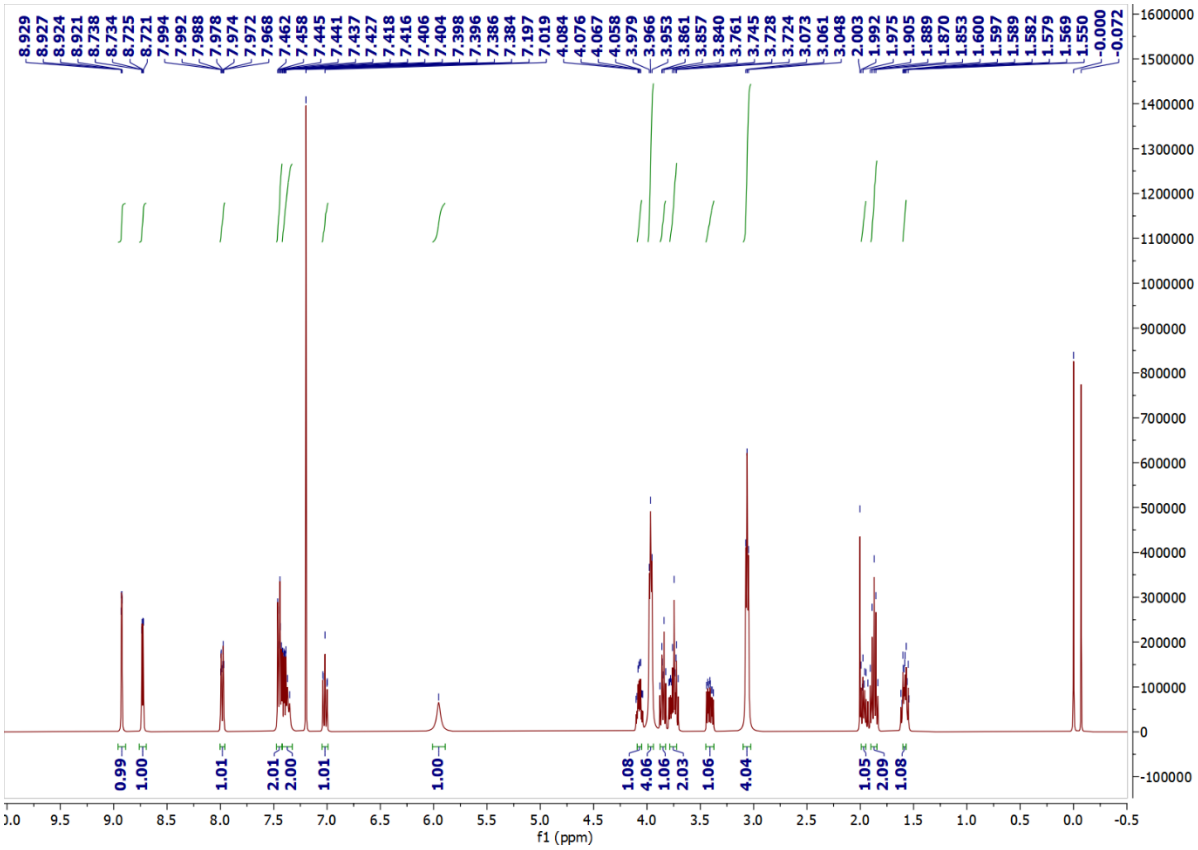

Figure S37: ^{1}H NMR Spectra of **31**.

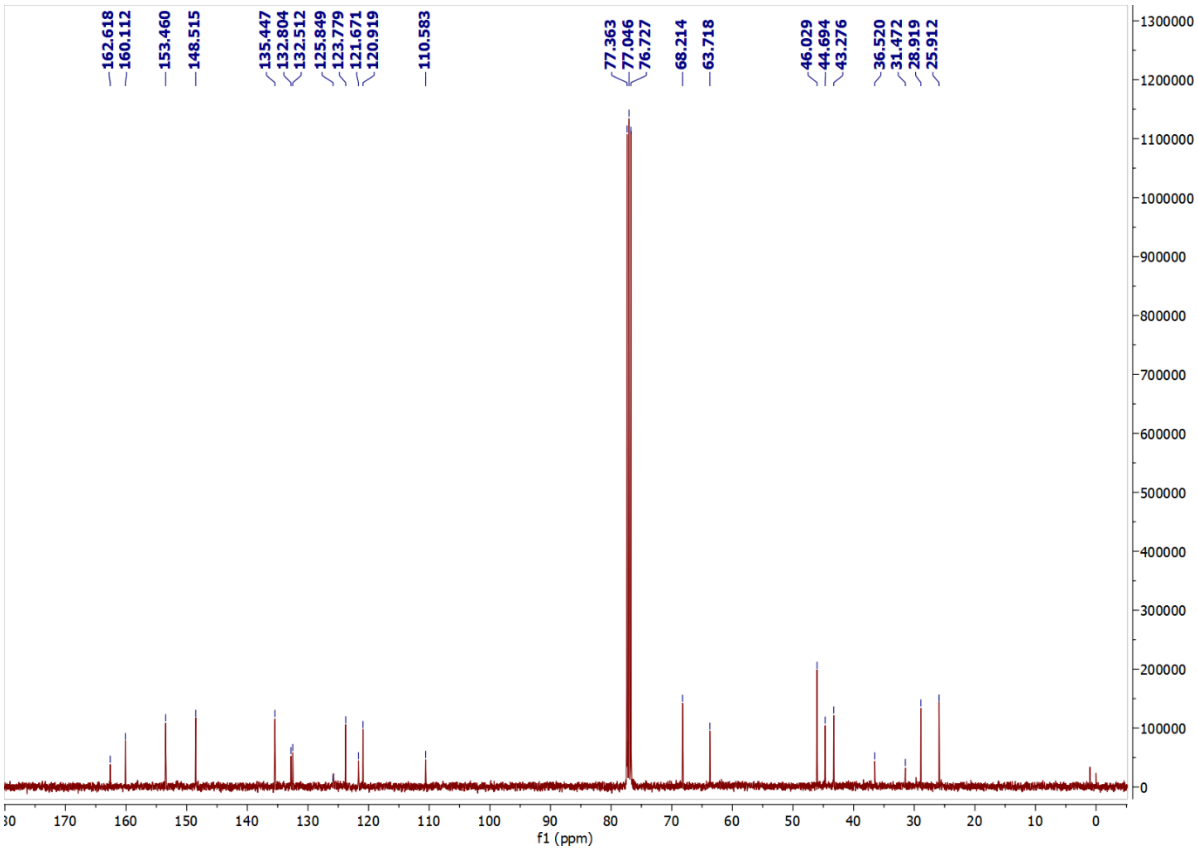

Figure S38: ^{13}C NMR Spectra of **31**.

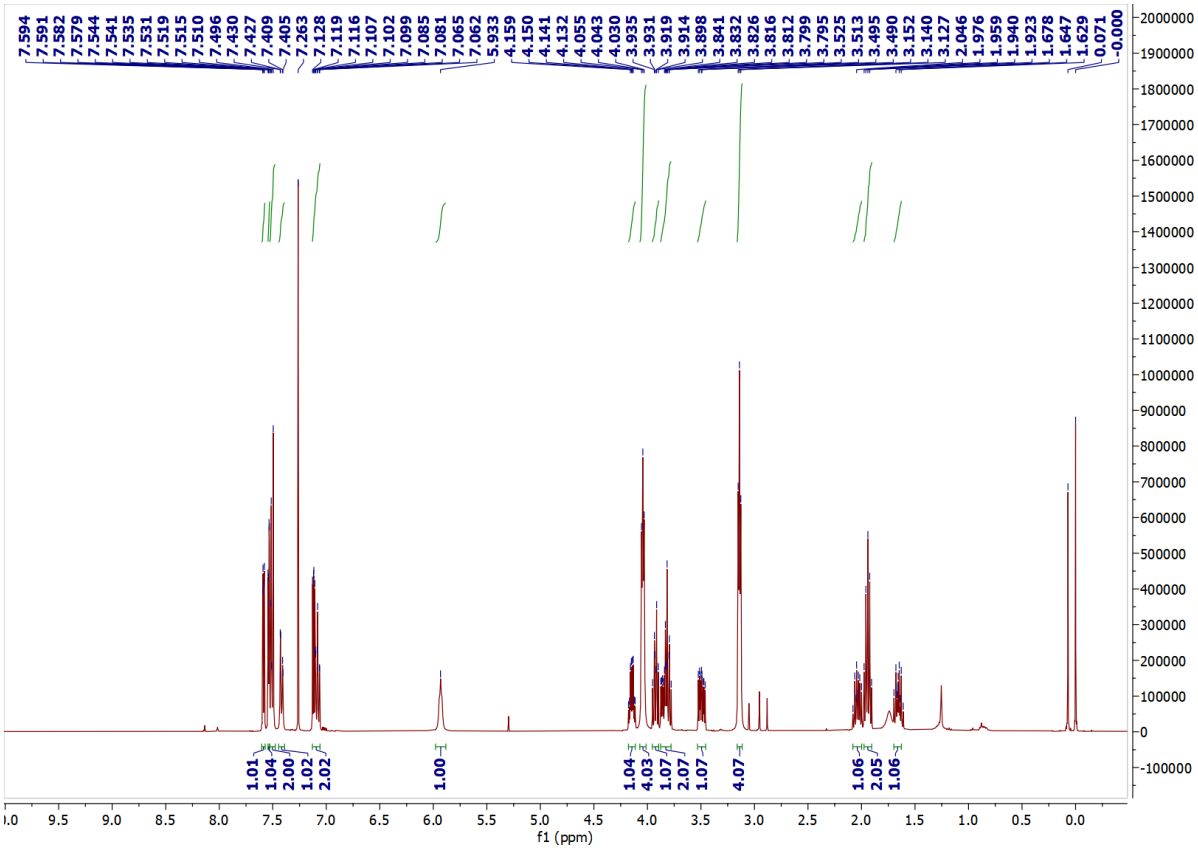

Figure S39: ^{1}H NMR Spectra of **32**.

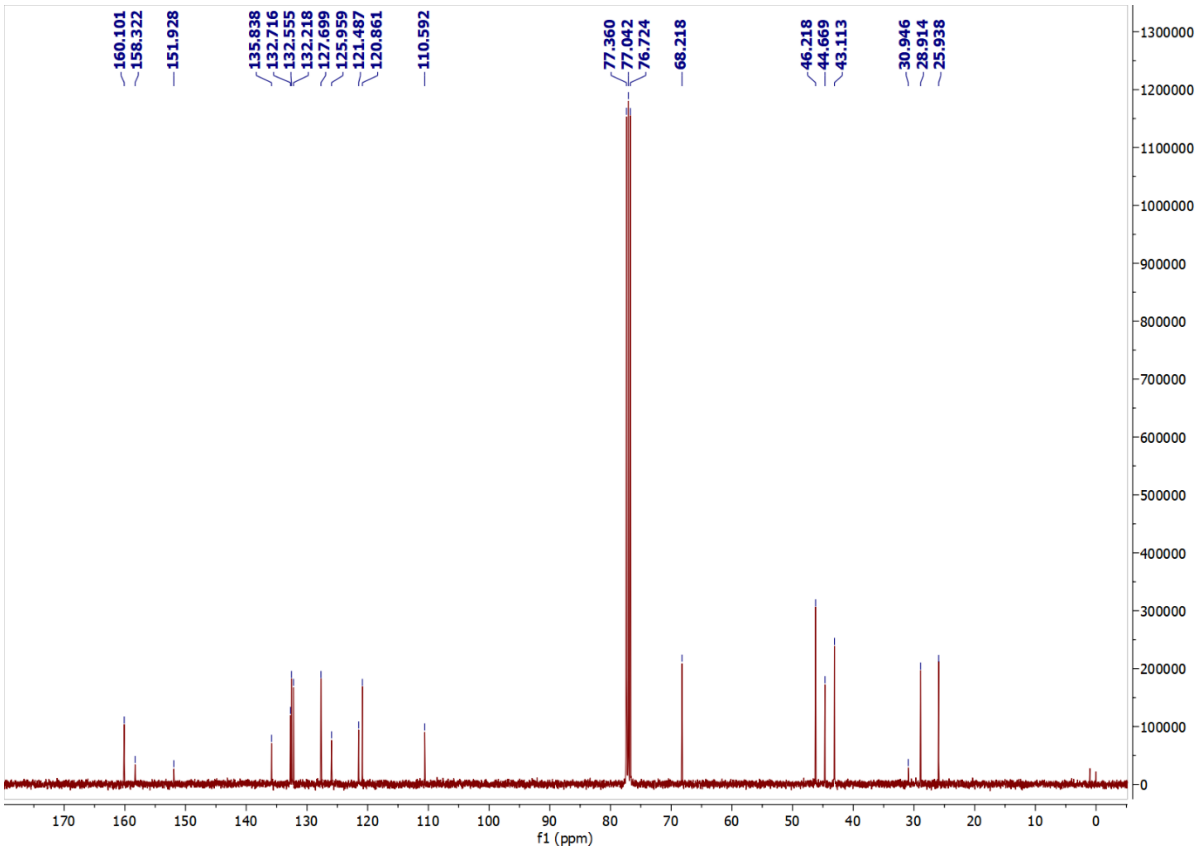

Figure S40: ^{13}C NMR Spectra of **32**.

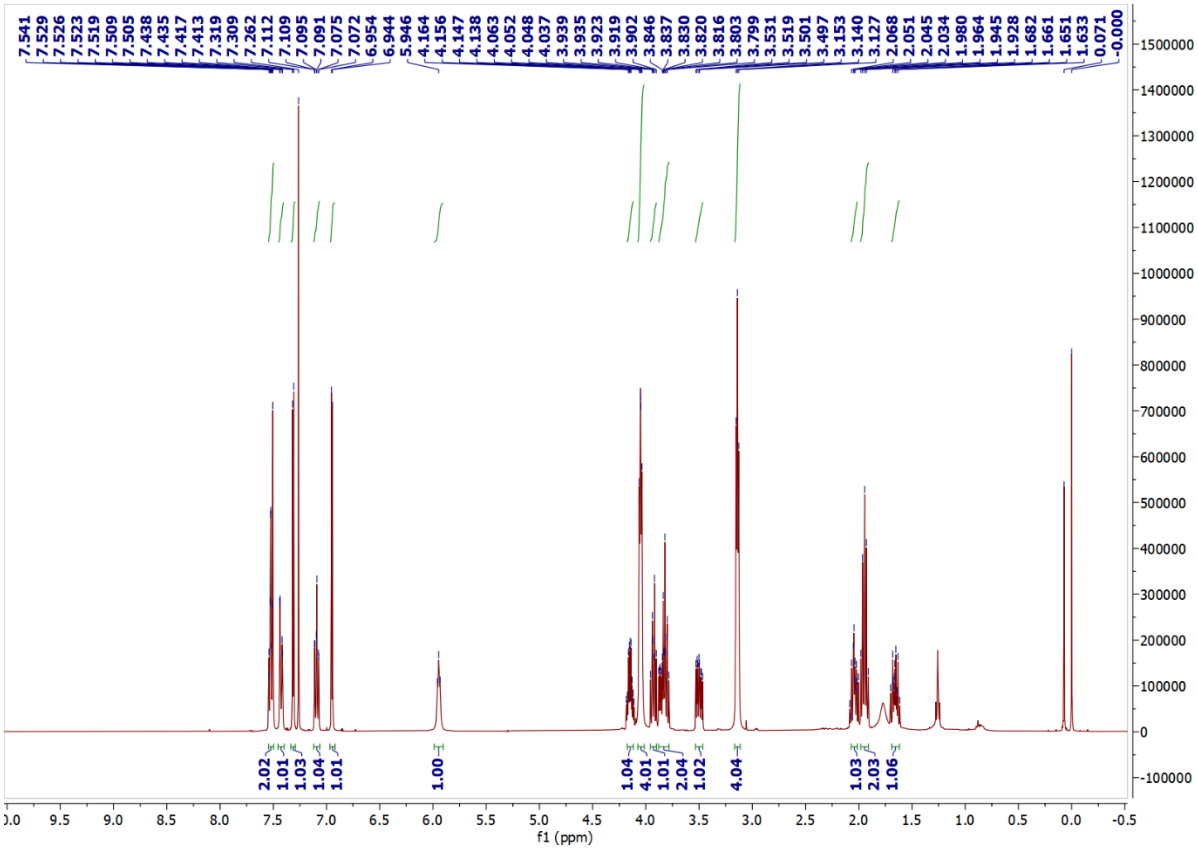

Figure S41: ^{1}H NMR Spectra of **33**.

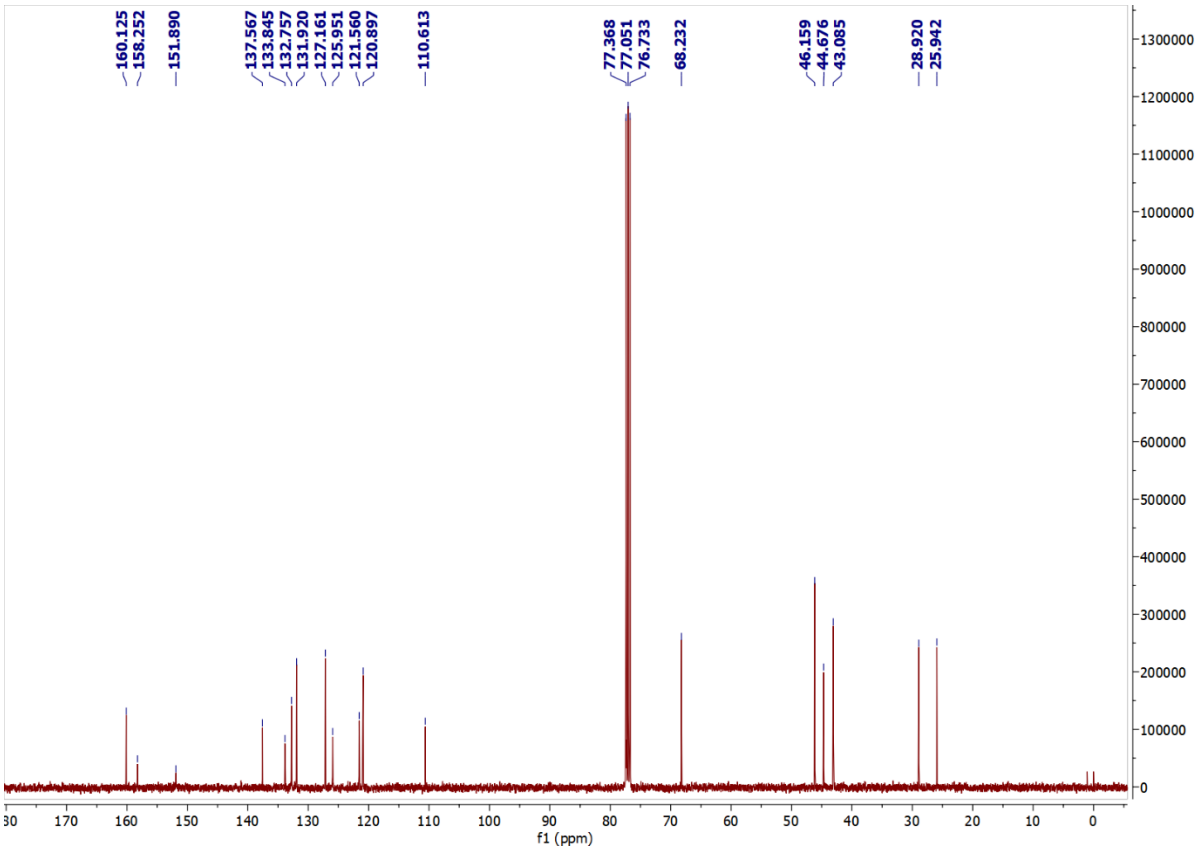

Figure S42: ^{13}C NMR Spectra of **33**.

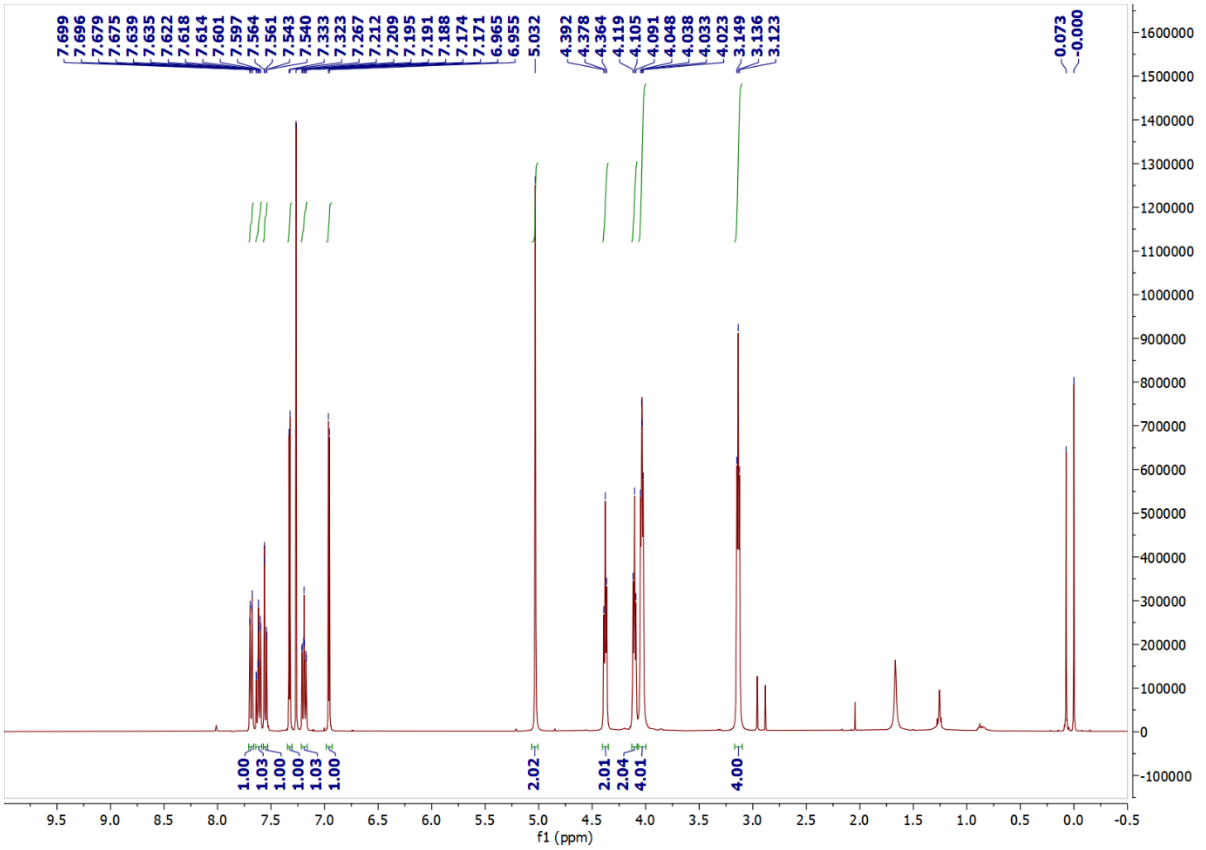

Figure S43: ^{1}H NMR Spectra of **34**.

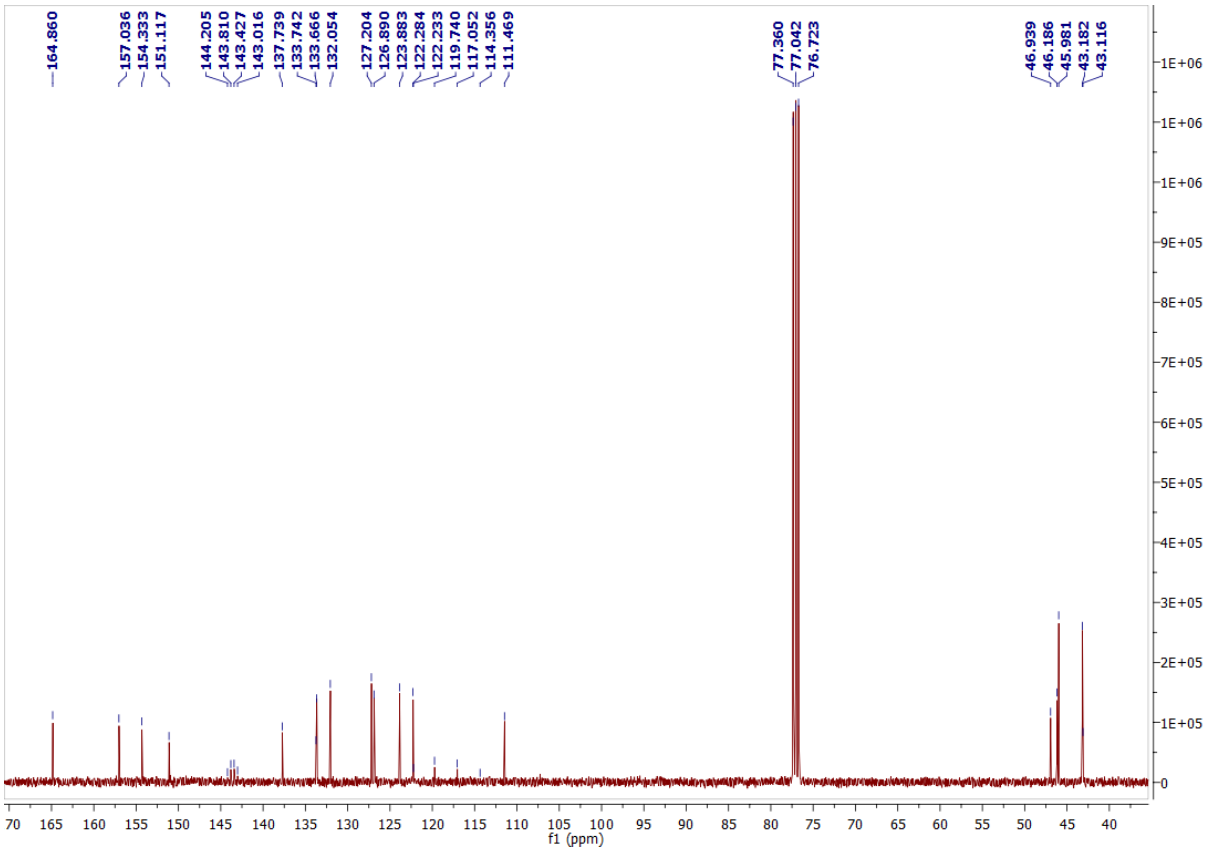

Figure S44: ^{13}C NMR Spectra of **34**.

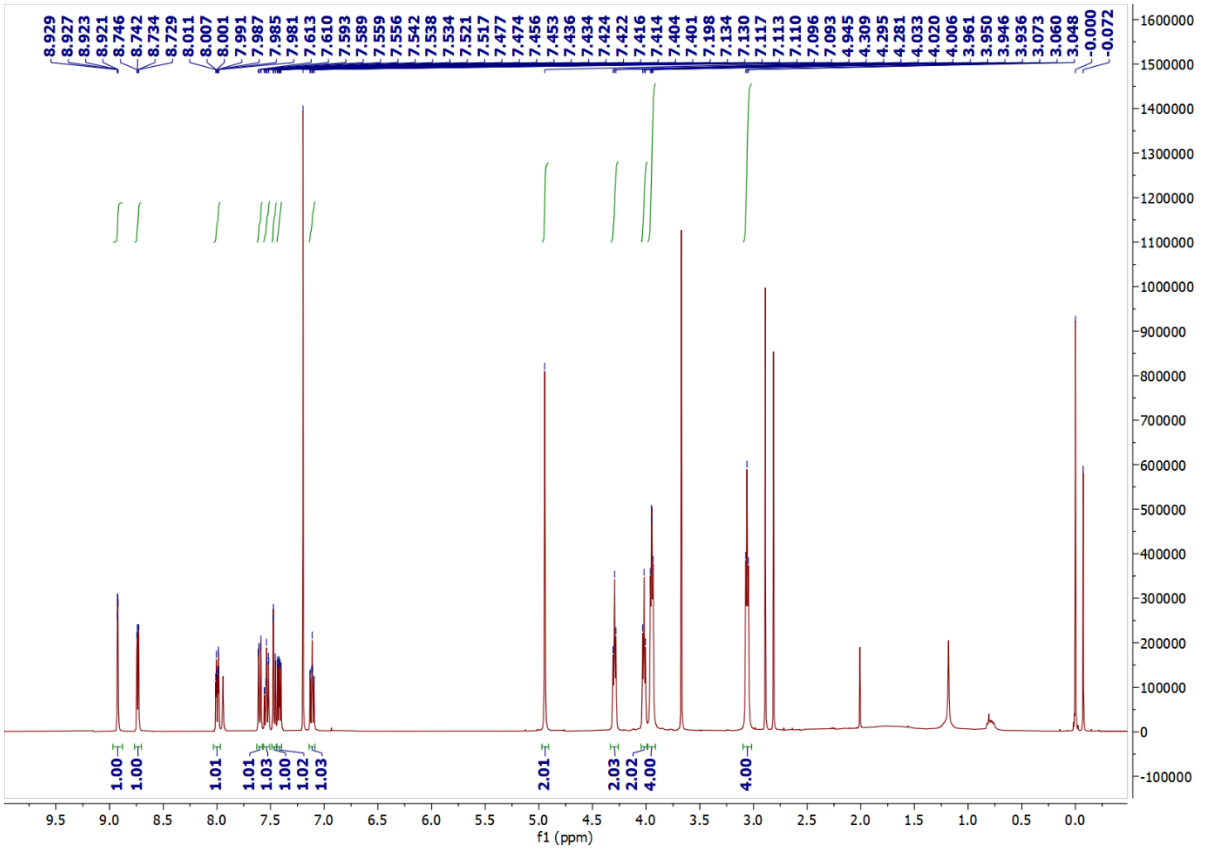

Figure S45: ^{1}H NMR Spectra of **35**.

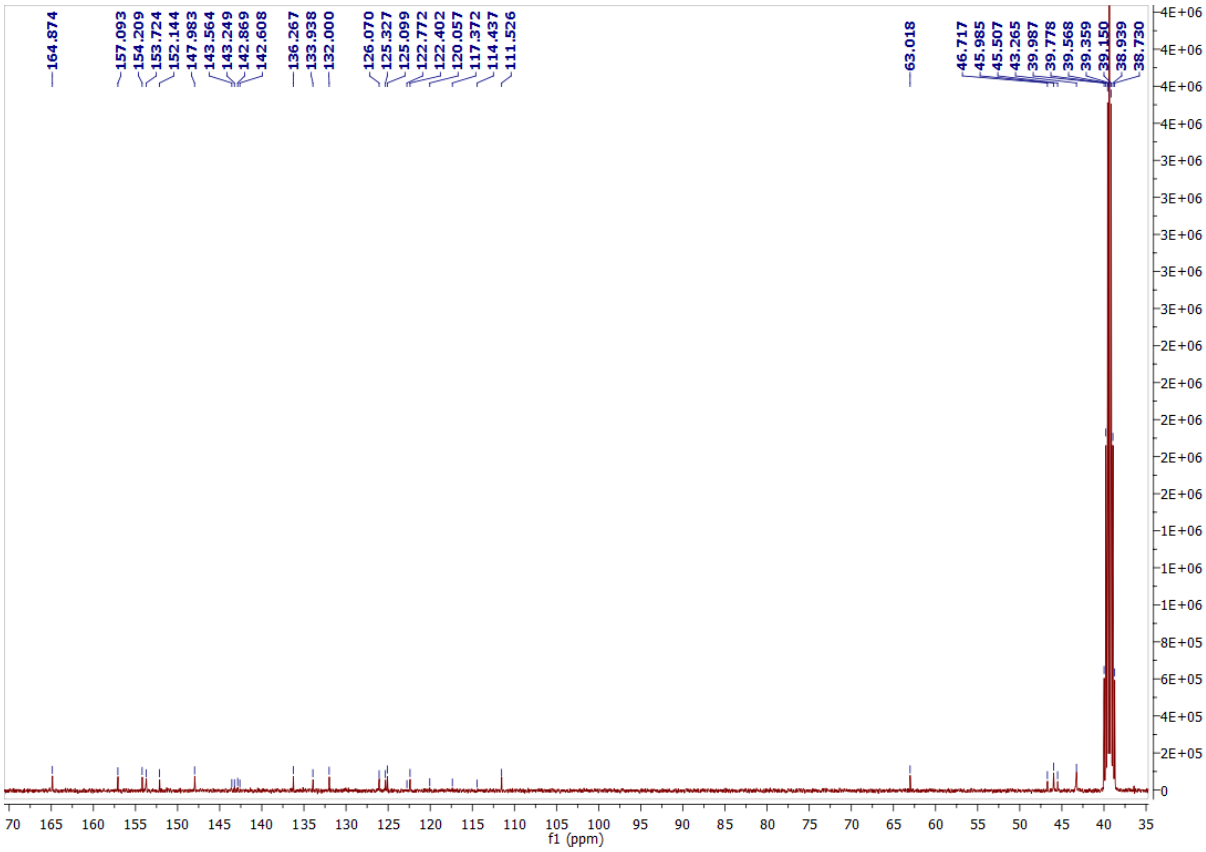

Figure S46: ^{13}C NMR Spectra of **35**.

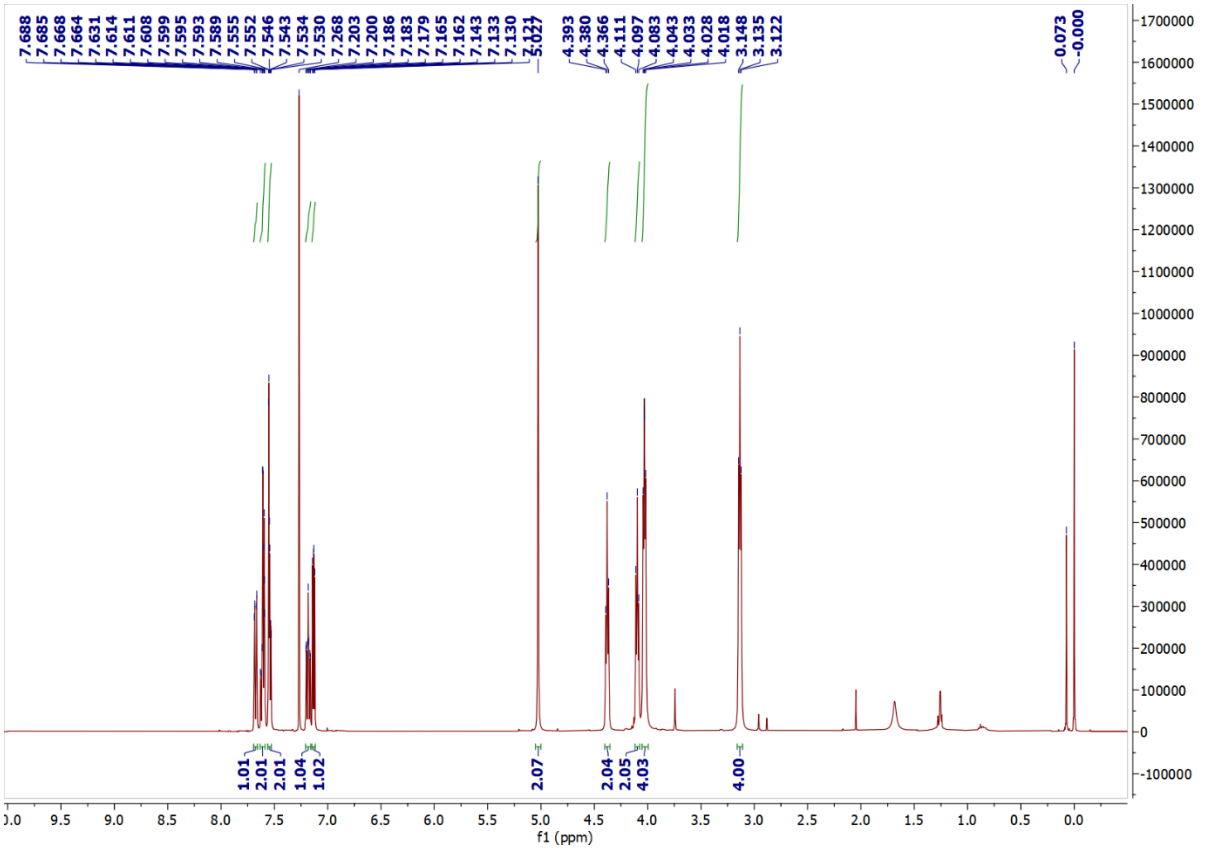

Figure S47: ^{1}H NMR Spectra of **36**.

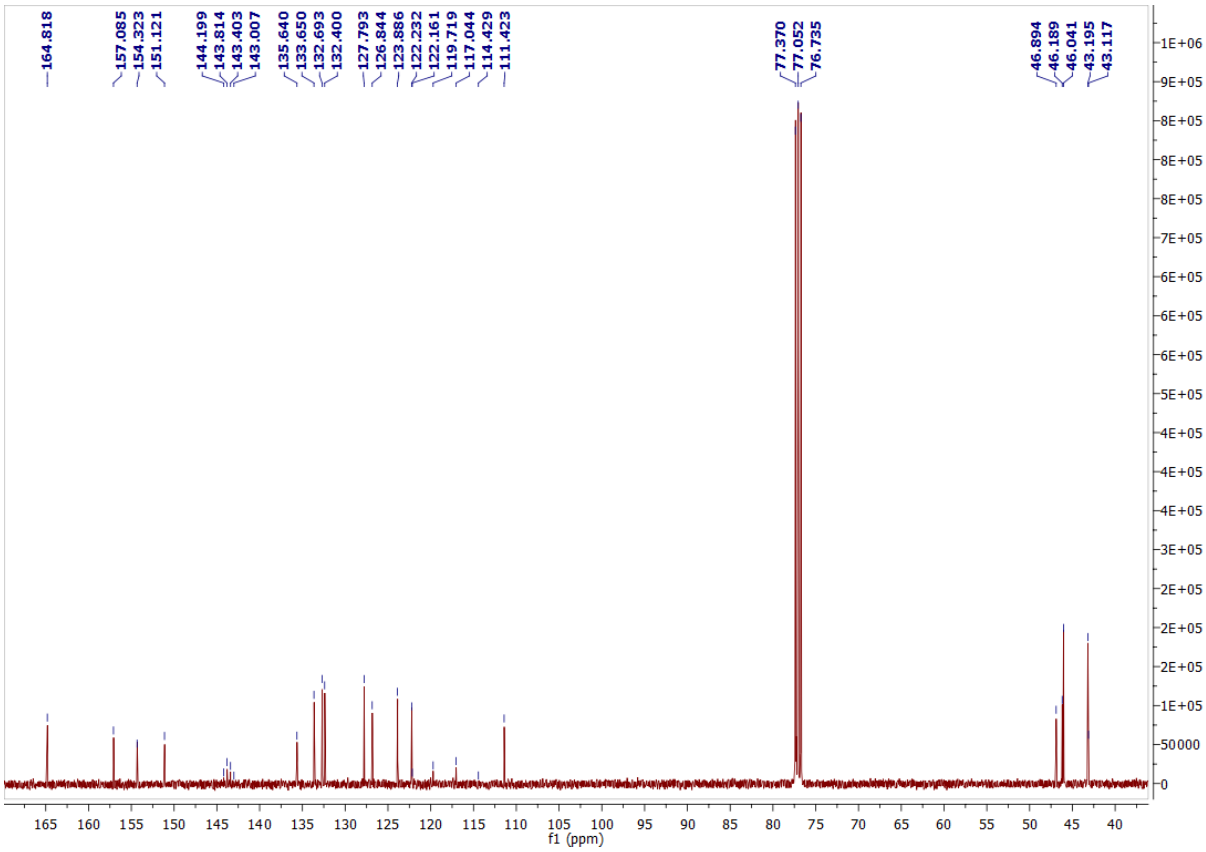

Figure S48: ^{13}C NMR Spectra of **36**.

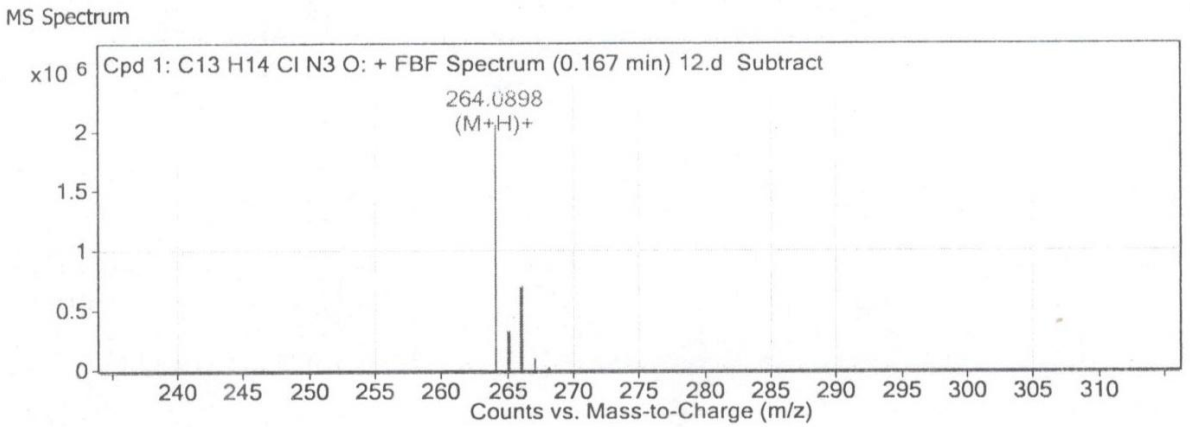

Figure S49: HRMS of Compound **13**. Observed molecular ion peak at 264.0898 (m/z), which corresponds to $[M+H]^+$.

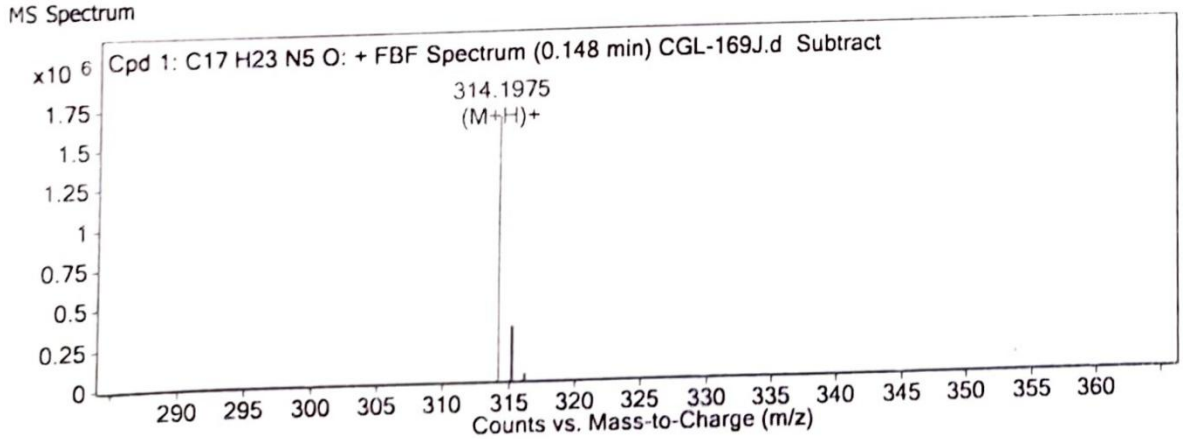

Figure S50: HRMS of Compound **14a**. Observed molecular ion peak at 314.1975 (m/z), which corresponds to $[M+H]^+$.

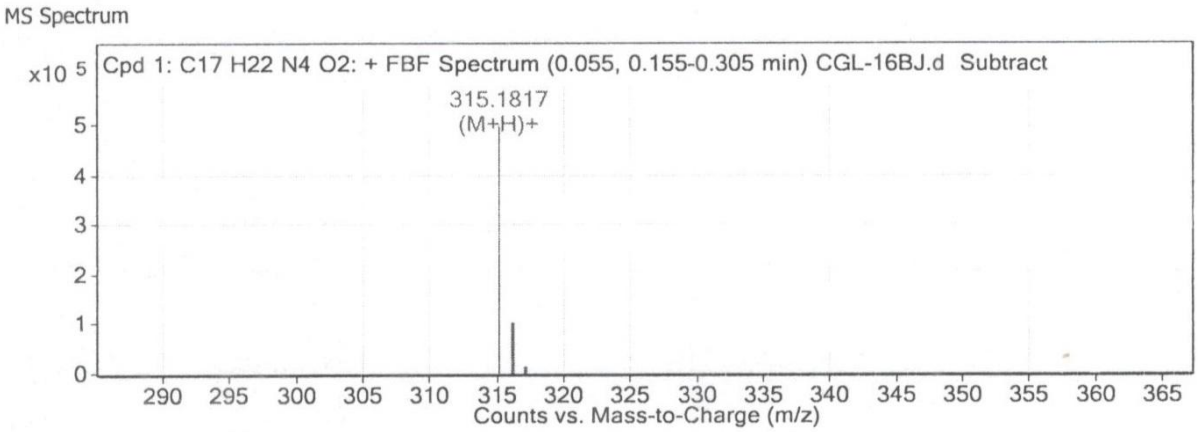

Figure S51: HRMS of Compound **14b**. Observed molecular ion peak at 315.1817 (m/z), which corresponds to $[M+H]^+$.

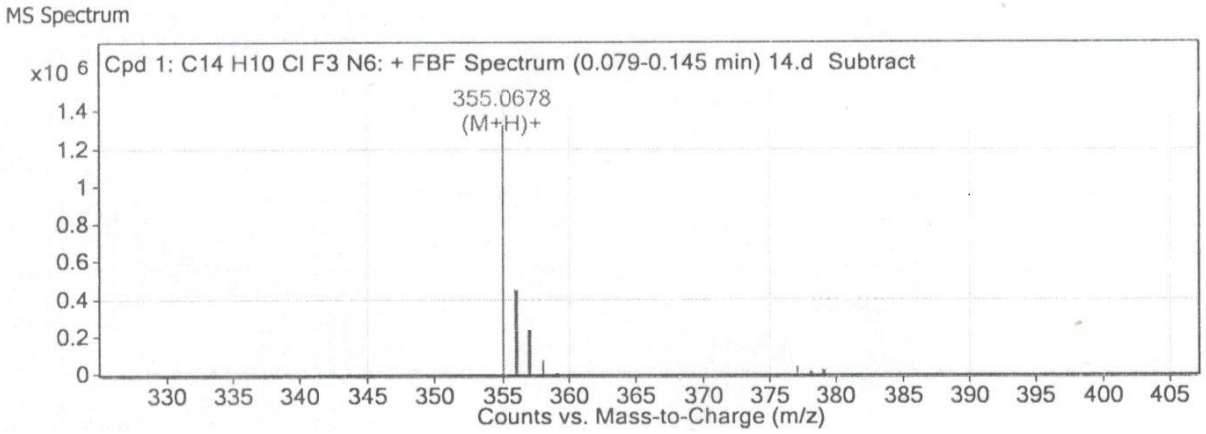

Figure S52: HRMS of Compound **16**. Observed molecular ion peak at 355.0678 (m/z), which corresponds to $[M+H]^+$.

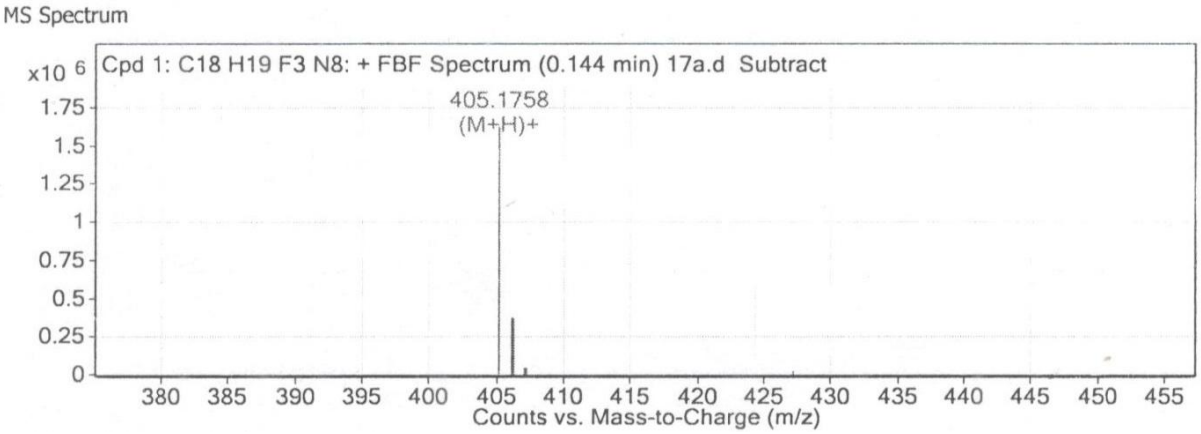

Figure S53: HRMS of Compound **17a**. Observed molecular ion peak at 405.1758 (m/z), which corresponds to $[M+H]^+$.

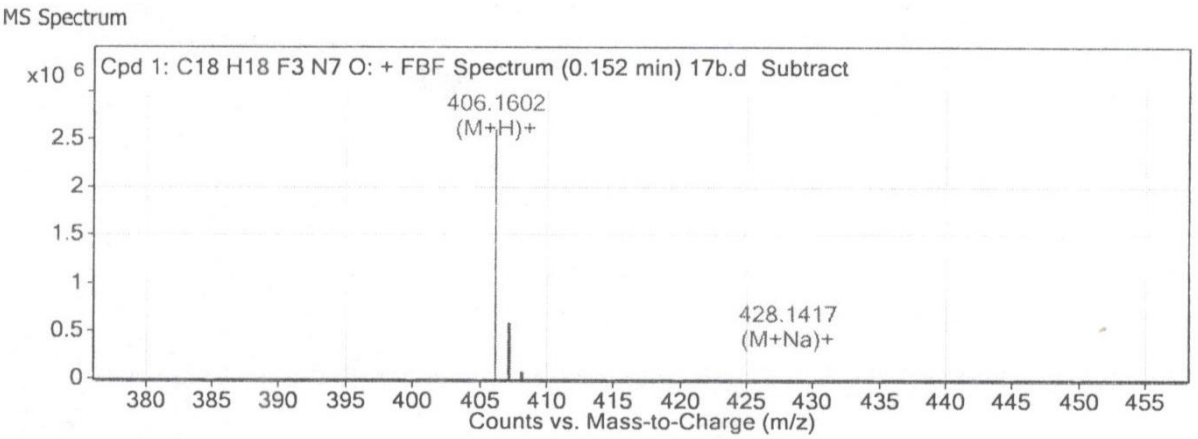

Figure S54: HRMS of Compound **17b**. Observed molecular ion peak at 406.1602 (m/z), which corresponds to $[M+H]^+$.

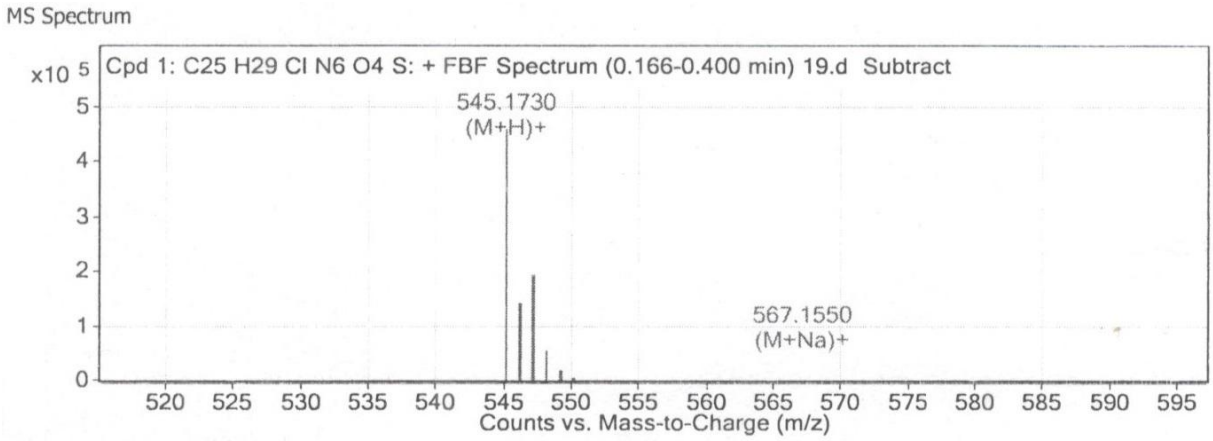

Figure S55: HRMS of Compound **19**. Observed molecular ion peak at 545.1730 (m/z), which corresponds to $[M+H]^+$.

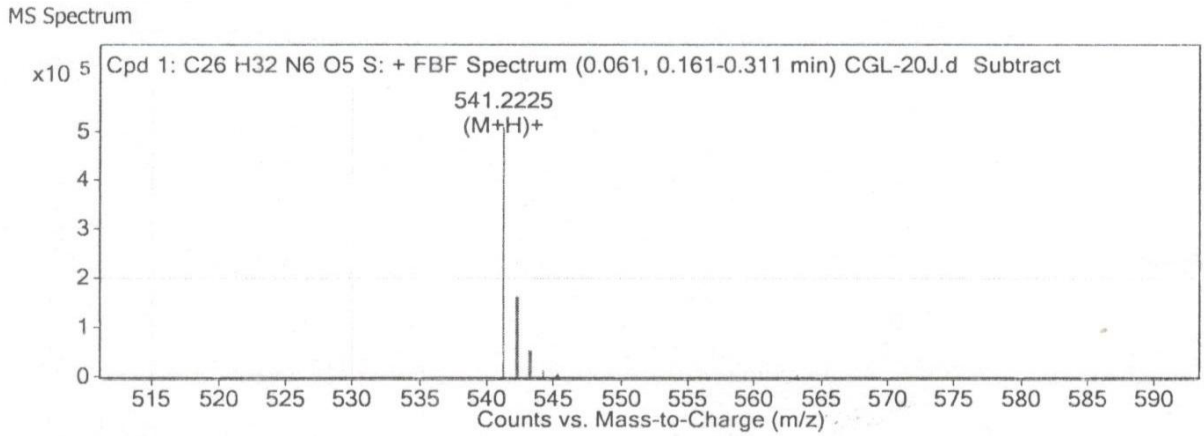

Figure S56: HRMS of Compound **20**. Observed molecular ion peak at 541.2225 (m/z), which corresponds to $[M+H]^+$.

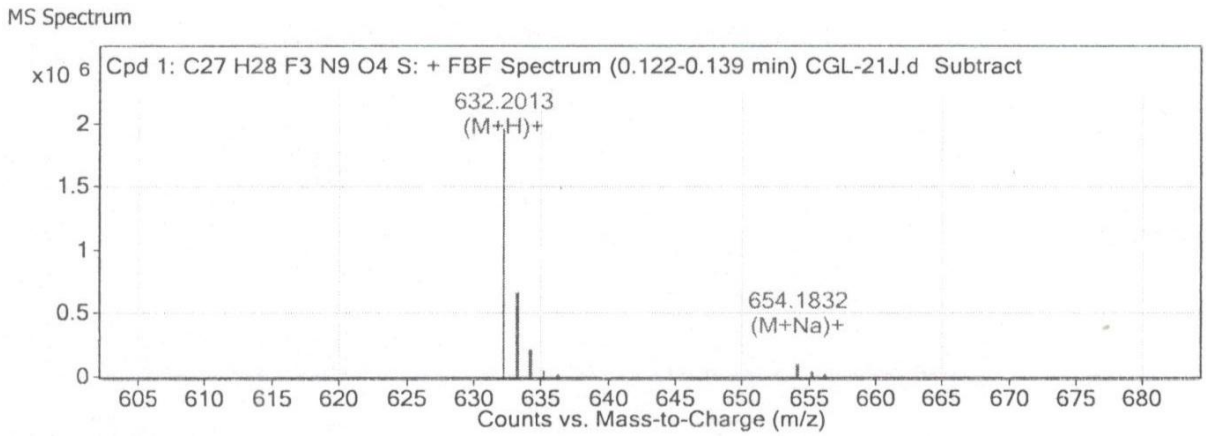

Figure S57: HRMS of Compound **21**. Observed molecular ion peak at 632.2013 (m/z), which corresponds to $[M+H]^+$.

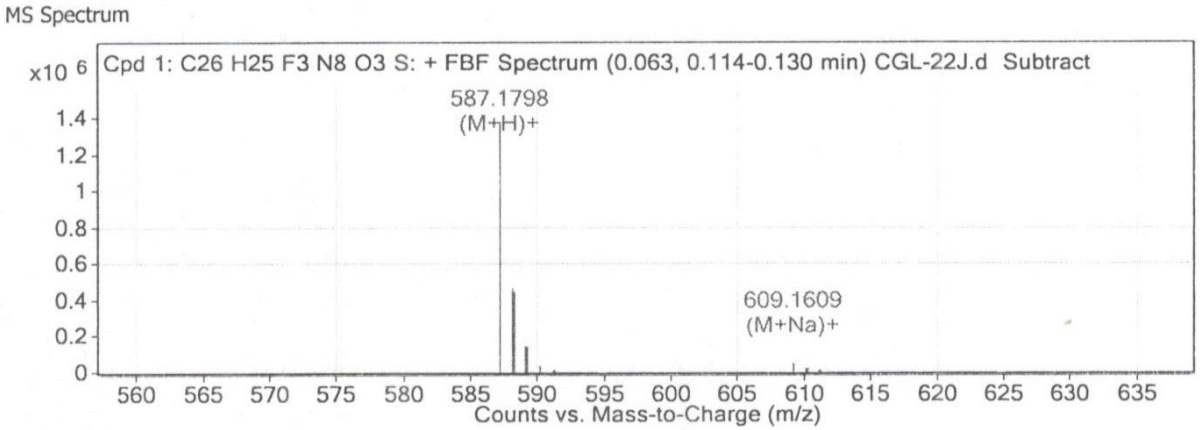

Figure S58: HRMS of Compound **22**. Observed molecular ion peak at 587.1798 (m/z), which corresponds to $[M+H]^+$.

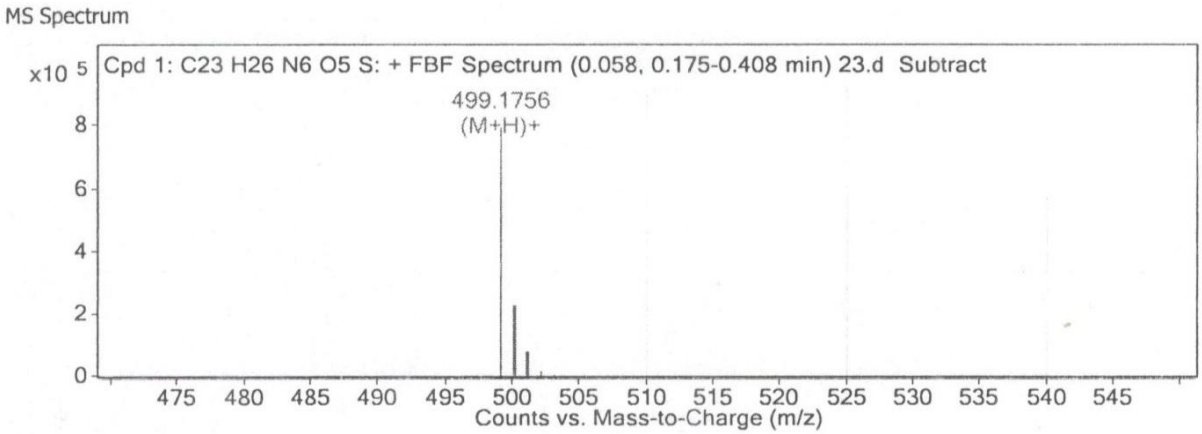

Figure S59: HRMS of Compound **23**. Observed molecular ion peak at 499.1756 (m/z), which corresponds to $[M+H]^+$.

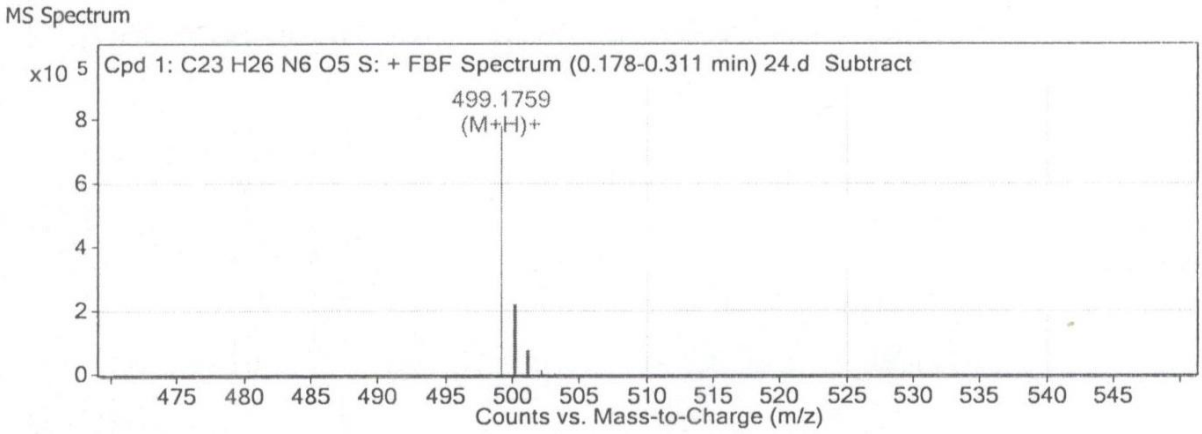

Figure S60: HRMS of Compound **24**. Observed molecular ion peak at 499.1759 (m/z), which corresponds to $[M+H]^+$.

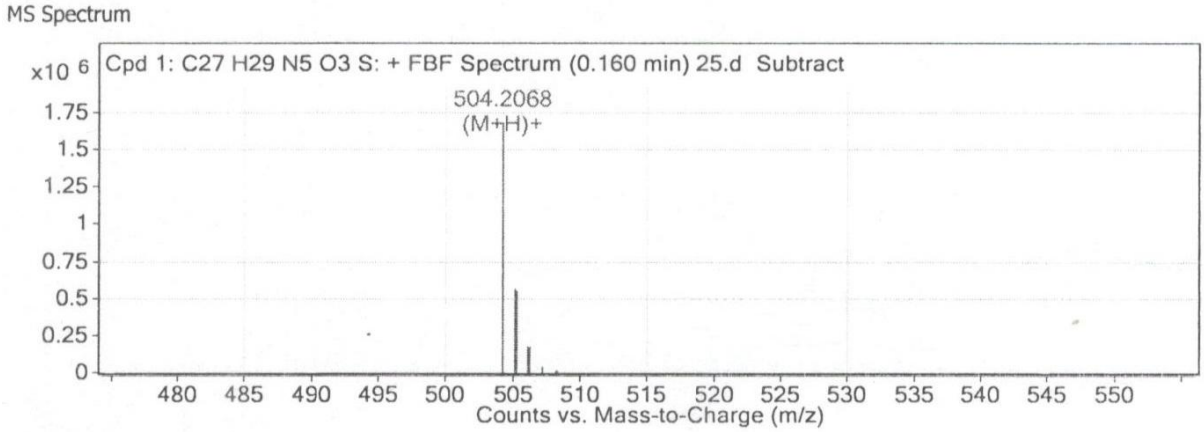

Figure S61: HRMS of Compound **25**. Observed molecular ion peak at 504.2068 (m/z), which corresponds to $[M+H]^+$.

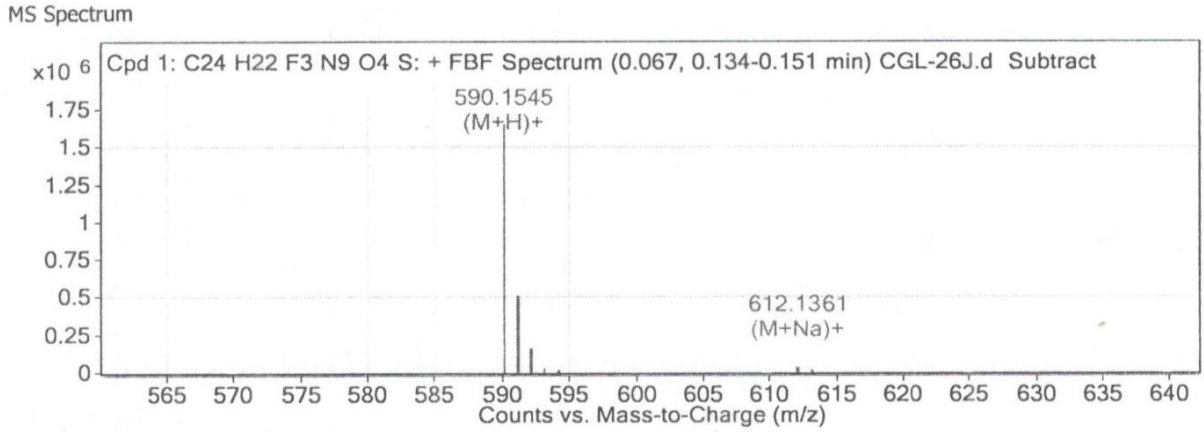

Figure S62: HRMS of Compound **26**. Observed molecular ion peak at 590.1545 (m/z), which corresponds to $[M+H]^+$.

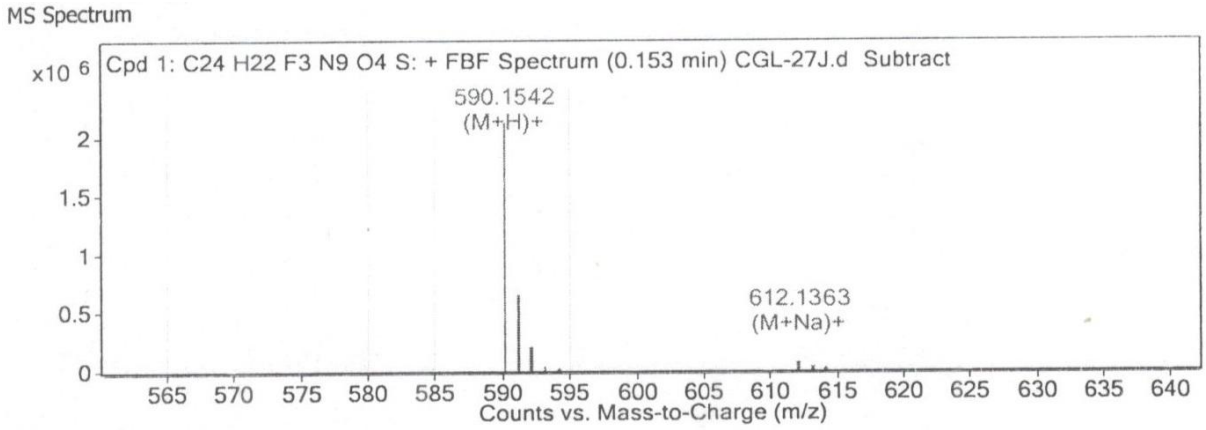

Figure S63: HRMS of Compound **27**. Observed molecular ion peak at 590.1542 (m/z), which corresponds to $[M+H]^+$.

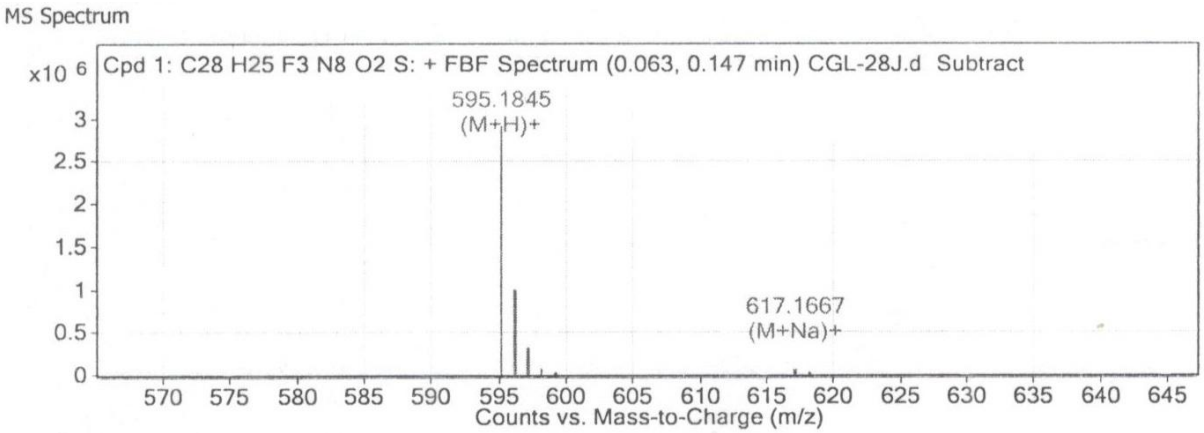

Figure S64: HRMS of Compound **28**. Observed molecular ion peak at 595.1845 (m/z), which corresponds to $[M+H]^+$.

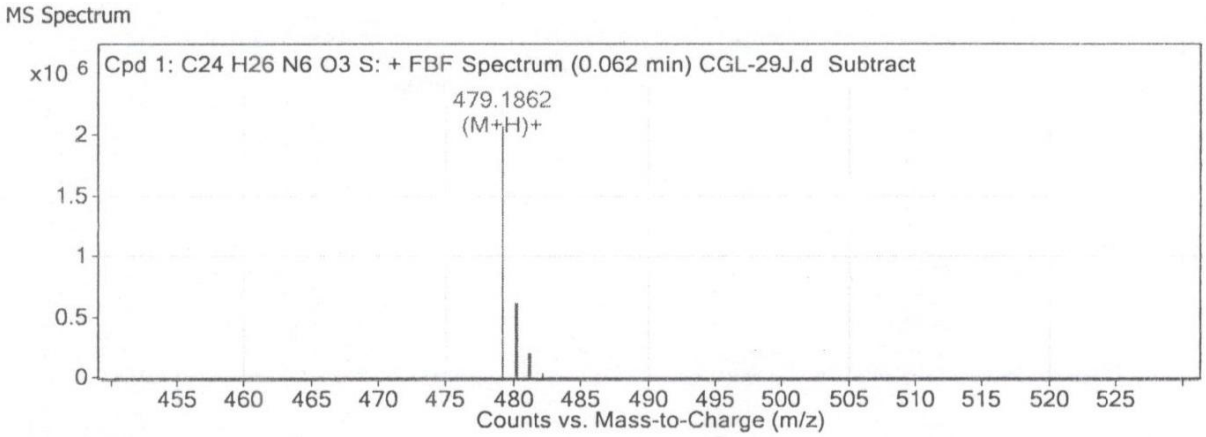

Figure S65: HRMS of Compound **29**. Observed molecular ion peak at 479.1862 (m/z), which corresponds to $[M+H]^+$.

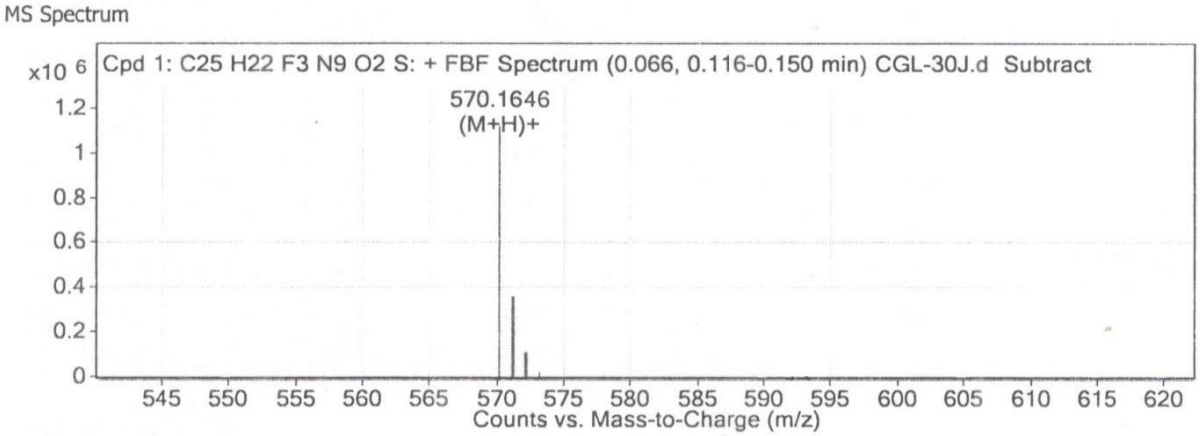

Figure S66: HRMS of Compound **30**. Observed molecular ion peak at 570.1646 (m/z), which corresponds to $[M+H]^+$.

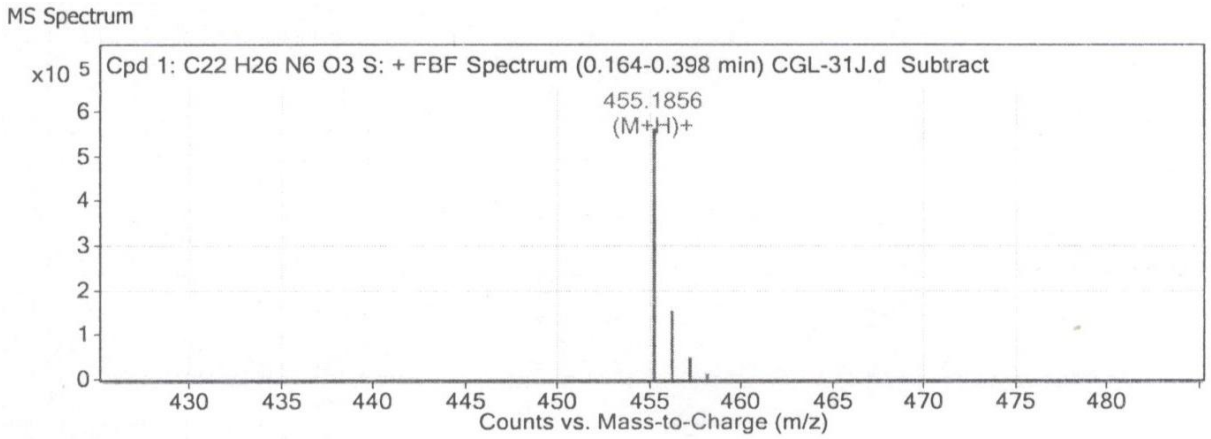

Figure S67: HRMS of Compound **31**. Observed molecular ion peak at 455.1856 (m/z), which corresponds to $[M+H]^+$.

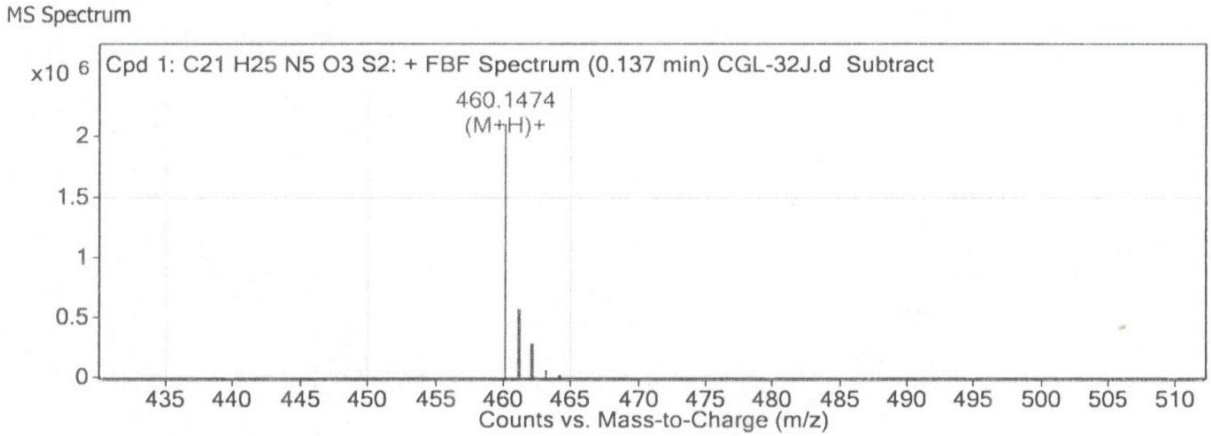

Figure S68: HRMS of Compound **32**. Observed molecular ion peak at 460.1474 (m/z), which corresponds to $[M+H]^+$.

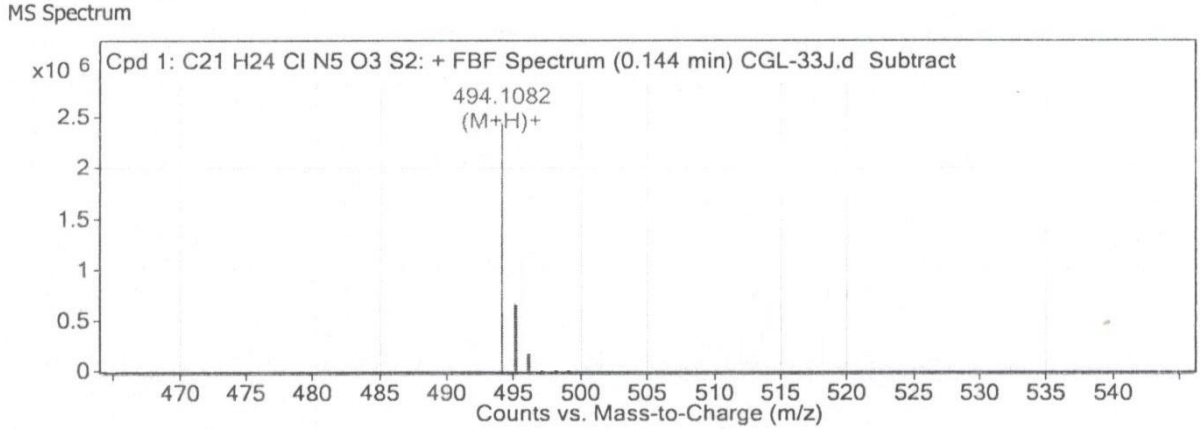

Figure S69: HRMS of Compound **33**. Observed molecular ion peak at 494.1082 (m/z), which corresponds to $[M+H]^+$.

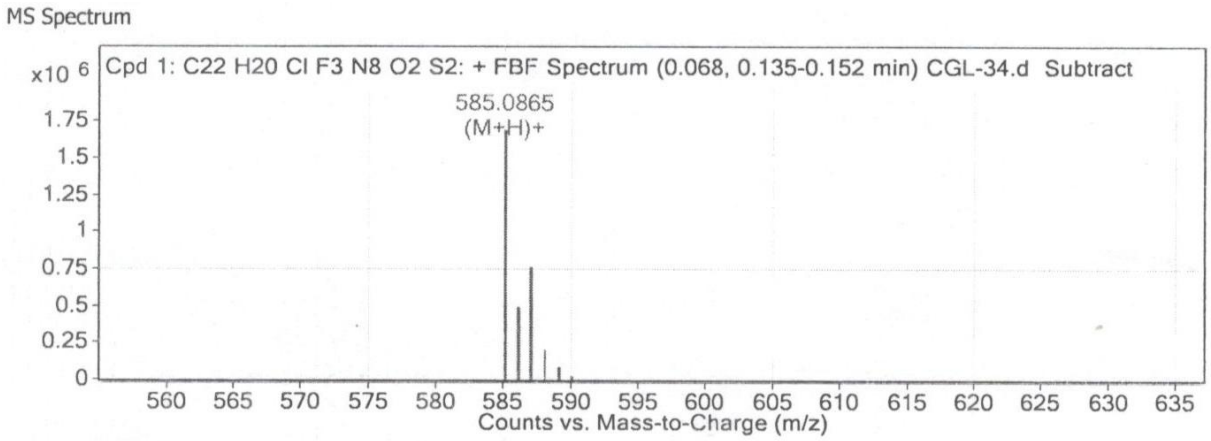

Figure S70: HRMS of Compound **34**. Observed molecular ion peak at 585.0865 (m/z), which corresponds to $[M+H]^+$.

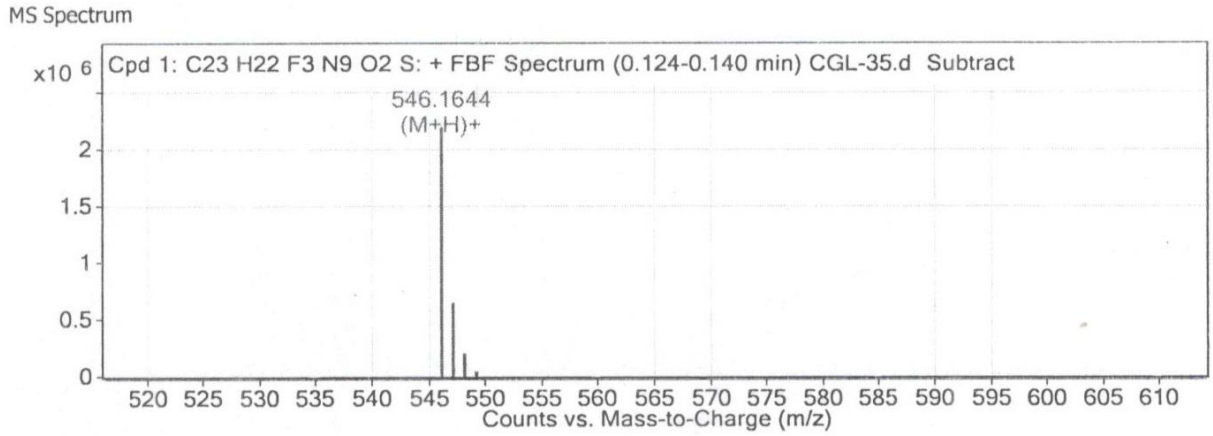

Figure S71: HRMS of Compound **35**. Observed molecular ion peak at 546.1644 (m/z), which corresponds to $[M+H]^+$.

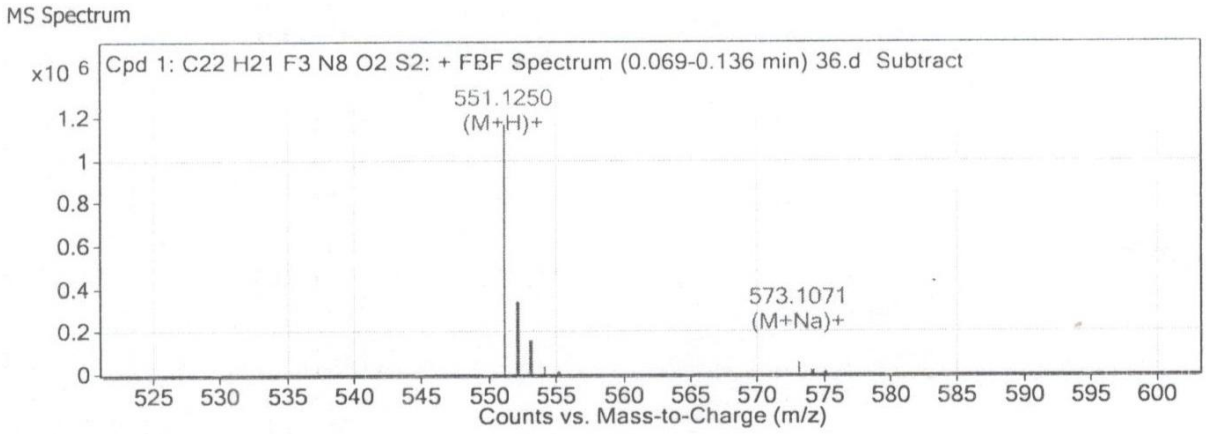

Figure S72: HRMS of Compound **36**. Observed molecular ion peak at 551.1250 (m/z), which corresponds to $[M+H]^+$.

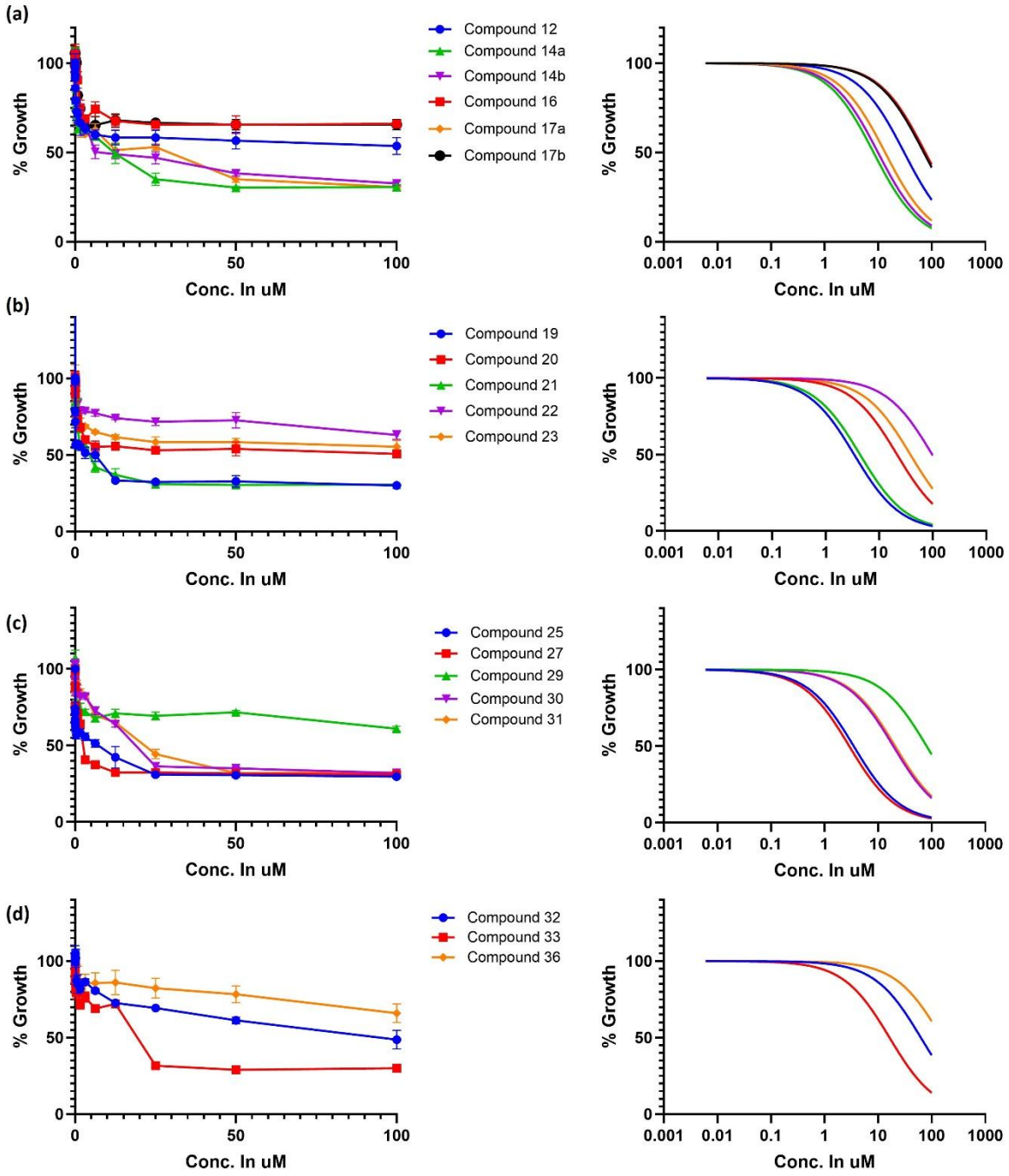

Figure S73: Parasite per cent growth inhibition plots at different concentrations of the test compounds. The initial concentration of the test compounds was 100 µM.

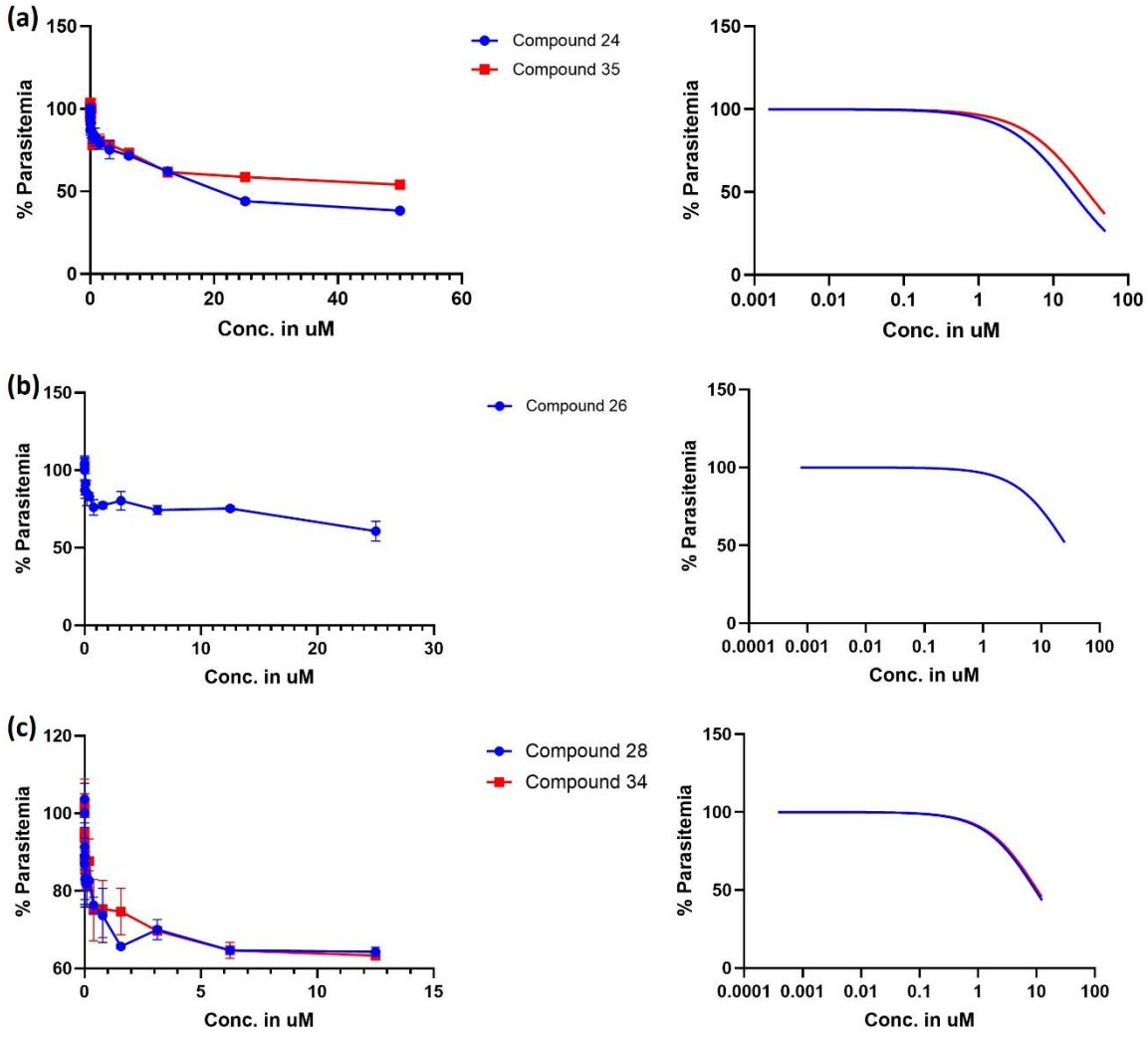

Figure S74: Parasite per cent growth inhibition plots at different concentrations of the test compounds. The initial concentration of the test compounds was 50 µM for (a), 25 µM for (b), and 12 µM for (c).

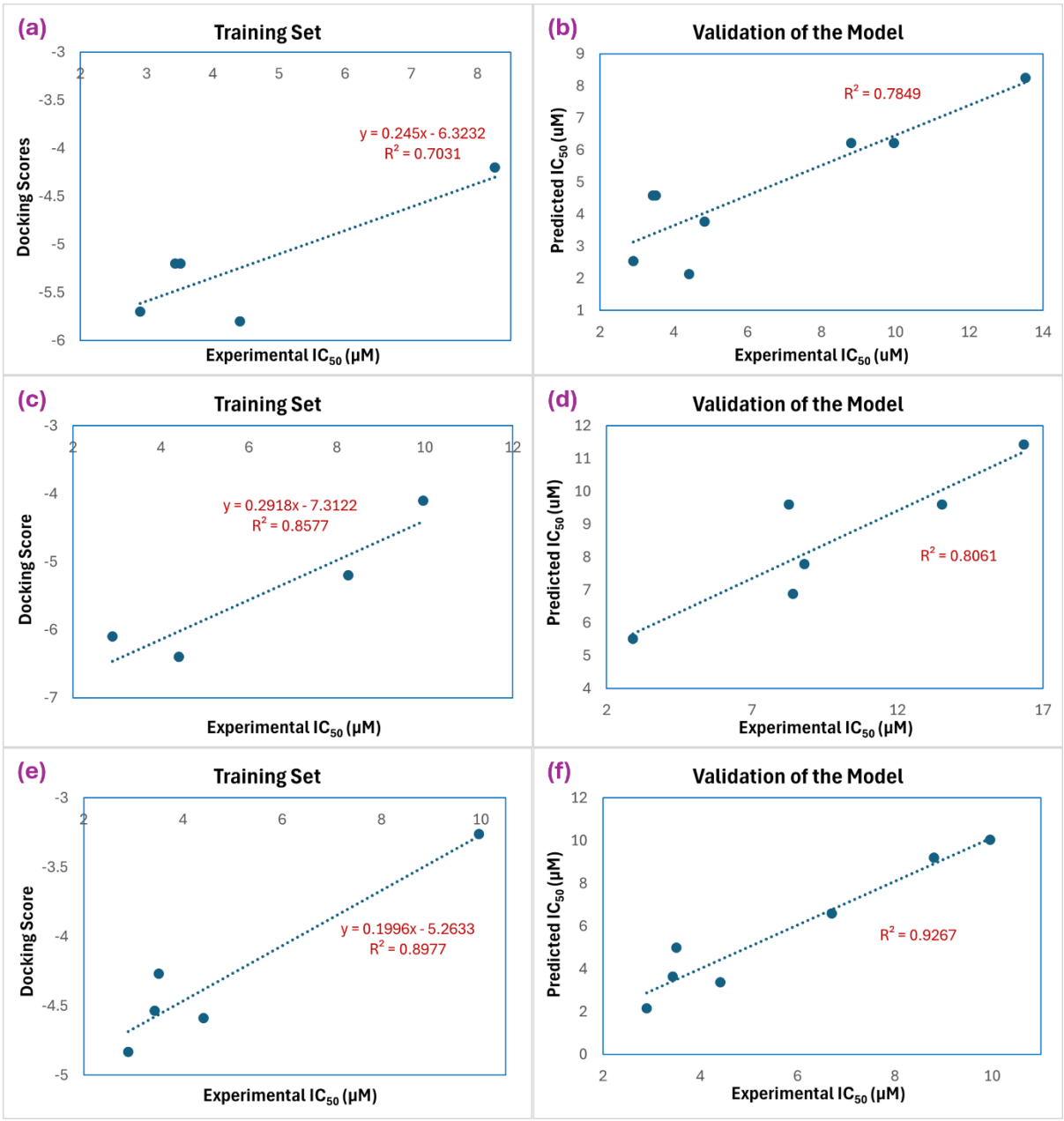

Figure S75: Correlation curve for validation of docking study; (**a** and **b**) for *Pf*FP2; (**c** and **d**) for *Pf*FP3; (**e** and **f**) for *Pf*FLN. The variables in the equation of a straight line are defined as y = docking score; x = predicted IC_{50} value.

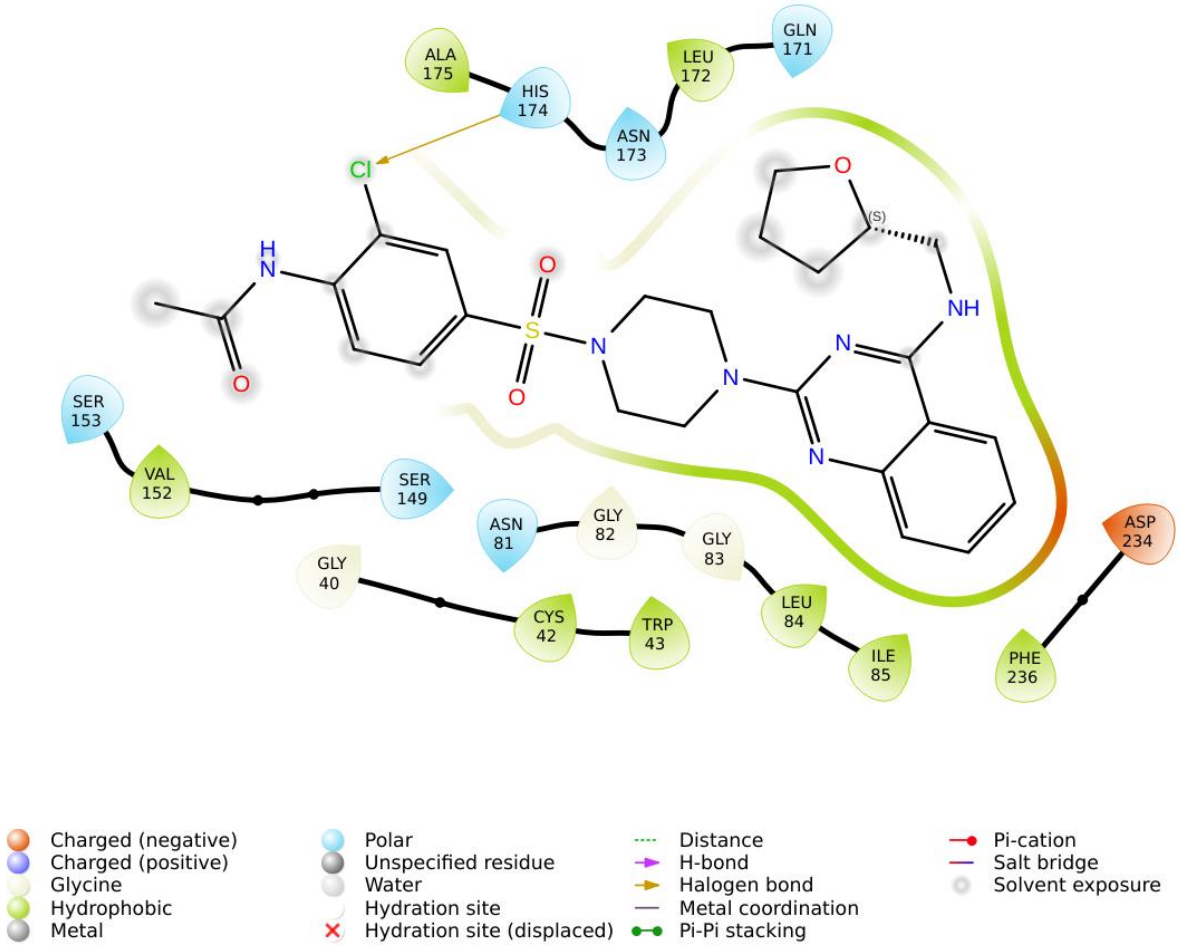

Figure S76: 2D ligand-protein interaction presentation for complex **19**-*Pf*FP2.

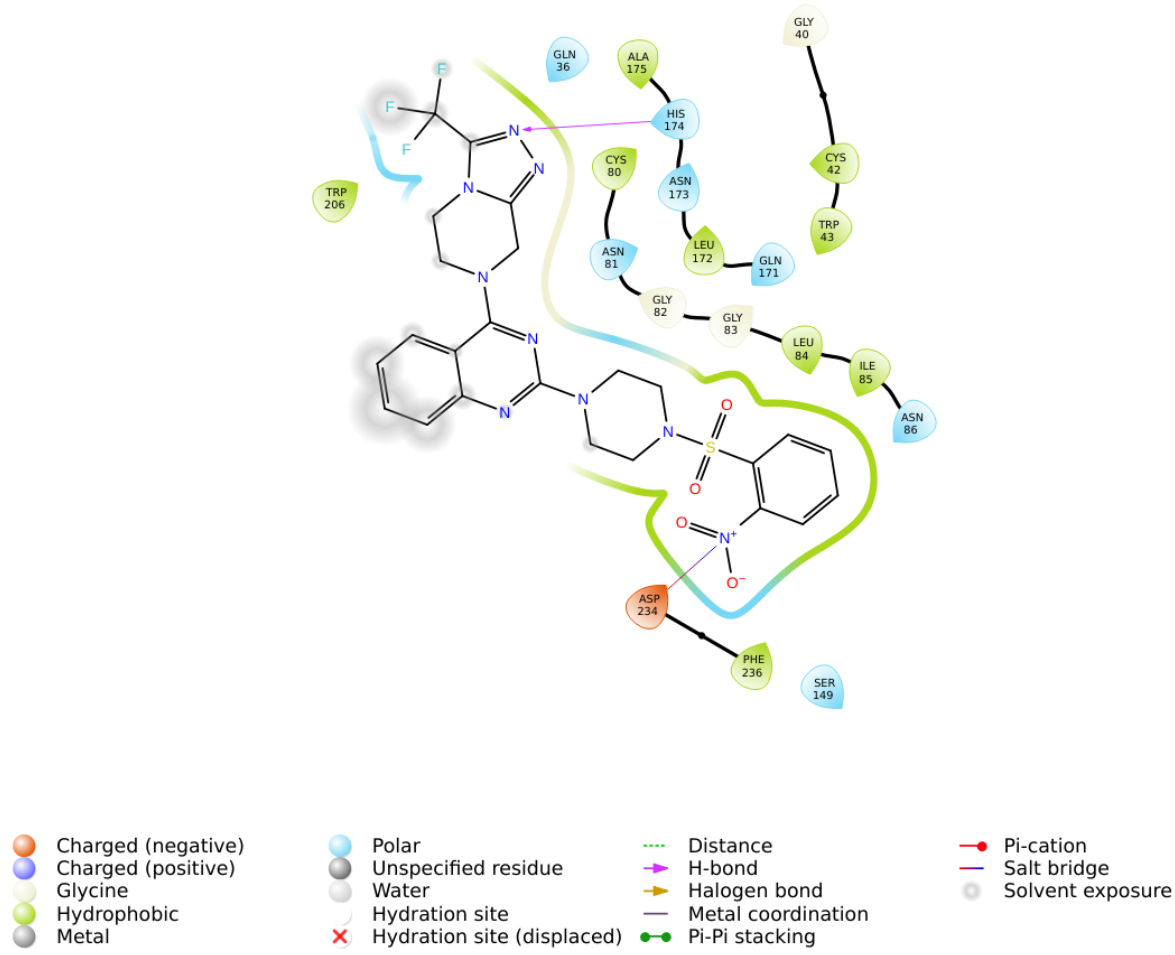

Figure S77: 2D ligand-protein interaction presentation for complex **27**-*Pf*FP2.

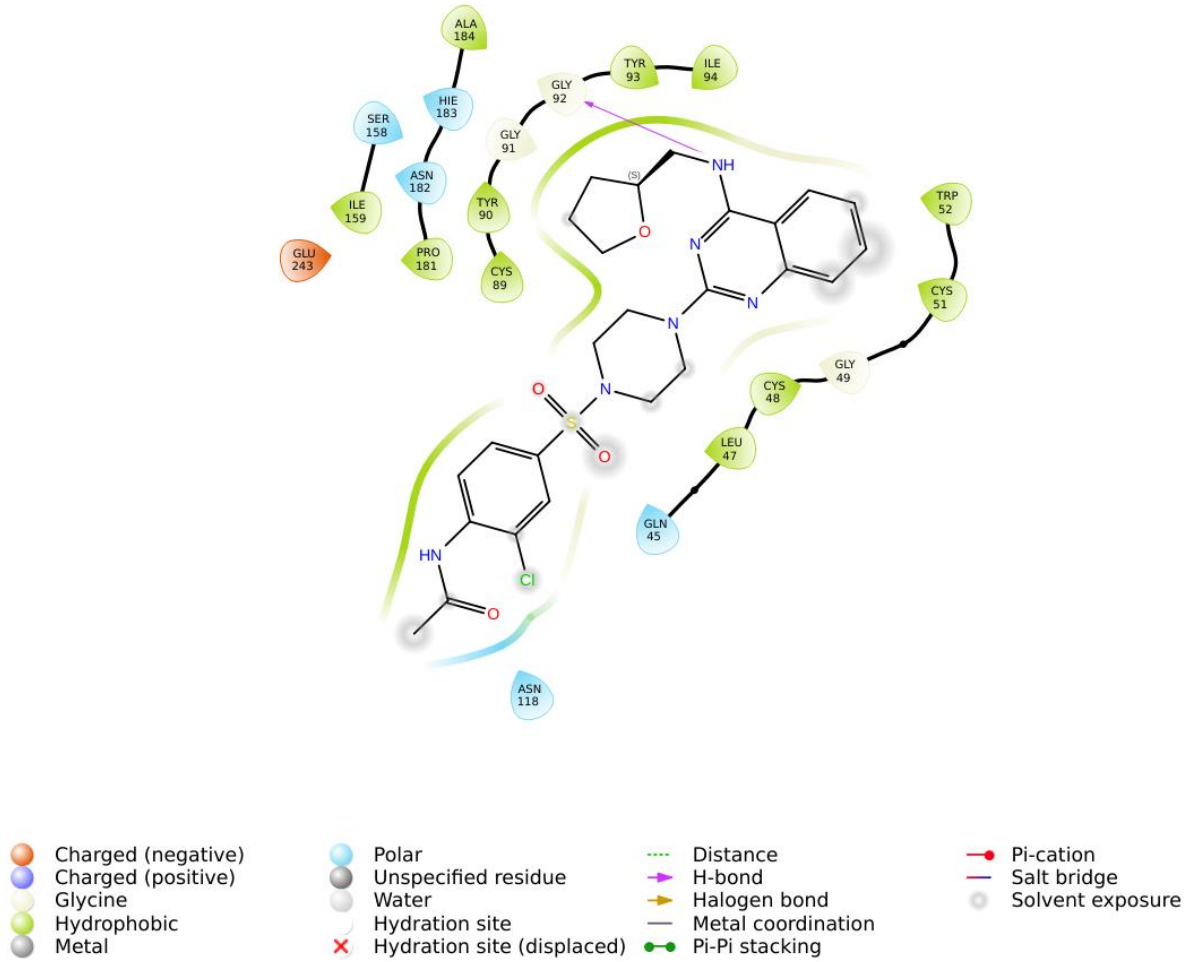

Figure S78: 2D ligand-protein interaction presentation for complex **19**-*Pf*FP3.

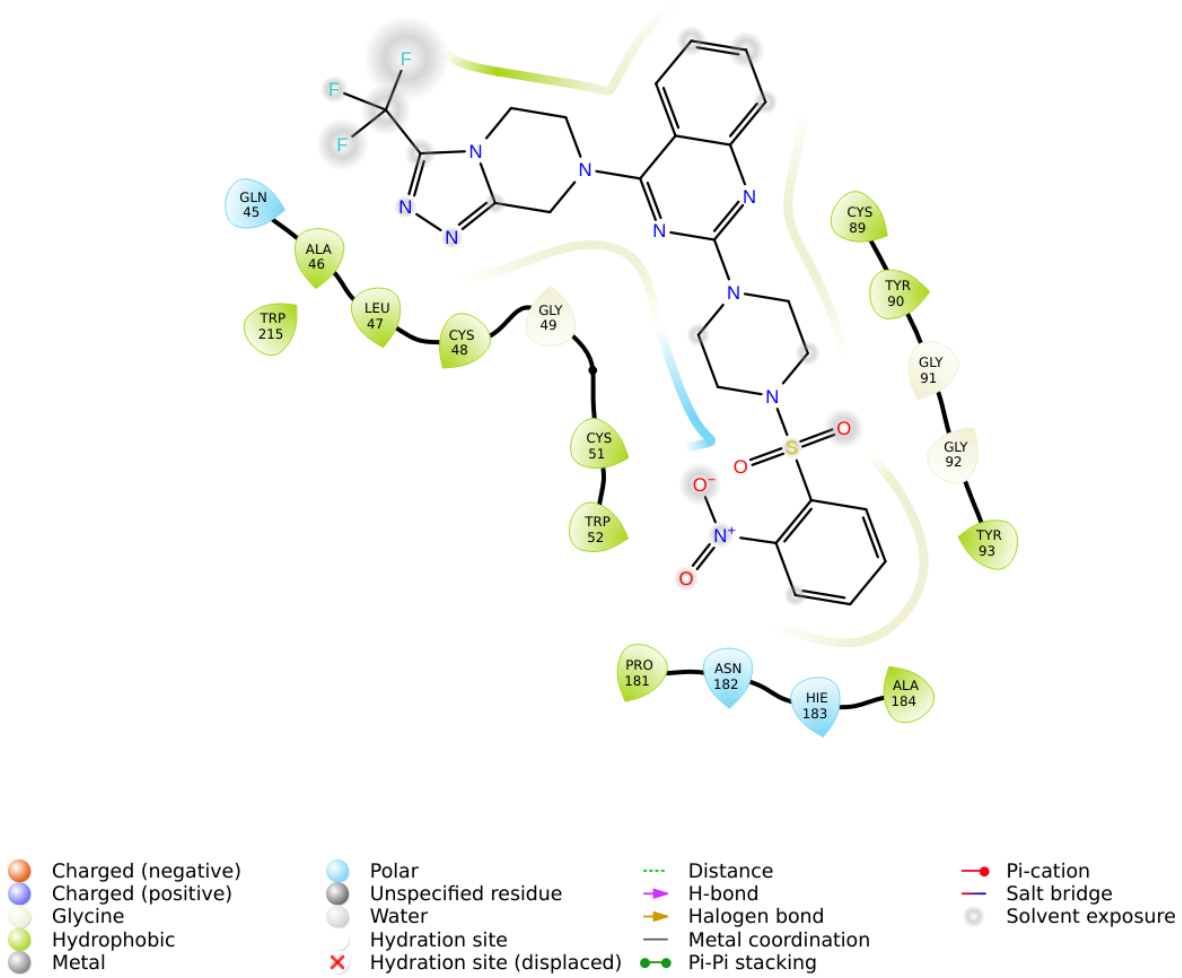

Figure S79: 2D ligand-protein interaction presentation for complex **27**-*Pf*FP3.

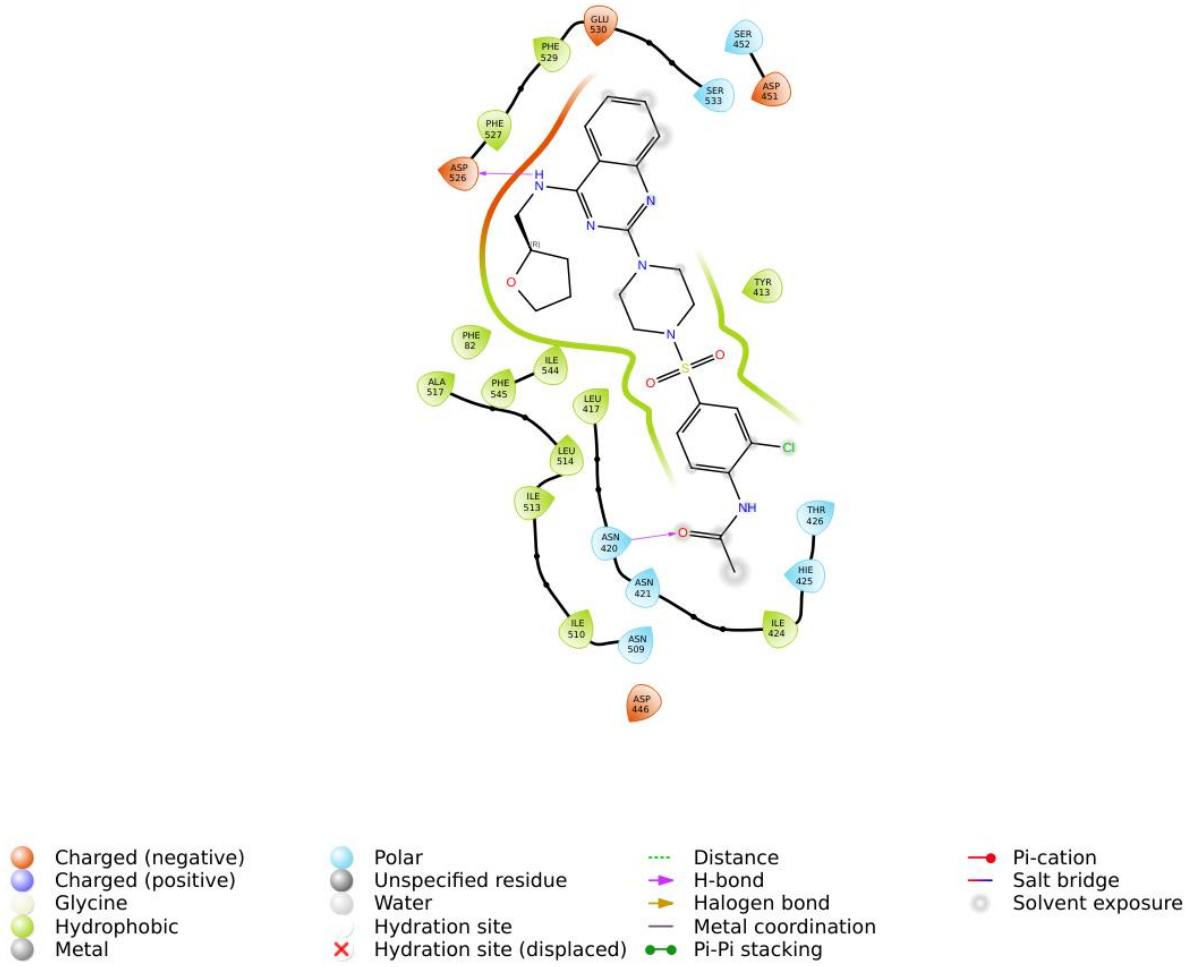

Figure S80: 2D ligand-protein interaction presentation for complex **19**-*Pf*FLN.

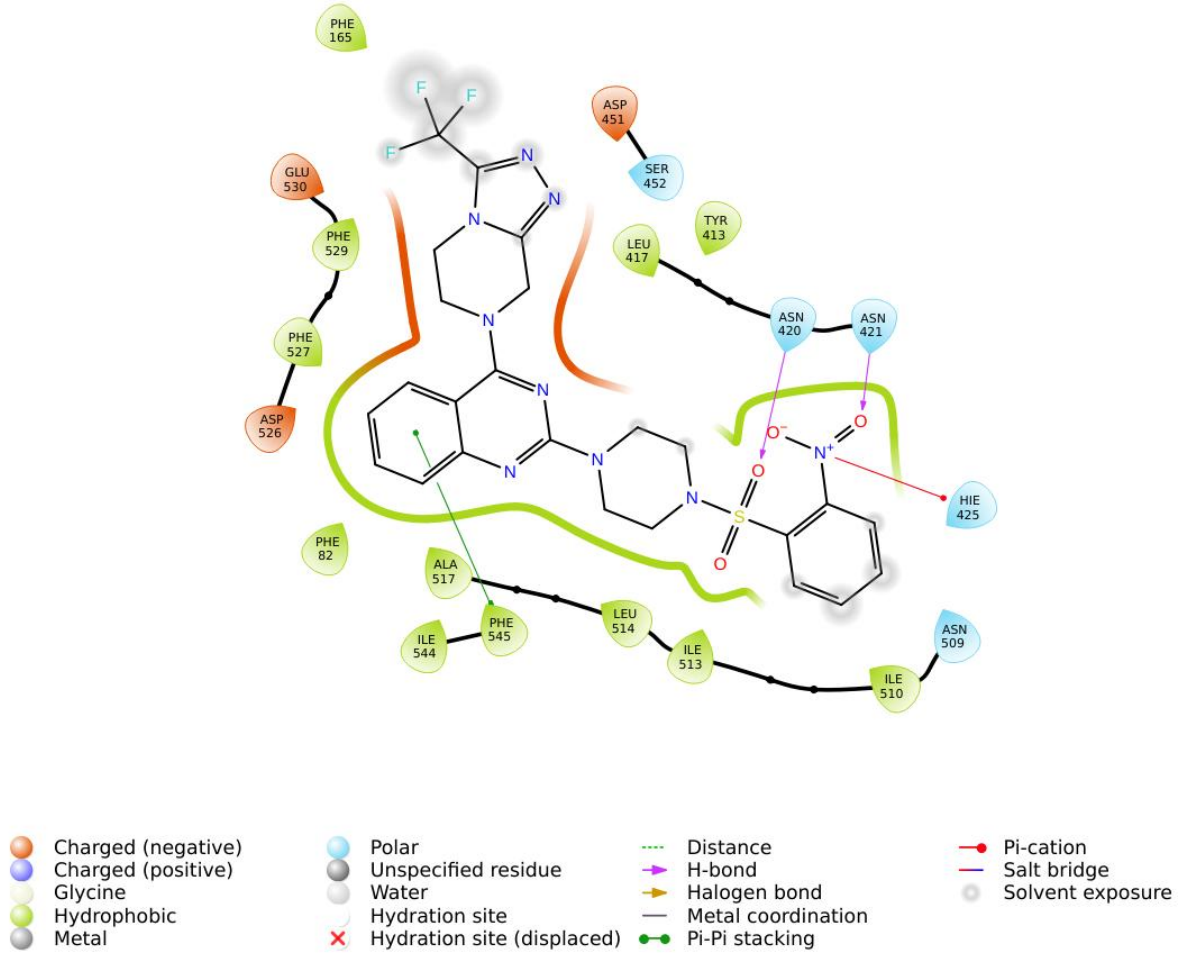

Figure S81: 2D ligand-protein interaction presentation for complex **27**-*Pf*FLN.

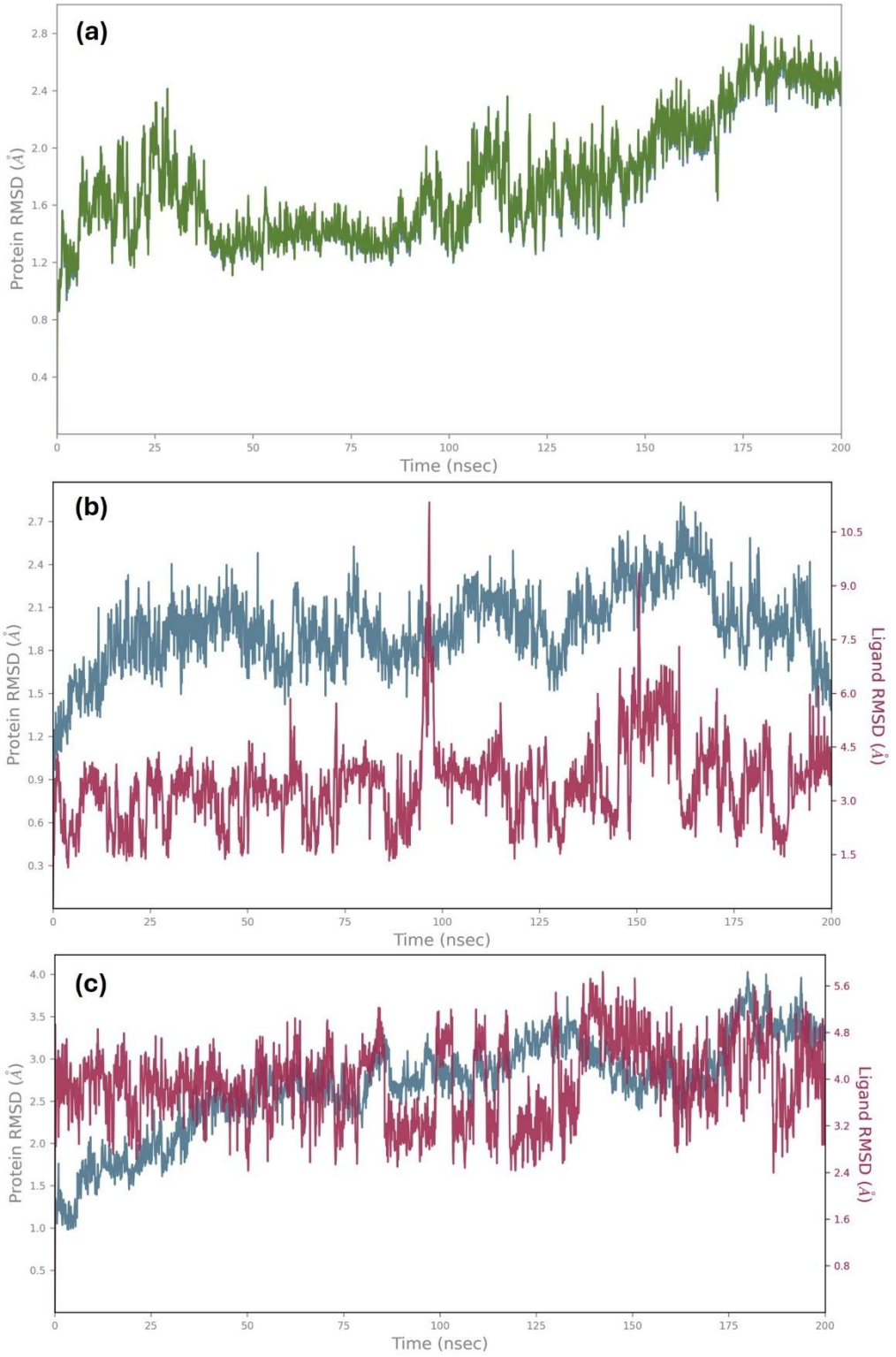

Figure S82: RMSD plots for the (a) apo *Pf*FP2, (b) *Pf*FP2-**19**, and (c) *Pf*FP3-**27** complexes.

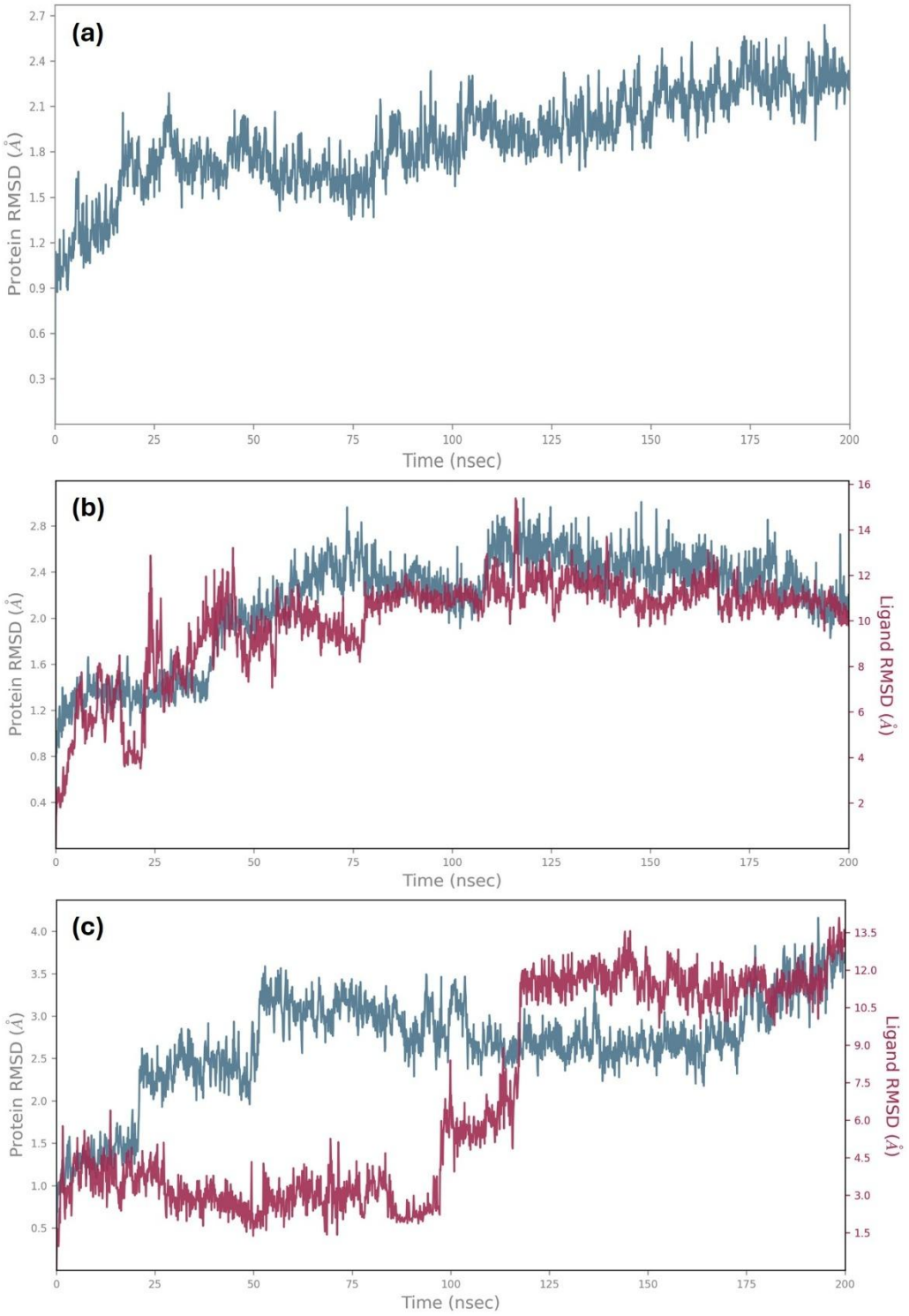

Figure S83: RMSD plots for the (a) apo *Pf*FP3, (b) *Pf*FP3-**19**, and (c) *Pf*FP3-**27** complexes.

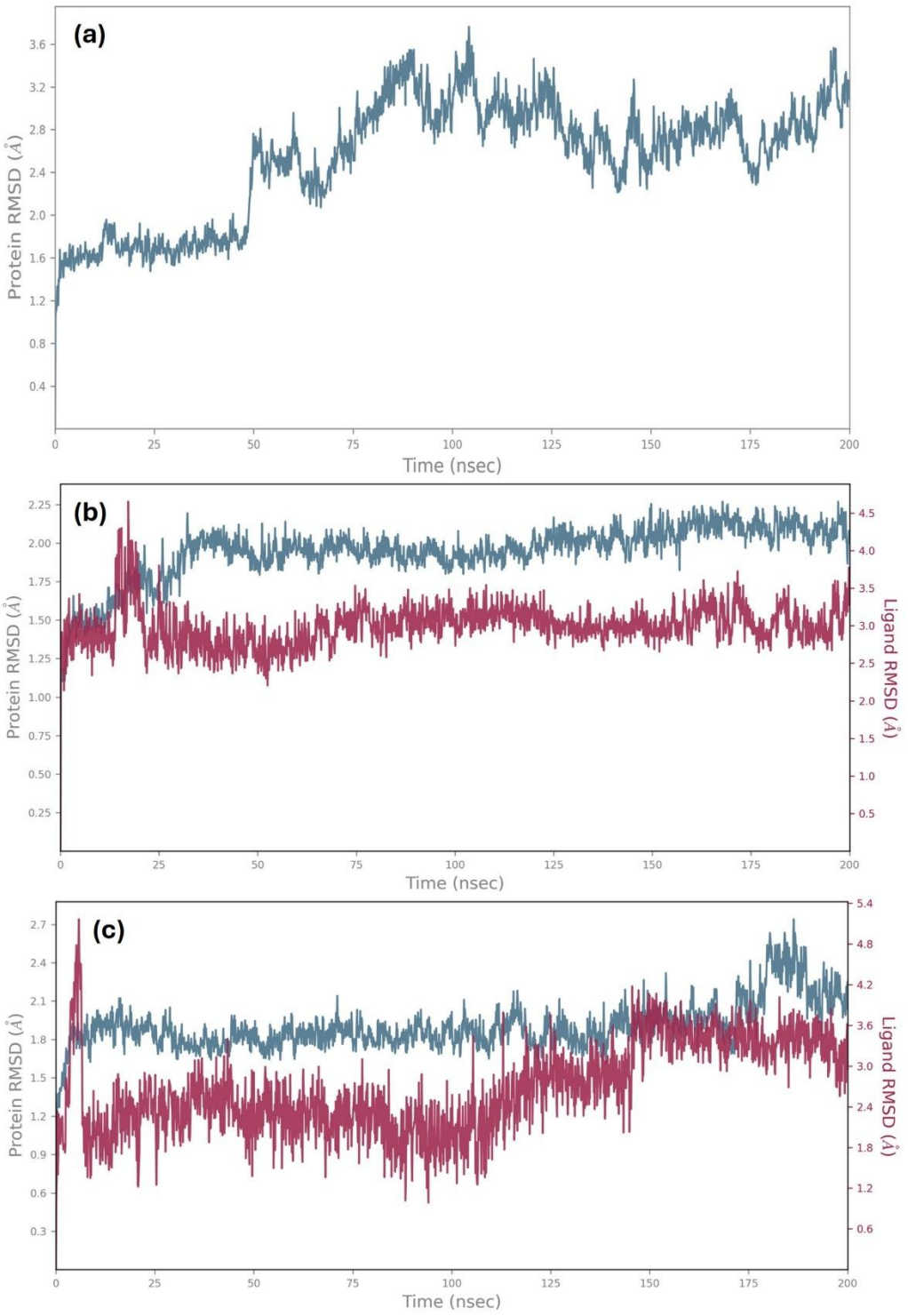

Figure S84: RMSD plots for the (a) apo *Pf*FLN, (b) *Pf*FLN-**19**, and (c) *Pf*FLN-**27** complexes.

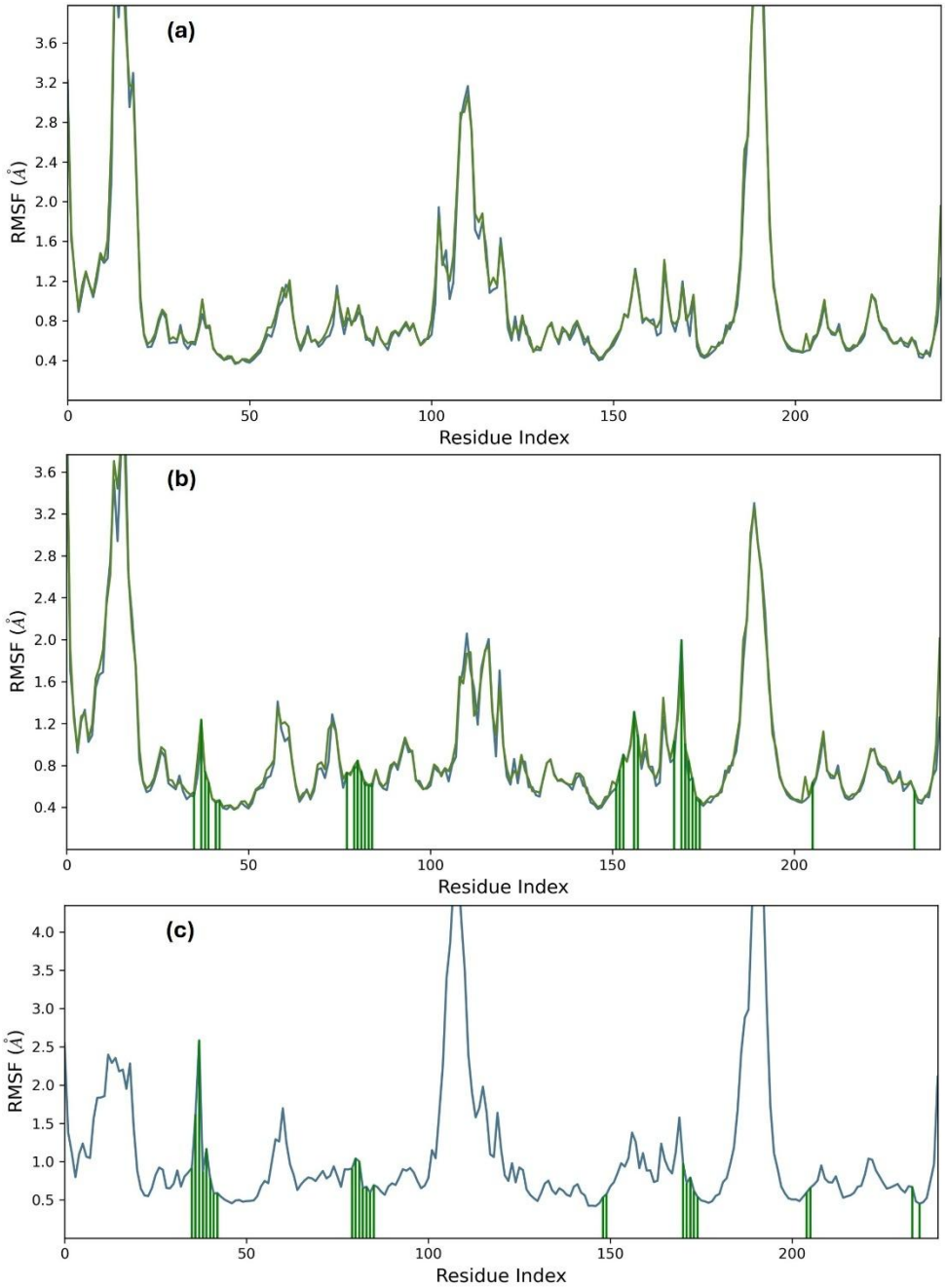

Figure S85: RMSF plots for the (a) apo *Pf*FP2, (b) *Pf*FP2-**19**, and (c) *Pf*FP2-**27** complexes.

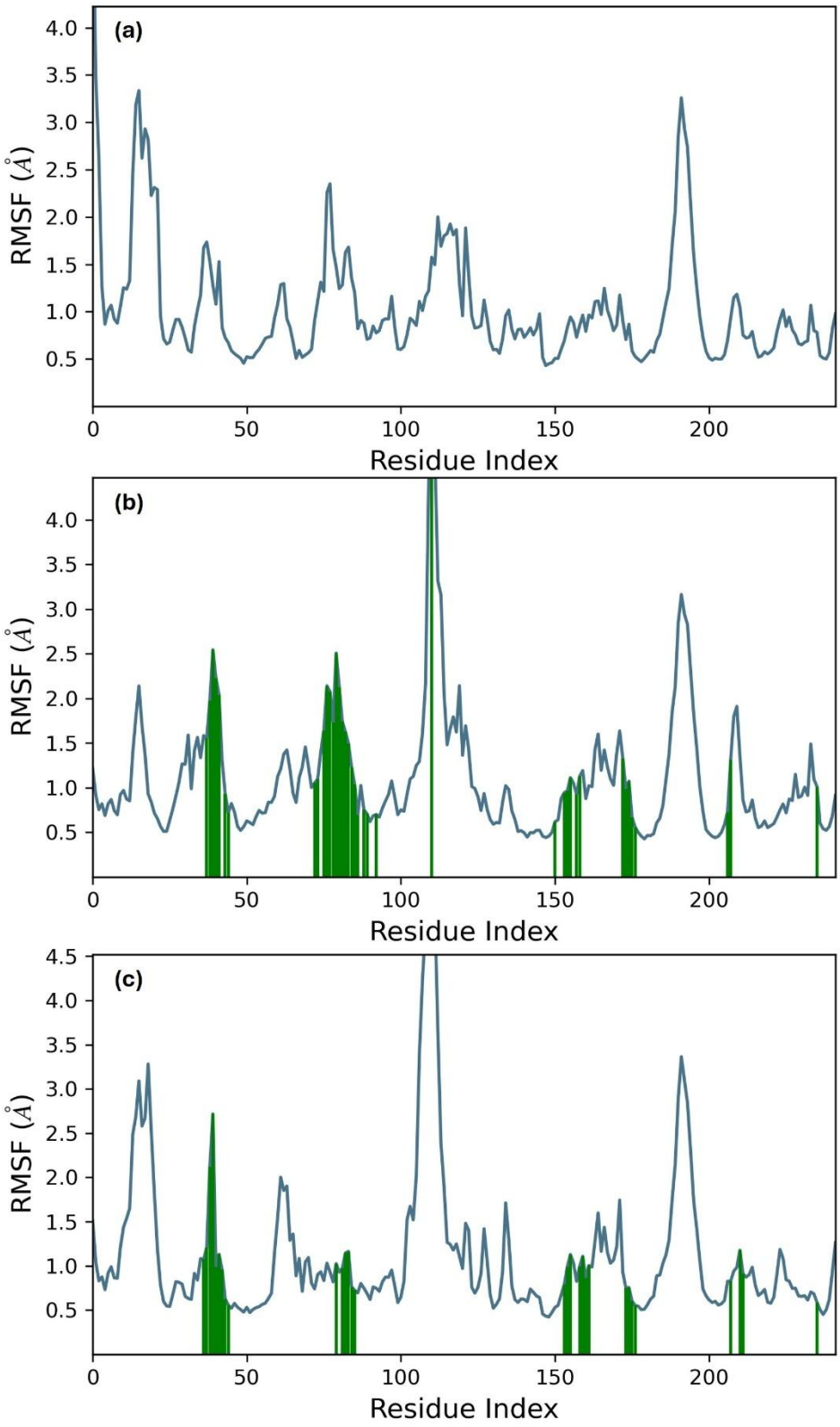

Figure S86: RMSF plots for the (a) apo *Pf*FP3, (b) *Pf*FP3-**19**, and (c) *Pf*FP3-**27** complexes.

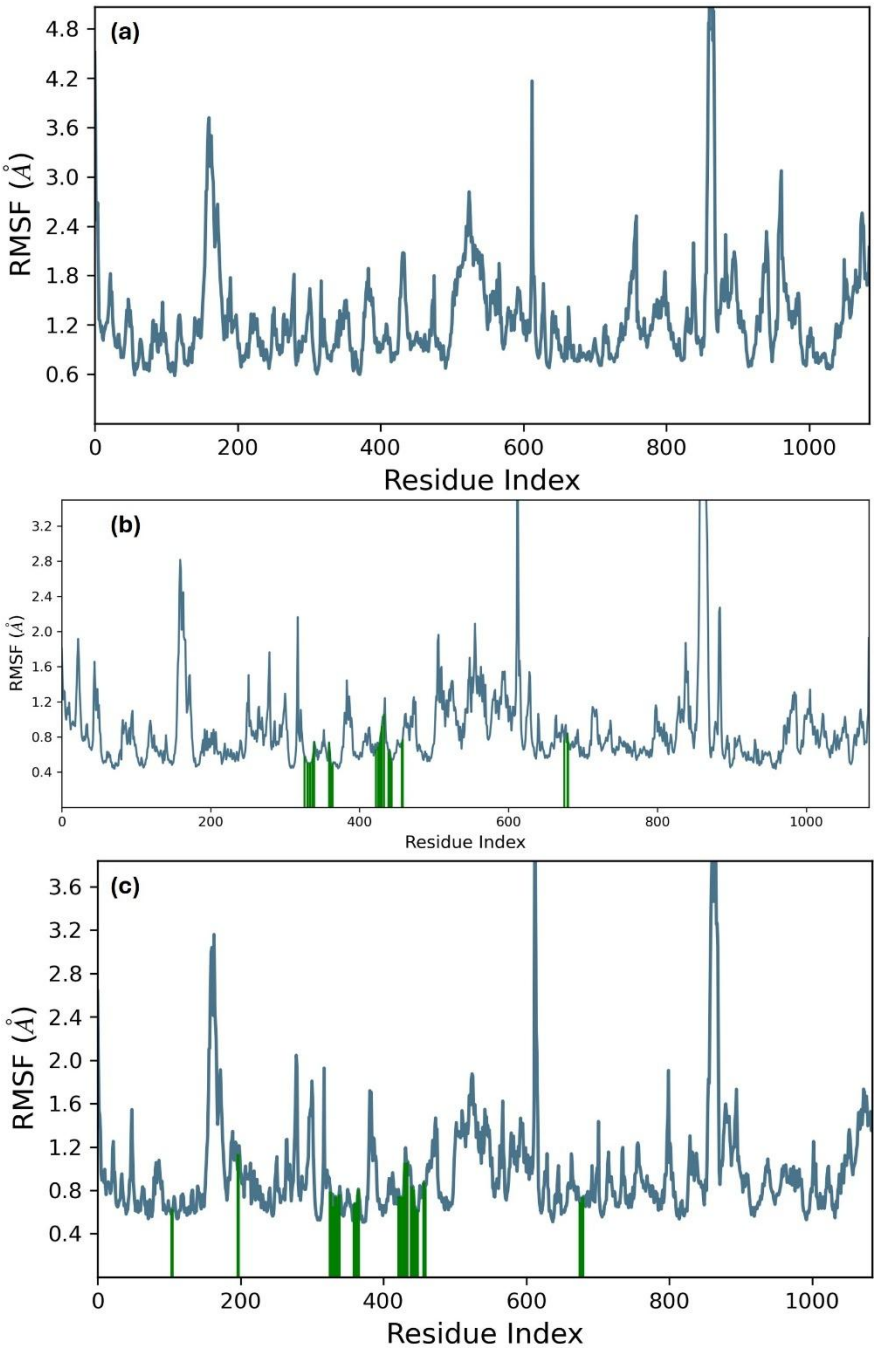

Figure S87: RMSF plots for the (a) apo *Pf*FLN, (b) *Pf*FLN-**19**, and (c) *Pf*FLN-**27** complexes.

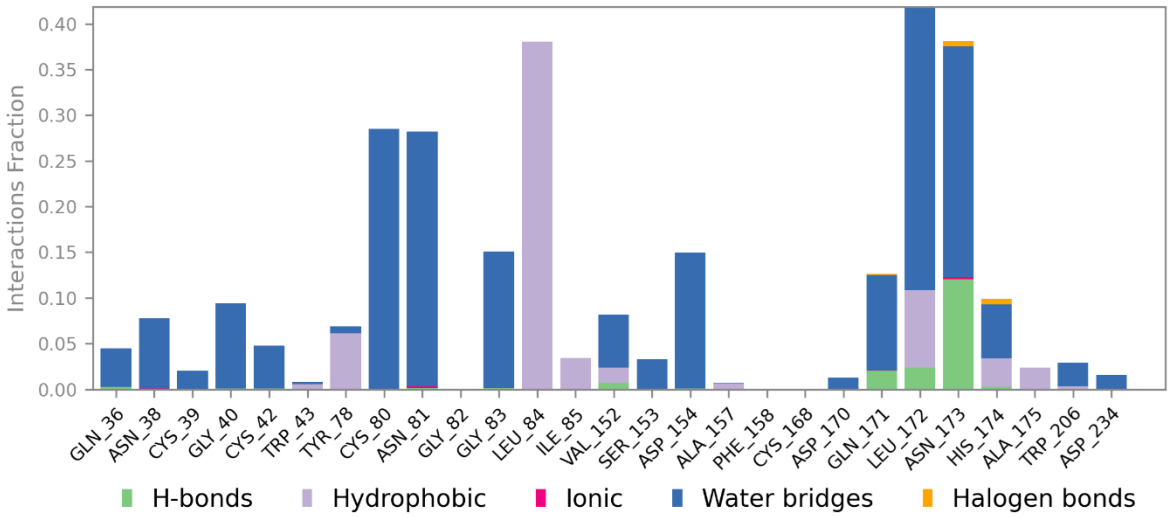

Figure S88: Protein-ligand contact histogram for *Pf*FP2-**19** complex during MD simulation. The value 0.1 suggests that 10% of the simulation time, the specific interaction was maintained.

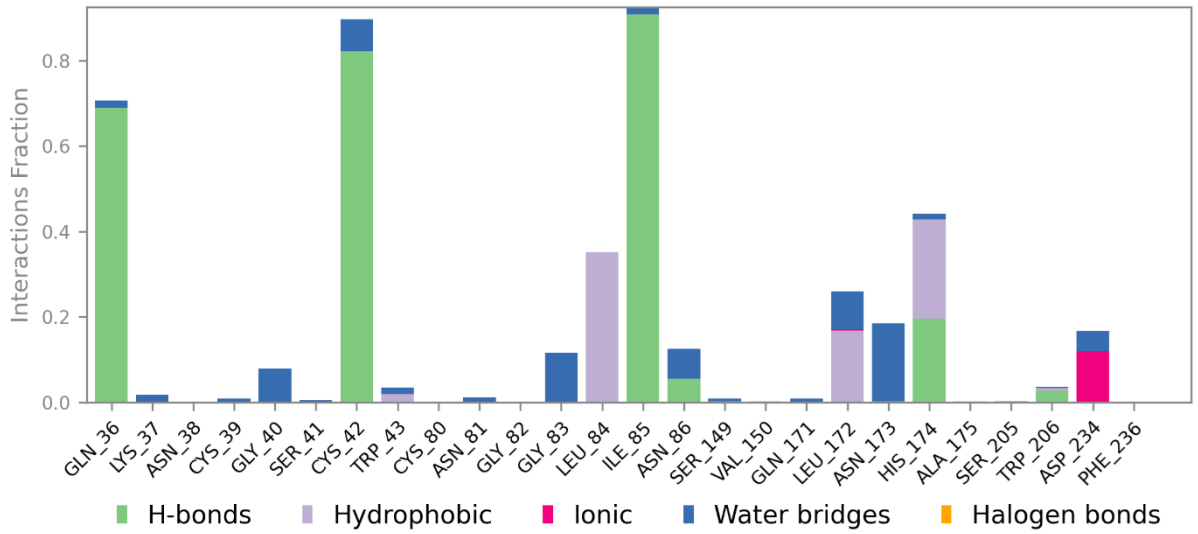

Figure S89: Protein-ligand contact histogram for *Pf*FP2-**27** complex during MD simulation.

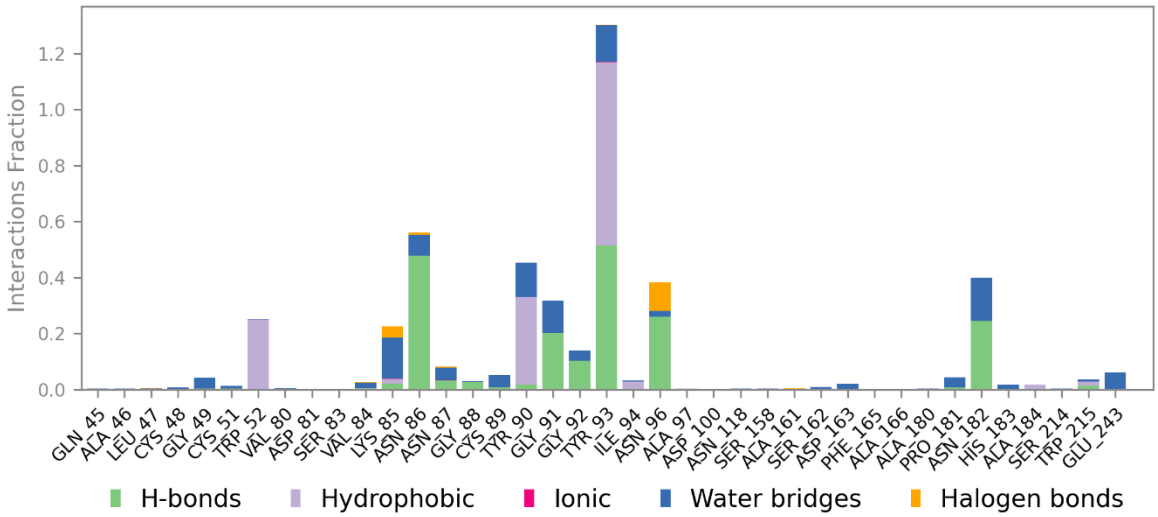

Figure S90: Protein-ligand contact histogram for *Pf*FP3-**19** complex during MD simulation. Note: it is possible to have interactions with >100% as some residues may have multiple interactions of a single type with the same ligand atom.

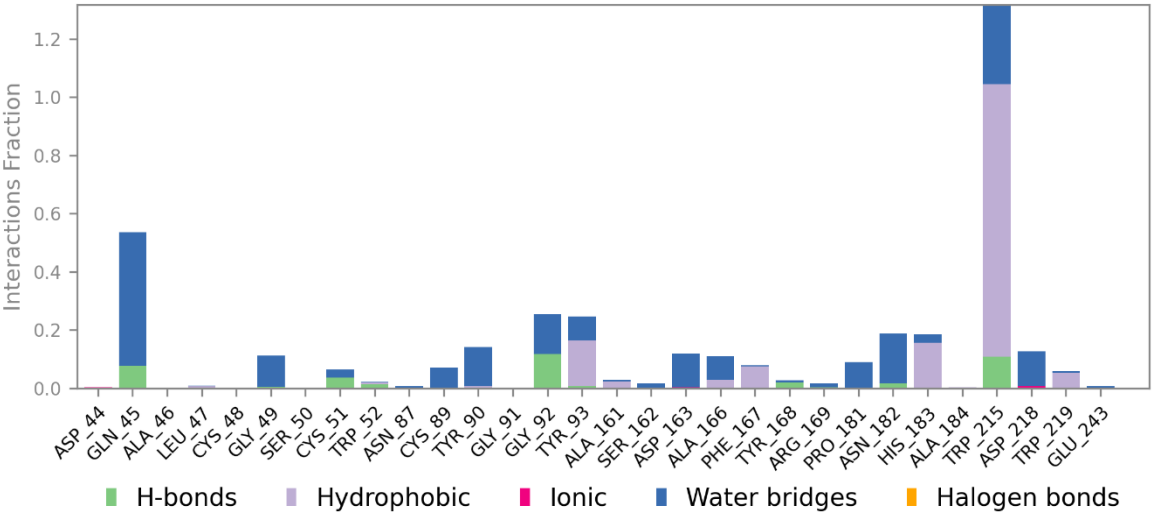

Figure S91: Protein-ligand contact histogram for *Pf*FP3-**27** complex during MD simulation.

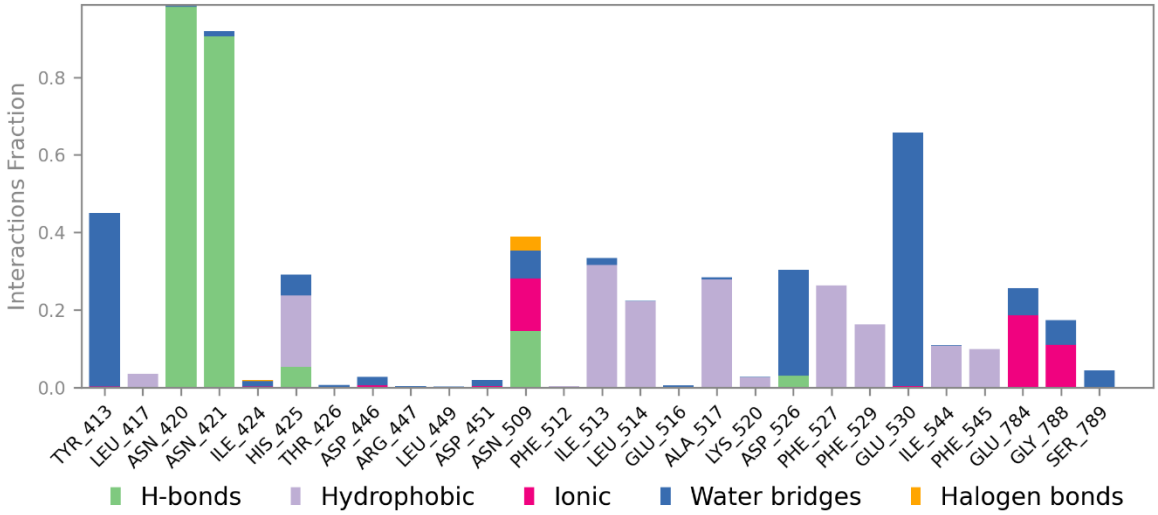

Figure S92: Protein-ligand contact histogram for *Pf*FLN-**19** complex during MD simulation.

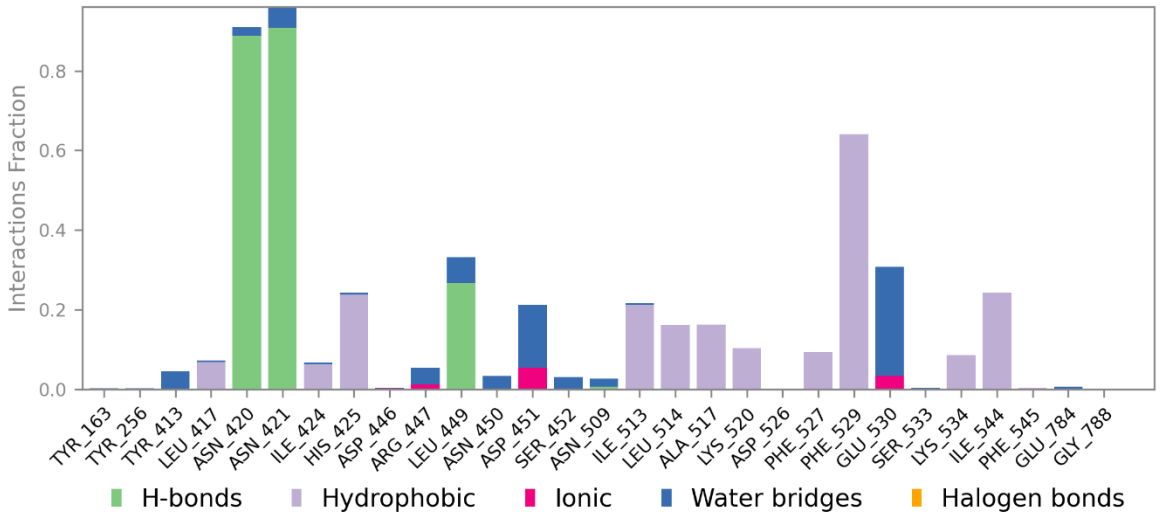

Figure S93: Protein-ligand contact histogram for *Pf*FLN-**27** complex during MD simulation.

ADME Prediction and Drug-Likeness of the Compounds

Physicochemical properties are one of the key factors to predict the drug-like nature of the test compound. The solvent-accessible surface area (SASA), hydrophilic and hydrophobic content of SASA, prediction of per cent human oral absorption, QPlogS, etc., are physicochemical parameters that significantly affect the ability of the compounds to interact with the target protein. Similarly, Lipinski's rule of five, rule of three, etc., are used to predict the oral bioavailability of the compounds. Therefore, FISA (a hydrophilic component of the SASA), FOSA (a hydrophobic component of the SASA), %HOA (per cent human oral absorption), QPlogS, $QPlogK_{hsa}$, rule of five, rule of three, SASA, molecular weight, number of hydrogen bond donors and acceptors, etc, were calculated and discussed in Table S1.

Table S1: Physicochemical and ADME properties of the compounds:

Compound	Mol. Wt.	QPlogPo/w	HBD	HBA	FISA	FOSA	%HOA	QPlogS	$QPlogK_{hsa}$	Violations		SASA
										Rule of five	Rule of three	
13	263.73	2.92	1.0	4.2	38.36	199.42	100.00	-3.42	-0.05	0	0	480.72
14a	313.40	2.29	2.0	6.2	53.58	344.76	91.98	-2.77	0.09	0	0	568.06
14b	314.39	3.15	1.0	6.4	23.20	370.92	100.00	-3.86	0.08	0	0	567.35

16	354.72	3.63	0.0	4.5	78.81	108.73	100.00	-5.06	0.16	0	0	549.06
17a	404.40	2.87	1.0	6.5	99.19	222.03	87.62	-3.83	0.38	0	0	584.62
17b	405.38	3.38	0.0	6.6	70.71	255.47	100.00	-4.47	0.06	0	0	596.83
19	545.06	3.91	2.0	11.7	142.42	433.59	84.25	-7.45	0.36	1	1	897.66
20	540.64	3.06	2.0	12.4	144.79	457.22	65.87	-5.90	0.07	2	1	847.80
21	631.64	3.48	1.0	12.7	177.77	349.15	62.74	-6.37	0.25	2	1	843.54
22	586.59	2.95	0.0	11.5	180.41	237.71	59.18	-4.70	-0.21	2	0	769.90
23	498.56	2.99	1.0	10.2	181.03	302.55	72.30	-5.58	0.16	1	0	779.22
24	498.56	3.39	1.0	10.2	152.05	309.43	79.57	-5.70	0.23	1	0	786.32
25	503.62	4.70	1.0	9.2	78.55	308.79	100.00	-6.78	0.58	1	1	816.00
26	589.55	2.88	0.0	10.5	220.16	160.13	52.06	-5.11	-0.09	2	0	763.01
27	589.55	3.10	0.0	10.5	175.72	154.21	60.90	-4.66	-0.14	2	0	739.42
28	594.62	4.72	0.0	9.5	125.49	168.55	91.87	-6.61	0.47	1	1	804.15
29	478.57	2.95	1.0	10.7	156.66	302.13	89.13	-6.41	0.04	0	1	780.56
30	569.57	2.81	0.0	11.0	195.67	160.12	55.78	-5.88	-0.23	2	1	764.35
31	454.55	2.81	1.0	10.7	106.96	308.90	96.77	-4.87	-0.13	0	0	739.98
32	459.58	3.66	1.0	9.2	81.44	308.34	100.00	-5.51	0.16	0	0	733.63
33	494.03	4.16	1.0	9.2	81.50	308.55	100.00	-6.26	0.27	0	1	759.49
34	585.02	4.24	0.0	9.5	130.57	171.48	88.18	-6.18	0.17	1	1	756.54
35	545.55	2.69	0.0	11.0	155.87	168.11	61.84	-4.48	-0.37	2	0	733.03
36	550.58	3.59	0.0	9.5	132.68	178.53	84.00	-5.17	0.02	1	0	723.79
CQ	319.87	1.95	1.0	3.0	24.08	373.47	100	-4.55	0.59	0	0	656.11

The ADME parameters were predicted using the QikProp module of Schrodinger 2021-2. SASA: Total solvent accessible surface area in square Å (300.0 – 1000.0); FOSA: Hydrophobic component of the SASA (0.0 – 750.0); FISA: Hydrophilic component of the SASA (7.0 – 330.0); QPlogS: Predicted aqueous solubility in mol/dm^3 (-6.5 – 0.5); #metab: The number of likely metabolic reactions (1 – 8); QPlogK_{hsa}: Prediction of binding to human serum albumin (-1.5 – 1.5); %HOA: Percent Human Oral Absorption (>80% is high, <25% is poor); Rule of Five: The rules are: mol_MW < 500, QPlogPo/w < 5, donorHB ≤ 5, accptHB ≤ 10. The compounds that follow this rule are considered more drug-like. The Rule of Three consists of three rules: QPlogS > -5.7. The compounds that follow this rule are considered more orally available.

The calculated and predicted physicochemical parameters of the compounds were compared with those of current mainline antimalarials, including chloroquine (CQ), primaquine (PQ), and artemether (AR). According to the biomolecular properties outlined in Table S1, a significant proportion of the compounds fall within the Schrödinger range, encompassing 95% of all known medications.